



**Magnetically Actuated Propellant  
Orientation Experiment, Controlling  
Fluid Motion With Magnetic Fields  
in a Low-Gravity Environment**  
(MSFC Center Director's Discretionary Fund Final Report,  
Project No. 93–18)

*J.J. Martin and J.B. Holt*

*Marshall Space Flight Center, Marshall Space Flight Center, Alabama*

## The NASA STI Program Office...in Profile

Since its founding, NASA has been dedicated to the advancement of aeronautics and space science. The NASA Scientific and Technical Information (STI) Program Office plays a key part in helping NASA maintain this important role.

The NASA STI Program Office is operated by Langley Research Center, the lead center for NASA's scientific and technical information. The NASA STI Program Office provides access to the NASA STI Database, the largest collection of aeronautical and space science STI in the world. The Program Office is also NASA's institutional mechanism for disseminating the results of its research and development activities. These results are published by NASA in the NASA STI Report Series, which includes the following report types:

- **TECHNICAL PUBLICATION.** Reports of completed research or a major significant phase of research that present the results of NASA programs and include extensive data or theoretical analysis. Includes compilations of significant scientific and technical data and information deemed to be of continuing reference value. NASA's counterpart of peer-reviewed formal professional papers but has less stringent limitations on manuscript length and extent of graphic presentations.
- **TECHNICAL MEMORANDUM.** Scientific and technical findings that are preliminary or of specialized interest, e.g., quick release reports, working papers, and bibliographies that contain minimal annotation. Does not contain extensive analysis.
- **CONTRACTOR REPORT.** Scientific and technical findings by NASA-sponsored contractors and grantees.

- **CONFERENCE PUBLICATION.** Collected papers from scientific and technical conferences, symposia, seminars, or other meetings sponsored or cosponsored by NASA.
- **SPECIAL PUBLICATION.** Scientific, technical, or historical information from NASA programs, projects, and mission, often concerned with subjects having substantial public interest.
- **TECHNICAL TRANSLATION.** English-language translations of foreign scientific and technical material pertinent to NASA's mission.

Specialized services that complement the STI Program Office's diverse offerings include creating custom thesauri, building customized databases, organizing and publishing research results...even providing videos.

For more information about the NASA STI Program Office, see the following:

- Access the NASA STI Program Home Page at <http://www.sti.nasa.gov>
- E-mail your question via the Internet to [help@sti.nasa.gov](mailto:help@sti.nasa.gov)
- Fax your question to the NASA Access Help Desk at (301) 621-0134
- Telephone the NASA Access Help Desk at (301) 621-0390
- Write to:  
NASA Access Help Desk  
NASA Center for AeroSpace Information  
7121 Standard Drive  
Hanover, MD 21076-1320



**Magnetically Actuated Propellant  
Orientation Experiment, Controlling  
Fluid Motion With Magnetic Fields  
in a Low-Gravity Environment  
(MSFC Center Director's Discretionary Fund Final  
Report, Project No. 93–18)**

*J.J. Martin and J.B. Holt*

*Marshall Space Flight Center, Marshall Space Flight Center, Alabama*

National Aeronautics and  
Space Administration

Marshall Space Flight Center • MSFC, Alabama 35812

## **Acknowledgments**

The authors would like to acknowledge Leslie Curtis of the Advanced Space Transportation Program Office for funding the CFX-4 computer model and its application to the problem. Also acknowledged are the efforts of Jeffrey Mullins, Kevin Pedersen, Robert Lake, Jr., Palmer Peters, Charles Sisk, Randy McNichol, Michael Lee, John Gibson, Shane Carpenter, Kerry Warner, Ricky Middleton, Sara Pauls, and Melissa Van Dyke of the Marshall Space Flight Center; the KC-135 flight and test crew at the Johnson Space Center; and project originator Susan Driscoll, formerly of the Marshall Space Flight Center.

## **TRADEMARKS**

Trade names and trademarks are used in this report for identification only. This usage does not constitute an official endorsement, either expressed or implied, by the National Aeronautics and Space Administration.

Available from:

NASA Center for AeroSpace Information  
7121 Standard Drive  
Hanover, MD 21076-1320  
(301) 621-0390

National Technical Information Service  
5285 Port Royal Road  
Springfield, VA 22161  
(703) 487-4650

## TABLE OF CONTENTS

1. INTRODUCTION .....	1
1.1 Background .....	1
1.2 Need .....	2
1.3 Objective .....	2
1.4 Approach .....	2
2. TEST ARTICLE .....	3
2.1 Test Hardware Description .....	3
2.2 Test Fluid Description .....	5
2.3 Flight Test Environment .....	6
3. NUMERICAL MODELING .....	9
3.1 Magnetic Influences .....	9
3.2 Model Description .....	10
4. TEST RESULTS .....	12
4.1 Test Matrix .....	12
4.2 Acceleration Axes and Data Histories .....	12
4.3 Experimental and Model Results .....	14
4.4 Discussion .....	30
5. CONCLUSIONS .....	38
APPENDIX A—DETAILED DRAWING SET FOR TEST PACKAGE HARDWARE .....	39
APPENDIX B—MAGNETIC FIELD MEASUREMENTS OVER TEST TANK VOLUME .....	51
APPENDIX C—MAGNETIZATION MEASUREMENTS OF WATER-BASED MAGNETIC FLUID .....	56
APPENDIX D—ACCELEROMETER EXPERIMENTAL DATA .....	66
REFERENCES .....	94

## LIST OF FIGURES

1.	MAPO test package .....	3
2.	MAPO free floating .....	3
3.	MAPO test tank .....	4
4.	MAPO ring magnet .....	5
5.	MAPO float zone in aircraft .....	7
6.	MAPO initial fluid orientations .....	7
7.	MAPO tank grid structure .....	10
8.	Surface shape comparison: Numerical and exact solutions .....	10
9.	Surface shape benchmark for MAPO tank .....	11
10.	MAPO acceleration axes .....	13
11.	Typical test acceleration profiles .....	13
12.	Baseline water test 5 image frames at 2, 11, 12.5, 14, 15.5, and 18.5 sec .....	15
13.	Baseline water test 23 image frames at 6, 12, 13.5, 16, 20, and 25 sec .....	15
14.	Mixture 133:1 test 30 image frames at 1.5, 3, 6, 8.5, 11, and 12.5 sec .....	17
15.	Mixture 30:1 test 48 image frames at 1.5, 6, 9.5, 14, 18, and 21 sec .....	19
16.	Mixture 30:1 test 59 image frames at 0.5, 6.5, 9, 13, 17, and 22 sec .....	21
17.	Mixture 30:1 test 74 image frames at 6, 15, 17, 20, 23, and 26.5 sec .....	23
18.	Mixture 10:1 test 90 image frames at 3.5, 7, 13, 16, 19, and 22.5 sec .....	25
19.	Mixture 10:1 test 97 image frames at 4, 8, 12.5, 16.5, 20, and 25 sec .....	27
20.	Mixture 10:1 test 106 image frames at 4.5, 10.5, 12, 13.5, 16, and 18.5 sec .....	29

## LIST OF FIGURES (Continued)

21.	<i>B</i> <sub>0</sub> for LO <sub>2</sub> and ferromagnetic solution .....	31
22.	<i>B</i> <sub>0</sub> and <i>B</i> <sub>0mags</sub> for ferromagnetic solutions .....	32
23.	<i>B</i> <sub>0</sub> and <i>B</i> <sub>0mags</sub> for LO <sub>2</sub> .....	33
24.	LO <sub>2</sub> motion simulation No. 1 for 1×, 2×, and 6× baseline magnetic field .....	34
25.	LO <sub>2</sub> motion simulation No. 2 for 1×, 2×, and 6× baseline magnetic field .....	36
26.	MAPO assembly sheet 1 .....	39
27.	MAPO frame layout sheet 2 .....	40
28.	MAPO frame layout sheet 3 .....	41
29.	MAPO frame layout sheet 3a .....	42
30.	MAPO test tank assembly sheet 4 .....	43
31.	MAPO test tank assembly sheet 4a .....	44
32.	MAPO test tank assembly sheet 4b .....	45
33.	MAPO test tank assembly sheet 4c .....	46
34.	MAPO test tank assembly sheet 4d .....	47
35.	MAPO test tank assembly sheet 4e .....	48
36.	MAPO hand rail assembly sheet 5 .....	49
37.	MAPO camera assembly sheet 6 .....	50
38.	Test magnet .....	51
39.	Magnet and tank layout .....	51
40.	Magnetization of Nd <sub>2</sub> O <sub>3</sub> standard .....	57
41.	Magnetization of 170:1 ratio .....	58

## LIST OF FIGURES (Continued)

42.	Ferro- $\chi$ of 170:1 ratio .....	58
43.	Magnetization of 133:1 ratio .....	59
44.	Ferro- $\chi$ of 133:1 ratio .....	59
45.	Magnetization of 83:1 ratio .....	60
46.	Ferro- $\chi$ of 83:1 ratio .....	60
47.	Magnetization of 30:1 ratio .....	61
48.	Ferro- $\chi$ of 30:1 ratio .....	61
49.	Magnetization versus concentration curve .....	62
50.	Magnetization of 10:1 ratio .....	63
51.	Ferro- $\chi$ of 10:1 ratio .....	63

## LIST OF TABLES

1.	Selected MAPO tests .....	12
2.	Drawing list .....	39
3.	Magnetic field measurements—four intervals .....	53
4.	Average magnetic field measurement .....	55
5.	Ferro- $\chi$ for a concentration ratio of 133:1 .....	64
6.	Ferro- $\chi$ for a concentration ratio of 30:1 .....	64
7.	Ferro- $\chi$ for a concentration ratio of 10:1 .....	65
8.	MAPO test number 5 data .....	67
9.	MAPO test number 23 data .....	70
10.	MAPO test number 30 data .....	73
11.	MAPO test number 48 data .....	76
12.	MAPO test number 59 data .....	79
13.	MAPO test number 74 data .....	82
14.	MAPO test number 90 data .....	85
15.	MAPO test number 97 data .....	88
16.	MAPO test number 106 data .....	91

## LIST OF ACRONYMS AND SYMBOLS

<i>Bo</i>	bond number
<i>Bomag</i>	magnetic bond number
CDDF	Center Director's Discretionary Fund
CFD	computational fluid dynamics
CFM	cryogenic fluid management
cgs	centimeter/gram/second system of units
ferro- $\chi$	ferro-susceptibility
JSC	Johnson Space Center
LH <sub>2</sub>	liquid hydrogen
LO <sub>2</sub>	liquid oxygen
MSFC	Marshall Space Flight Center
MAPO	magnetic actuated propellant orientation
PMD	propellant management device
TOS	tank on side
TUD	tank upside down
TUR	tank upright

## NOMENCLATURE

$a$	acceleration
$B$	magnetic field strength
$Bo$	bond number
$Bomag$	magnetic bond number
$\vec{F}_M$	body force, pondermotive (vector)
$F_M$	body force, pondermotive (magnitude)
G	gauss (measure of magnetic field strength)
$\mathfrak{g}, \mathfrak{g}_x, \mathfrak{g}_y, \mathfrak{g}_z$	gravity, gravity vectors
$\vec{H}$	magnetic intensity (vector)
$H$	magnetic intensity (magnitude)
$l$	tank length
$\vec{M}$	magnetization (vector)
$R$	tank radius
$\rho$	density
$\sigma$	surface tension
$\mu_o$	permeability of free space
$\chi$	susceptibility

## TECHNICAL MEMORANDUM

# **MAGNETICALLY ACTUATED PROPELLANT ORIENTATION EXPERIMENT, CONTROLLING FLUID MOTION WITH MAGNETIC FIELDS IN A LOW-GRAVITY ENVIRONMENT (MSFC Center Director's Discretionary Fund Final Report, Project No. 93-18)**

## **1. INTRODUCTION**

### **1.1 Background**

In a low-gravity (low-g) environment the acquisition and transfer of vapor-free propellant is not as straightforward as similar operations on the ground. The indeterminate location of the bulk liquid within the propellant tank complicates the design of engine feed and transfer systems for resupply that rely on proper liquid orientation and an understanding of fluid motion in response to thermal conditions, disturbances, and imposed accelerations. Traditional approaches included the application of periodic thruster burns to settle propellant over the tank outlet or the use of screen channel and vane propellant management devices (PMD's) to capture and hold propellant at specific locations within the tank.<sup>1,2</sup> Although these techniques have been used successfully in storable propellant applications, there are technology issues associated with using PMD's in cryogenic systems. Also, propellant settling burns complicate flight operations and require additional hardware systems and propellant.

An alternative to traditional methods exploits the inherent magnetism of propellants like liquid oxygen (LO<sub>2</sub>) and liquid hydrogen (LH<sub>2</sub>) to control liquid orientation. This idea is not new.<sup>3,4</sup> LO<sub>2</sub>, a paramagnetic substance, moves toward the regions of higher field strength when subjected to a non-uniform magnetic field (i.e., attracted to a magnet). On the other hand LH<sub>2</sub>, a weakly diamagnetic substance, moves away from regions of high magnetic field strength (i.e., repelled from a magnet) and therefore can be levitated.<sup>5</sup> With the advent of high-temperature superconductors and the potential for lightweight, rare Earth magnets (providing high field strength-to-mass ratios), renewed interest in using magnetic control has surfaced. This technology has the potential of opening up several promising applications in the handling of both paramagnetic and diamagnetic cryogens in low-g conditions.

To investigate this phenomenon, a Center Director's Discretionary Fund (CDDF) project was awarded to the Marshall Space Flight Center's (MSFC's) Propulsion Laboratory to design, fabricate, and test hardware in a relevant environment.

## 1.2 Need

Cryogenic fluid management (CFM) is a technology area common to virtually every space transportation propulsion concept envisioned. Storage, supply, transfer, and handling of subcritical cryogenic fluids are basic capabilities that have long been needed by multiple programs and the need is expected to continue in the future.<sup>6</sup> The use of magnetic fields provides another method which could replace or augment current approaches, potentially simplifying vehicle operational constraints.

The magnetically actuated propellant orientation (MAPO) program effort focused on the use of magnetic fields to control fluid motion as it relates to positioning; i.e., orientation and acquisition, of a paramagnetic substance such as LO<sub>2</sub>. Current CFM state-of-the-art systems used to control and acquire propellant in low-g environments rely on liquid surface tension devices which employ vanes, fine screen mesh channels, and baskets. These devices trap and direct propellant to areas where it is needed and have been used routinely with storable (noncryogenic) propellants.<sup>7</sup> However, almost no data exists regarding their operation in cryogenics, and the use of such devices confronts designers with a multitude of significant technology issues. Typical problems include a sensitivity to screen dryout (due to thermal loads and pressurant gas) and momentary adverse accelerations, generated from either internal or external sources.<sup>8,9</sup> Any of these problems can potentially cause the acquisition systems to ingest or develop vapor and fail.

The use of lightweight, high field strength magnets may offer a valuable means of augmenting traditional systems potentially mitigating or at least easing operational requirements. Two potential uses of magnetic fields include (1) strategically positioning magnets to keep vent ports clear of liquid (enabling low-g vented fill operations) and (2) placing magnets in the center or around the walls of the tank to create an insulating vapor pocket (between the liquid and the tank wall) which could effectively lower heat transfer to the liquid (enabling increased storage time).

## 1.3 Objective

Assess feasibility of employing magnets to control orientation of cryogenic fluids in zero-g. This test program was focused on producing experimental data regarding the interaction between a magnetic field and ferromagnetic fluid, and using the data to verify a computational fluid dynamics (CFD) code called CFX-4 that had been modified to account for pertinent magnetic forces. The verified CFD model could then be used to predict motion for other fluids, magnetic field distributions, hardware geometries, and imposed accelerations.

## 1.4 Approach

Experimental hardware was fabricated and tested with fluids including a nonmagnetic water baseline and several magnetic solutions of varying strength. With the intent of making this test program simple from the standpoint of safety and handling, a commercially available water-based ferromagnetic material was selected as the magnetic test fluid. Experimental data were collected in the form of videotape and accelerometer readings aboard the NASA Reduced-Gravity Workshop, a KC-135A aircraft.

## 2. TEST ARTICLE

### 2.1 Test Hardware Description

The MAPO test hardware, illustrated in figures 1 and 2, was designed, fabricated, and assembled at MSFC. This hardware package consisted of an aluminum tubular frame providing structural support for components and handrails on all sides to ease handling. The hardware had an overall envelope of 52-in. length  $\times$  23-in. width  $\times$  16-in. height and a flight weight of  $\approx$ 150 lb. The size and weight were kept at a minimum in an effort to maximize the amount of free float time. The package also contained its own power and lighting sources so that no connections to the aircraft were required. Appendix A provides a detailed drawing set for the test package hardware. The components contained within the frame structure consisted of the test tank, a rare Earth magnet, video camera, a three-axis accelerometer package, and a laptop computer.

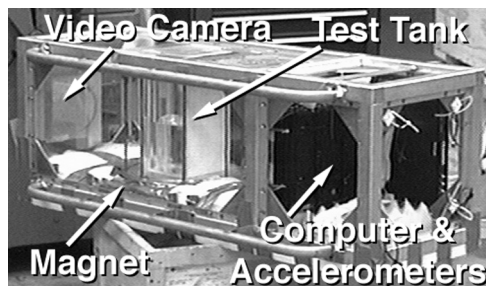


Figure 1. MAPO test package.



Figure 2. MAPO free floating.

The cylindrical test tank, shown in figure 3, has a 6-in. internal diameter and a total height of 10 in. It was fabricated by boring through a 6.5 in.  $\times$  6.5 in.  $\times$  10 in. section of rectangular Plexiglas<sup>®</sup> stock. This process provided a flat front surface, allowing a better view of the motion inside the cylindrical interior. The tank was sealed on each end with 1/2-in.-thick Plexiglas caps equipped with rubber O-rings. The tank was pneumatically proof tested and tagged for an operational pressure of 11.2 psig. Although the tank was not attached to a pressurant system, in the event of KC-135 cabin decompression, the test tank would be exposed to the low ambient pressure at 35,000-ft altitude. The top Plexiglas cap was equipped with a 3/8-in. fitting through which water and ferromagnetic solutions were added. For all testing, the tank was filled to  $\approx$ 50-percent capacity.

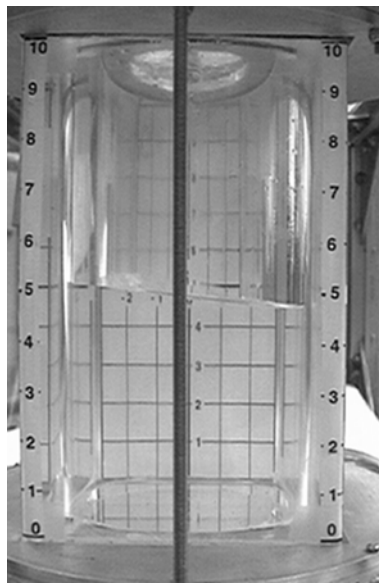


Figure 3. MAPO test tank.

The permanent rare Earth magnet, shown in figure 4, was of a ring design with a weight of 25 lb, a thickness of 1.5 in., and inner and outer diameters of 4 and 10 in., respectively. The maximum magnetic field strength, measured at the surface, was 6,000 G. The magnet was mounted directly beneath the test tank with a resulting magnetic field strength ranging from a high of 1,400 G at the bottom corners of the tank to 45 G at the top of the tank. The magnetic field was weaker at the bottom center of the tank,  $\approx$ 600 G, because of the magnet ring shape. The hardware dimensions and layout were selected in order to position the magnet sufficiently far away from sensitive electronic devices. Appendix B contains information regarding detailed measurements of the magnetic field within the test tank envelope.

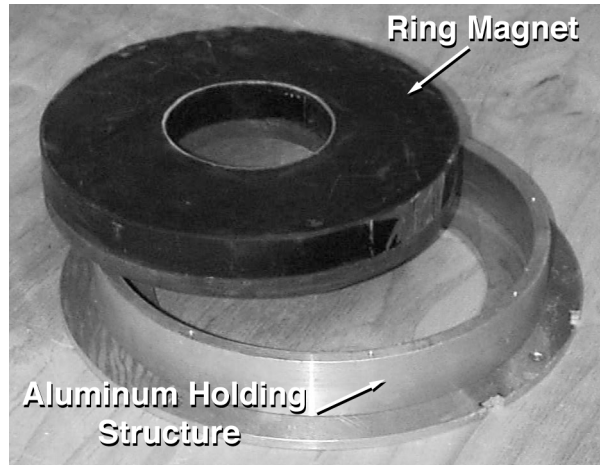


Figure 4. MAPO ring magnet.

The video camera, three-axis accelerometer package, and laptop computer were used to measure and record test data. To reduce the chances of data corruption, each device was positioned beyond the magnet minimum safe distance (app. B) and with sufficient foam padding to protect against rough handling and flight loads. The video camera was attached to the front of the package, providing a clear view of the test tank and fluid motion. This camera location also made it the most vulnerable component on the test package. The accelerometer pack and computer were positioned at the rear of the test package in an open compartment so that a crew member could interact with the computer and issue the start command at the beginning of each free-float interval.

To protect against accidental spills or leaks of fluid, the compartment containing the test tank was enclosed with Plexiglas and aluminum panels. Several of these panels had small holes cut through them to allow for cabling, video imaging, and rapid venting in case of an aircraft decompression. These holes were covered with plastic and tape to prevent liquid leakage without interfering with the emergency vent function. In addition, absorbent material was attached along the bottom of the sealed compartment to absorb any potential spillage.

The test package was designed to satisfy the handling, structural, electrical, and safety requirements identified in four Johnson Space Center (JSC) documents.<sup>10-13</sup> Based on this information, a test article data package was assembled outlining the program objectives, test hardware, structural/electrical analyses, test requirements, and test article hazards analysis. This package was provided to both the MSFC reviewers and the JSC Reduced Gravity Office for test article approval. The hardware was then required to pass a final test readiness review involving a hardware walkdown prior to loading aboard the KC-135 aircraft.

## 2.2 Test Fluid Description

The water-based ferromagnetic test fluid was manufactured by a commercial company, Ferrofluidics Corporation. This fluid selection enabled simplification of the overall program safety requirements. Safety requirements would have been significant had a kerosene-based simulant or actual oxygen been used. The ferromagnetic material was a colloidal dispersion of very fine iron oxide

particles within a water base. The main drawback was its very dark nature and a tendency to coat surfaces rendering them opaque, an undesirable effect for systems requiring visual observation. The ferromagnetic solution, designated EMG-805, was diluted with distilled water for testing at ratios of 10:1, 30:1, and 133:1 by volume. These ratios were chosen to cover a range of strengths corresponding to that of  $\text{LO}_2$  (see app. C). The distilled water was also treated with a wetting agent (Triton X-100 manufactured by Union Carbide Corporation) in an attempt to lower the surface tension. However, to prevent potential foaming of the wetting agent, an antifoaming agent (FG-10 manufactured by Dow Corning) was added. The wetting agent was added at  $\approx 0.1$  percent by volume and antifoaming agent was added until no foaming occurred when agitated. The average fluid surface tension was measured to be 31.5 dyn/cm using a dynamic contact angle analyzer model DCA 315 (Cahn Instruments Inc.).

In order to accurately model and test fluid motion resulting from magnetic field interactions, it is necessary to obtain the slope of the fluid magnetization versus the applied magnetic field. This term is commonly referred to as the fluid's susceptibility ( $\chi$ ) and is a constant for a paramagnetic material such as oxygen. However, for a ferromagnetic fluid, such as that used in this experiment,  $\chi$  is not a constant; hence, discrete values must be calculated at each location within the magnetic field for a given fluid dilution. The impact of this situation is that a single ferromagnetic mixture cannot be made to simulate oxygen throughout the entire test tank. This ferrosusceptibility (ferro- $\chi$ ) range can be rather significant; for example, the 30:1 mixture ranges from approximately  $800 \times 10^{-6}$  (cgs) at the top of the tank (low magnetic field) to  $\approx 40 \times 10^{-6}$  (cgs) at the bottom of the tank near the magnet. For the KC-135 flight experiments, the stronger ferromagnetic mixtures were chosen for use due to the short low-g float interval and the uncertainty in gravity levels. The stronger mixtures responded more quickly to the magnetic field and were more resistant to small perturbation. Appendix C provides a detailed discussion regarding the measurement and calculation of the ferrosusceptibilities for the ferromagnetic mixtures used on the MAPO project.

### **2.3 Flight Test Environment**

All testing was performed aboard the NASA KC-135 Reduced Gravity Workshop operated by JSC out of Ellington Field, Houston, Texas. The test hardware was loaded onto the aircraft and secured with several cargo straps. The MAPO float zone extended from Station 880 to 1140, which used approximately one-third of the aircraft open space, as illustrated in figure 5. The large float zone provided the space necessary for maximizing the low-g float time (before the test package drifted into the aircraft walls). Also, since there is a tendency for free-floating articles to migrate rearward during a free float, the rear position assisted in keeping the test package away from other experiments. The typical duration of the low-g float interval (or parabola) flown by the aircraft was  $\approx 25$  sec. However, the usable portion of the interval was typically much shorter with time consumed by the test package transition and release process.

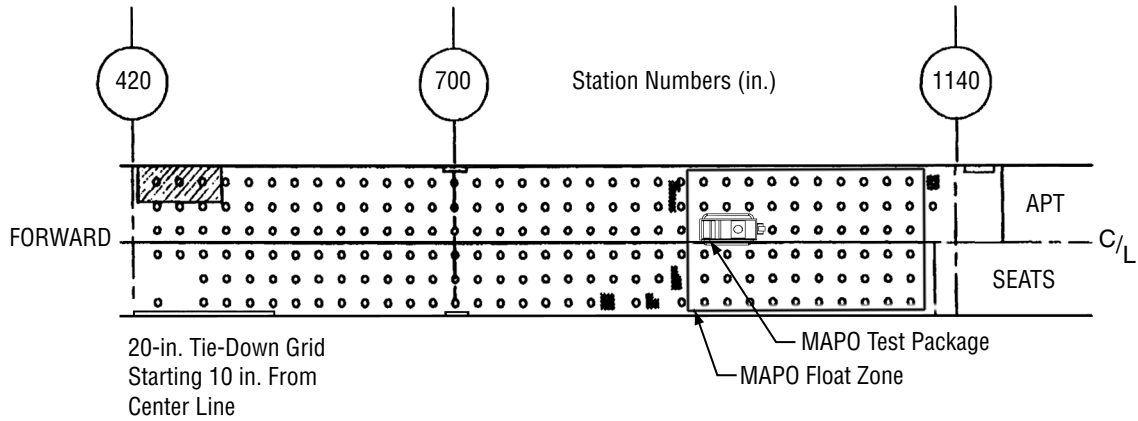


Figure 5. MAPO float zone in aircraft.

The MAPO hardware was tested in three different orientations used to provide an initial fluid position prior to the low-g test interval. These orientations included: (1) Upright position which placed the fluid on the bottom of the tank against the magnet, (2) on-side position which placed the fluid against the side wall of the tank, and (3) upside-down position which placed the fluid against the top of the tank opposite the magnet. The fluid motion was then observed during the low-g test interval as the magnetic field acted on the ferromagnetic fluid (tending to move it toward the magnet). These initial orientations are illustrated in figure 6.

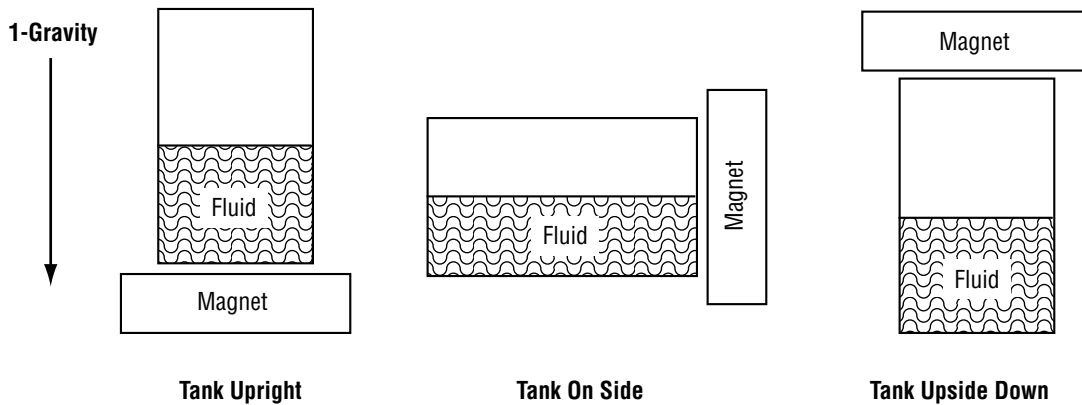


Figure 6. MAPO initial fluid orientations.

Typical operations during a flight day included mixing the correct ferromagnetic solution ratio, charging batteries, setting up the computer, and securing the test package prior to lift-off. Once at altitude, the package was released and oriented in one of the three positions on the aircraft floor. Each package orientation was free floated for a minimum of 10 low-g parabolas in an attempt to get at least one good float with minimum agitation and the longest possible float duration. It was found that free floating the package was extremely difficult at best, due to the complex nature of the interactions between the crew members, test package, and aircraft. Minor disturbances induced by either the crew or the aircraft could result in the package very quickly (within seconds) contacting the floor, walls, or ceiling, significantly agitating the tank contents and effectively terminating that free float. However, usually 1 of 10 parabolas resulted in a clean release and a slow float through the cabin, providing 10–15 sec of low-g coast time. Two crew members were required to control the test package release and capture operations. Additional crew members assisted in the float, monitored the video recording, operated the computer data acquisition system, and maintained a logbook detailing the outcome of each low-g parabola. During a typical flight day 40 low-g parabolas were flown.

### 3. NUMERICAL MODELING

#### 3.1 Magnetic Influences

The use of a magnetic field provides an additional body force, ponderomotive, which can be written as

$$\vec{F}_M = \mu_0 (\vec{M} \cdot \nabla) \vec{H} \quad (1)$$

where

$\mu_0$  = permeability of free space

$\vec{M}$  = magnetization

$\vec{H}$  = magnetic intensity.

For paramagnetism and ferromagnetism, the magnetization vector  $\vec{M}$  is parallel to the external field that causes it. Furthermore, the magnetization  $\vec{M}$  is proportional to the magnetic intensity  $\vec{H}$  for paramagnetic and diamagnetic fluids. Assuming the fluid is electrically nonconducting, the displacement current is negligible and the fluid is linear in the magnetic sense, equation (1) can be written as

$$\vec{F}_M = \mu_0 \chi H \nabla H \quad (2)$$

where

$\chi$  = magnetic susceptibility

$H$  = magnitude of the magnetic intensity.

With the above assumptions, the relation for the magnetic field strength and the magnetic field intensity can be written as

$$B = \mu_0 (1 + \chi) H \quad (3)$$

The measured magnetic parameters for the MAPO experiment included the magnetic field strength  $B$ , magnetic field direction, and the ferromagnetic solution magnetic susceptibility  $\chi$ . These values were used in equation (2) to compute the magnetic force on the fluid throughout the volume of the MAPO test tank.

### 3.2 Model Description

The CFD code selected for this project is a commercially available product called CFX-4 distributed by AEA Technology. This three-dimensional code contains a solver for predicting laminar and turbulent flow and heat transfer. Additional models for multiphase flows, combustion, and particle transport are also included. The current MAPO model utilized the following CFX-4 options: surface tension model, incompressible, two phase (liquid/gas), laminar, isothermal, transient, and buoyant flow. The grid structure for the MAPO test tank analyses, shown in figure 7, consisted of five blocks with a total of 40,700 volumes. The grid is primarily uniform with some clustering near the walls of the tank.

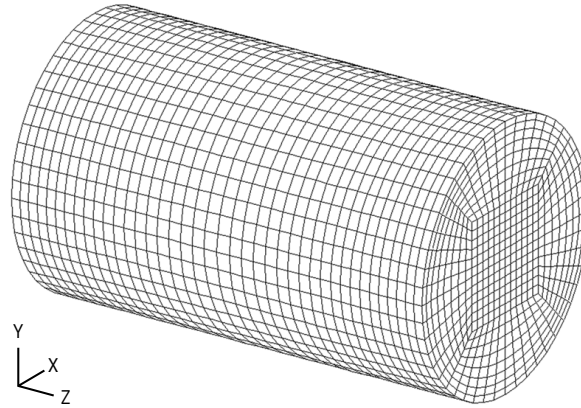


Figure 7. MAPO tank grid structure.

Exact free surface shapes for liquids in low-g have been developed by Myshkis et al.<sup>14</sup> Exact surface shapes were determined using Myshkis's method for a zero-g, axisymmetric, nonrotating cylinder with dimensions of 1 m high by 1 m diameter. Three fluid contact angles were selected, 0°, 20°, and 45° to benchmark the CFX-4 algorithms. A matrix of CFD cases was developed varying time-step size, grid spacing, surface sharpening algorithms, iterations per time step, and equation solvers. These cases were used to determine the most CPU-efficient CFX-4 code options to use while maintaining the highest possible surface shape accuracy for multiphase flow analysis. The predicted surface shapes with these CFX-4 options compare very well with the exact surface shapes, as illustrated in figure 8.

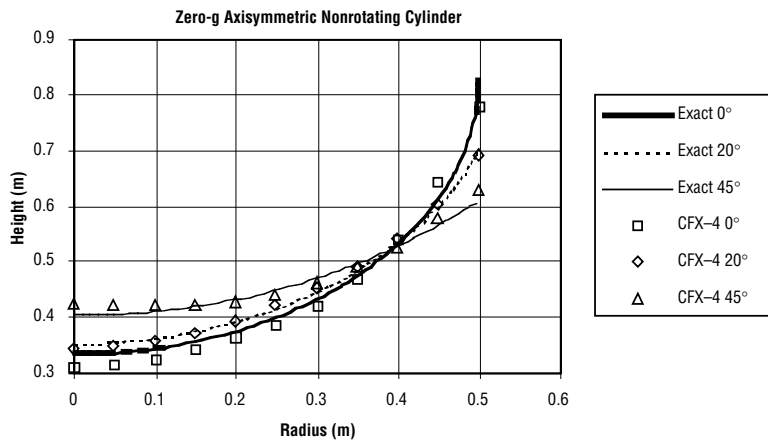


Figure 8. Surface shape comparison: Numerical and exact solutions.

An additional benchmark case was run using the MAPO tank and MAPO baseline test fluid (water with wetting agent). The fluid was initially settled at the 50-percent fill level at the beginning of the simulation. The predicted steady state surface level from the MAPO model under zero-g acceleration ( $g_x$ ,  $g_y$ , and  $g_z$ ) is compared with the exact surface level in figure 9. The CFX-4 MAPO model matches the exact liquid height solution (calculated by Myshkis's method) for the MAPO cylindrical test tank. This same CFX-4 MAPO model was also used for the two baseline water tests and produced excellent results.

The environmental influence due to the magnetic field was mapped over the computation space producing a constant force field applied to the fluid in the tank. The force magnitude was dependent on the fluid location inside the tank as well as the concentration of the ferromagnetic solution. The concentration of the ferromagnetic solution is assumed to be constant for any given test. However, different concentrations of ferromagnetic solution were used in the test program. The MAPO model includes programming for three ferromagnetic solution concentrations. The measured gravity level history, including perturbations, for each test case was input to the MAPO model. The MAPO model was used to simulate seven test cases employing the water-based ferromagnetic solution, producing very good results. The MAPO model also included programming for  $LO_2$  properties and was used to predict fluid motion with two initial fluid positions and three magnetic field strengths.

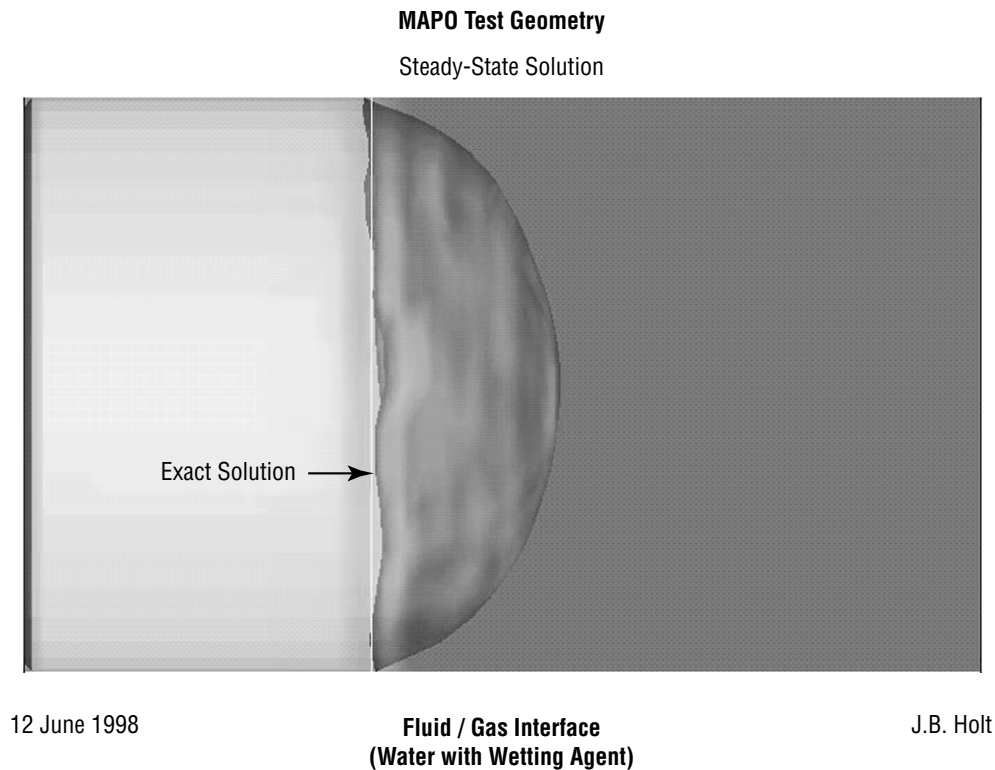


Figure 9. Surface shape benchmark for MAPO tank.

## 4. TEST RESULTS

### 4.1 Test Matrix

A total of 111 low-g float tests were performed during the three test days aboard the KC-135. After reviewing the video and accelerometer data, nine tests, listed in table 1, were selected as candidates to pursue further with computational modeling. The remaining tests were unacceptable due to shortness of float, agitation of fluid, poor visibility, or any combination of these problems. The transition and free-float intervals in the table refer to the time required to set the test package free in the low-g environment and the amount of time spent in free float before collision or capture, respectively. The video data offset column specifies the time difference between the video and computer clocks. The offset time must be subtracted from the video clock to synchronize it with the accelerometer data recorded by the computer.

Table 1. Selected MAPO tests.

Test No.	Mixture Ratio	Tank Position*	Transition Interval** (sec)	Free-Float Interval (sec)	Video/Data Offset*** (sec)
5	Water	TUR	3.5–14.5	14.5–20	1
23	Water	TOS	4–16	16–25	1
30	133:1	TUR	0–6	6–12.5	1
48	30:1	TUR	0–9.5	9.5–21	0
59	30:1	TOS	0–11	11–23	0
74	30:1	TUD	4.5–13	13–27	0
90	10:1	TUR	2.5–13	13–22.5	1
97	10:1	TOS	1.5–10	10–25	1
106	10:1	TUD	4–11	11–18.5	0

\*Tank position: Tank upright (TUR), tank on side (TOS), and tank upside down (TUD).

\*\*Transition includes release and handling/guiding of test package prior to low-g free float.

\*\*\*Time sync. error between video and accelerometers: Video time–Offset = Accelerometer data time.

### 4.2 Acceleration Axes and Data Histories

A three-axis accelerometer was mounted on the test package and hooked into the computer which sampled data at a rate of 128 Hz. These axes are fixed, as illustrated in figure 10, with the positive  $x$  directed toward the video camera, the positive  $y$  out the left side of the test tank, and the positive  $z$  out the bottom of the test tank (where the magnet is permanently positioned).

The acceleration data were then smoothed posttest using a 32-point centered average producing the “four samples per second” data listed for each test in appendix D. These listed data include both a raw  $g$ -level and a corrected  $g$ -level adjusted for an average accelerometer bias. The magnitude of this

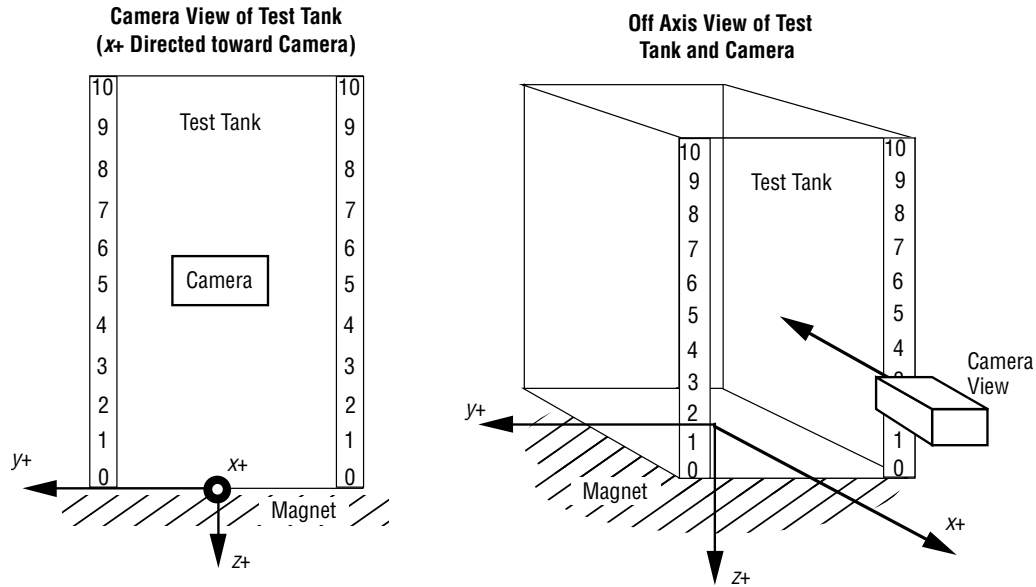


Figure 10. MAPO acceleration axes.

bias was calculated by averaging accelerometer data over a small time interval when the package was completely free floating (not being touched or bumped). Also, due to gain limitations in the computer data acquisition setup, there was minimal resolution of the accelerometer output below the one milli-g range and was assumed as zero below this point for modeling purposes. In all cases, the corrected values for g-level were used in all computational simulations. Figure 11 shows the typical g-levels recorded on each axis for a free-float test (these data taken from test 90). These figures illustrate the dramatic dropoff from the high 1.5+ g's experienced during aircraft pullout, down to one milli-g range during the low-g parabola. Minor bumps can be seen at approximately 8 and 13 sec followed by a clean interval extending out to 22 sec, at which time a major bump was encountered. The g-level then picked back up at 27 sec as the aircraft began its pullout to set up for the next parabola.

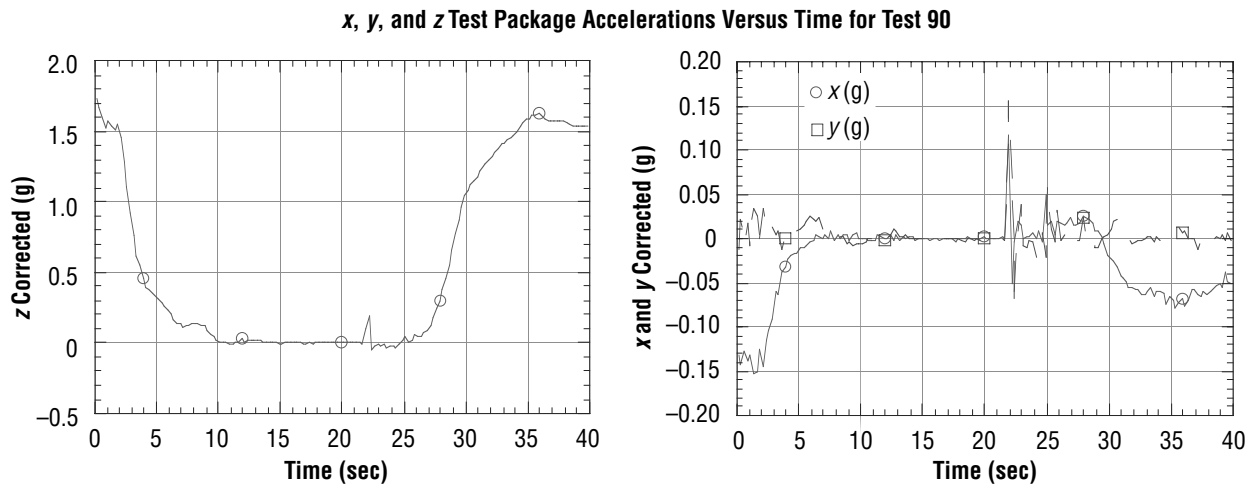


Figure 11. Typical test acceleration profiles.

### 4.3 Experimental and Model Results

The video and accelerometer data recorded during flight testing were transferred to the computer for processing so that it could be compared to the predictions from the CFD model. Nine computational simulations were performed examining tests 5, 23, 30, 48, 59, 74, 90, 97, and 106. To maximize the video camera's field of view, the camera was mounted sideways, giving the appearance that the test tank was laying on its side. For tests 5, 30, 48, and 90 the test package was placed with the tank upright (tank bottom against the aircraft floor) which shows the fluid initially settled to the right side of the image. On tests 23, 59, and 97 the test package was oriented so that the tank was on its side (tank side against the aircraft floor), which shows the fluid initially settled to the bottom of the image. Tests 74 and 106 both required the test package to be placed upside down (tank top against the aircraft floor), this shows the fluid initially settled to the left of the image.

The ferromagnetic solution used in tests 30 through 106 was very dark and had the undesired quality of opaquely coating the tank walls when agitated, obscuring subsequent fluid motion. As a result, the experiment video data were good visually up to the point where a slosh wave was generated. This condition placed critical importance on how the test package was released and handled during the transition into the low-g free-float environment. Once the aircraft began to pull out and standard gravity returned, the fluid would quickly settle, clearing the tank walls in preparation for the next test.

Two baseline water tests were performed showing the motion of a nonmagnetic fluid (water) in the presence of a magnetic field. These tests, 5 and 23, are illustrated in the image sequences depicted in figures 12 and 13, respectively. As expected, both tests show no tendency for the water to be attracted toward the magnet; however, they provided an excellent demonstration of the CFX-4 code's ability to model the basic motion of the liquid and its vapor interface. In test 5 (image sequence in fig. 12) the tank was placed upright as an initial condition, settling the water on the bottom against the magnet as shown in the image frame at 2 sec. The test package was released and guided into the free-float environment as the aircraft completed its high-g pullout and pushed over, creating the low-g flight path (parabola). Once free float began, small touches were required to center the package, introducing fluid slosh visible in image frames at 12.5 and 14 sec. This transition to low-g was completed at 14.5 sec followed by  $\approx 5.5$  sec of uninterrupted float time. During this float, the water completely surrounded the air space, forming a rippling bubble shown in the image frames at 15.5 and 18.5 sec. This tendency toward a spherically shaped bubble was an expected response since surface tension forces dominate in the low-g environment (spherical shape represents the lowest energy surface condition). At 20 sec the test package was captured producing severe agitation and terminating the test run. The results of this test showed that the magnet had no effect on the water as expected. The CFD model results show excellent correspondence with the test data. The model captured the low-g transition with slosh wave and eventual encapsulation of the air space as a bubble.

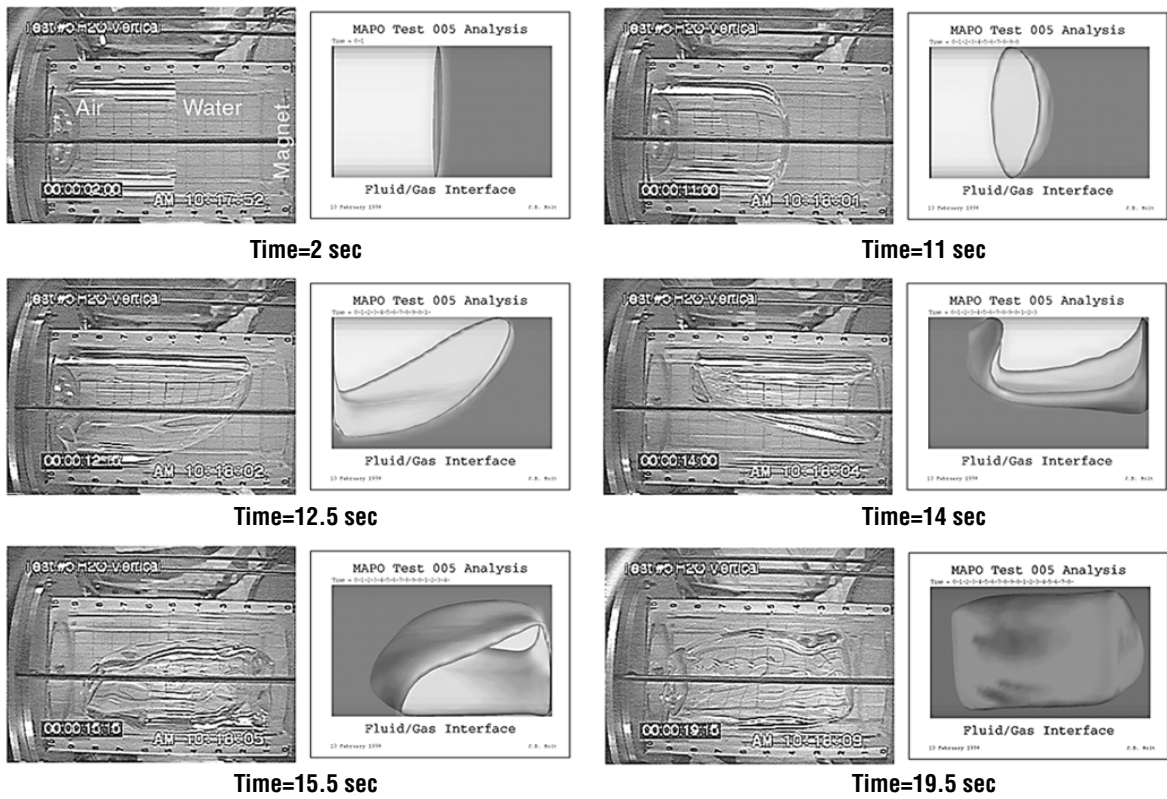


Figure 12. Baseline water test 5 image frames at 2, 11, 12.5, 14, 15.5, and 18.5 sec.

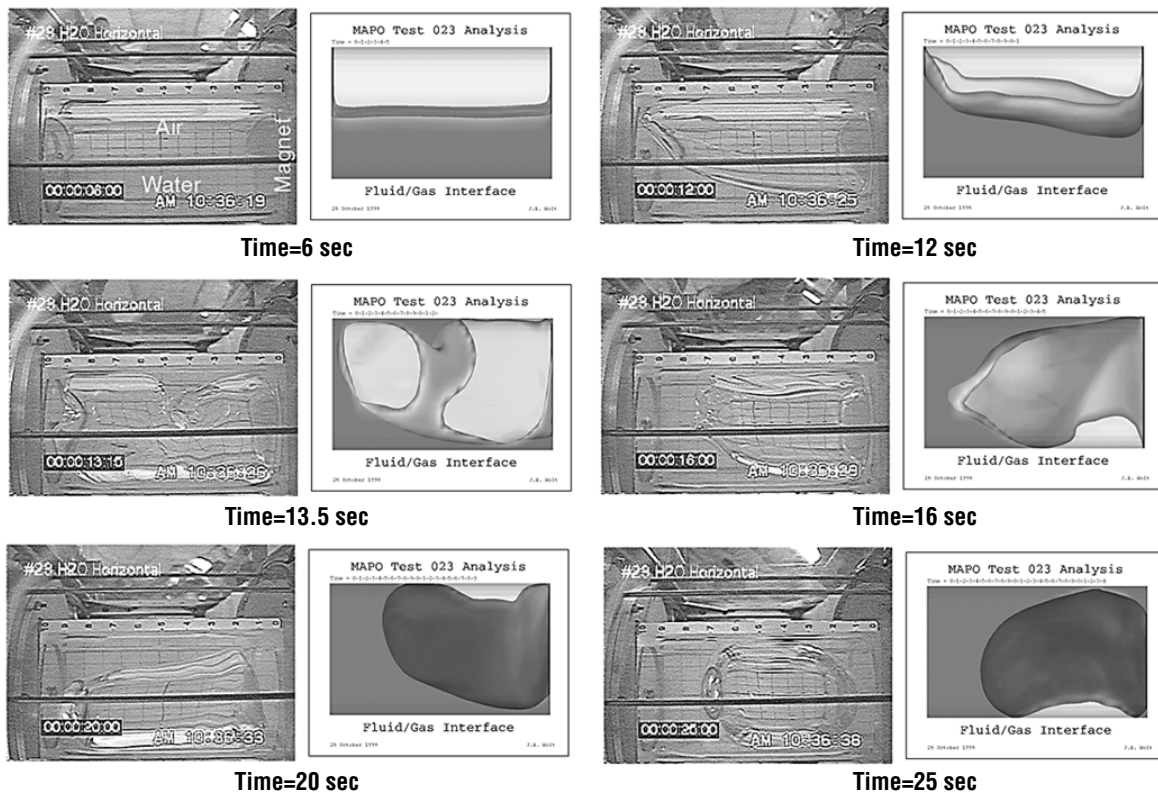


Figure 13. Baseline water test 23 image frames at 6, 12, 13.5, 16, 20, and 25 sec.

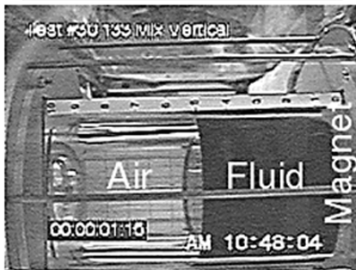
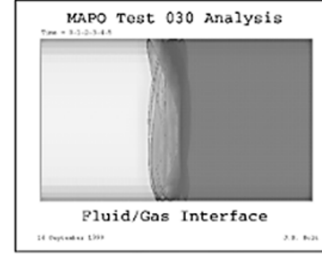
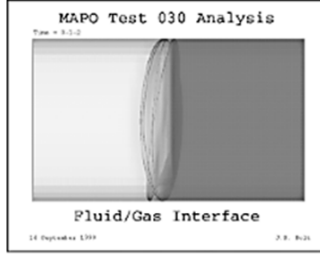
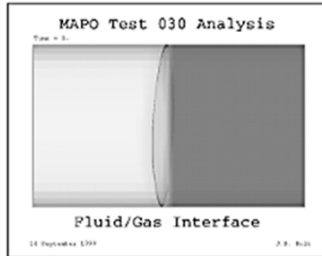
The image sequence for test 23, shown in figure 13, was the second baseline water test. The test tank was oriented on its side, producing a horizontal fluid surface as an initial condition, contacting both the bottom and top of the tank (the tank bottom and magnet are to the right in the image). The initial fluid vapor interface is barely visible, hidden behind a tank support rod, in the first image frame at 6 sec. The release and transition into the low-g environment was completed at  $\approx 16$  sec, introducing sloshing that is visible in the image frames at 12 and 13.5 sec. The uninterrupted low-g interval lasted 9 sec and is shown in the image frames at times 16, 20, and 25 sec. During this interval the air bubble achieves a nearly spherical shape with a position near the bottom of the tank. Again, this was an expected response and similar to the motion observed in baseline test 5. At 25.5 sec the test package was captured and the test run ended. As expected, the results of this test also show that the magnet had no effect on the water. The CFD results again show good correspondence with the fluid motion up to  $\approx 16$  sec. At this point the model prediction of the air bubble position deviated from that recorded in the test data (image frame at 20 sec). However, by the end of the simulation, 25 sec, the predicted air bubble was beginning to take on a spheroid shape positioned against the bottom of the tank.

Both water tests also served as a baseline in determining the accelerometer bias (offset) which would then be used in the computational models. Formation toward a sphere of the air bubble during the low-g period as seen in these tests resulted when the acceleration level is nearly zero-g (well below the magnitude recorded by the accelerometers due to instrument offset). Therefore, the difference in average recorded acceleration during this period and zero-g produce an approximate instrument bias. Bias values for all tests are listed in appendix D.

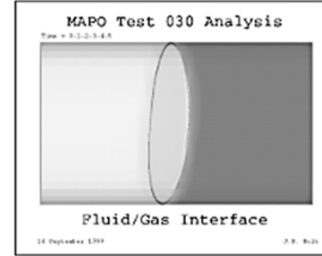
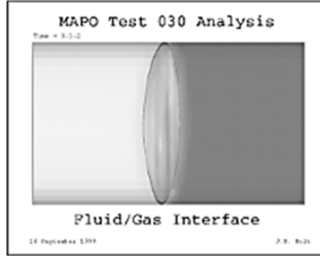
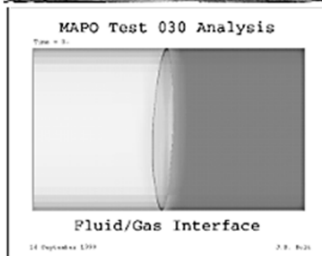
In test 30, illustrated in figure 14, the ferromagnetic material was added to the water, producing a mixture ratio of 133 parts water to 1 part ferromagnetic solution (133:1). The fluid mixture was given an initial settled condition against the bottom of the tank with the test package in an upright position, as can be seen in the image frame at 1.5 sec. The release and transition into the low-g environment proceeded smoothly for this test, producing only minor sloshing and was completed in  $\approx 6$  sec (shown in the image frames at 3 and 6 sec). The approximate duration of the low-g float interval was 6.5 sec as illustrated in the image frames at 8.5, 11, and 12.5 sec. The fluid sloshed slowly along the walls of the tank throughout the float interval; however, it remained well below the top of the tank, leaving a large portion of the air space clear. At  $\approx 13$  sec the test package was severely bumped, significantly agitating the fluid and effectively terminating the test.

The CFD model results for all tests involving ferromagnetic mixtures are displayed in two formats positioned above and below each experimental data image frame. The top CFD image represents the fluid-coated surface which tracks everywhere the fluid has been, providing a more realistic view of what the tank surface looks like after the sloshing fluid makes the walls opaque. The bottom CFD image represents the position of the bulk liquid and its vapor interface at the specific time. Overall, the model showed good correspondence with the experimental data. The predicted fluid surface shape agrees nicely with the test data up to the image frame at 8.5 sec, after which the fluid coating effect begins to obscure the motion of the test fluid. The model also predicts the fluid moving higher up the tank wall than what was shown in the test data in image frames at 8.5 and 11 sec. The model coated surface shape provided a fair representation of what was visible in the tank during the test interval.

Coated Surface



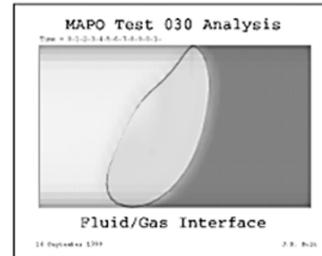
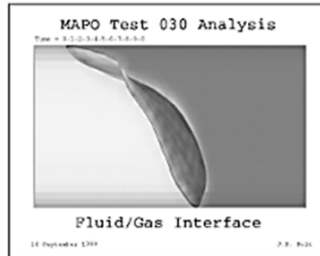
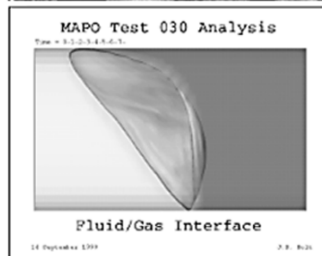
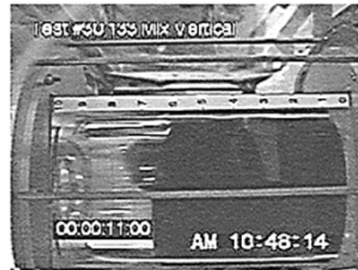
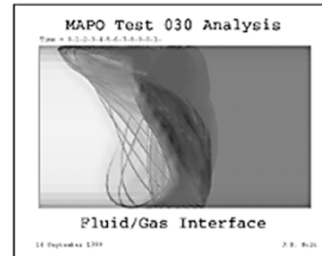
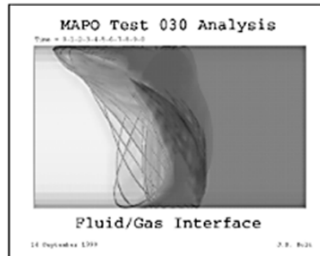
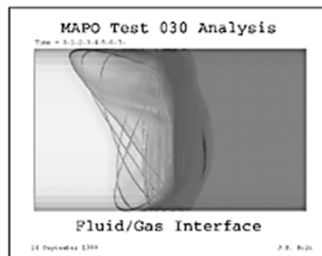
Fluid Surface



Time=1.5 sec

Time=3 sec

Time=6 sec



Time=8.5 sec

Time=11 sec

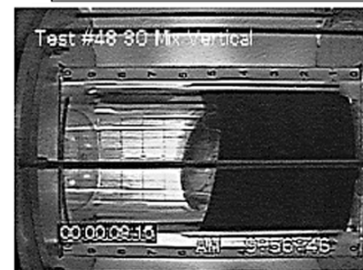
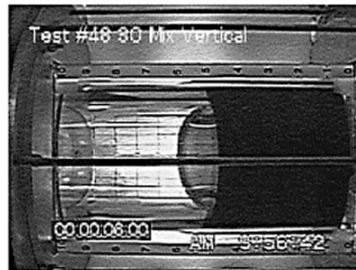
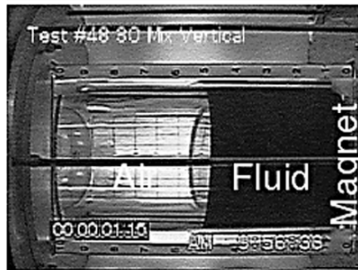
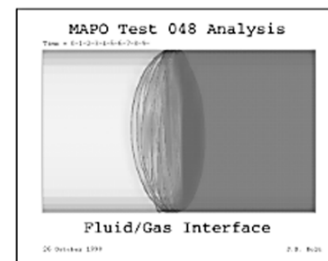
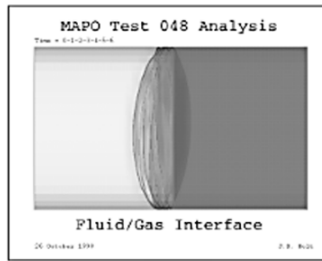
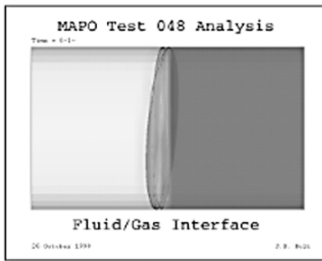
Time=12.5 sec

Figure 14. Mixture 133:1 test 30 image frames at 1.5, 3, 6, 8.5, 11, and 12.5 sec.

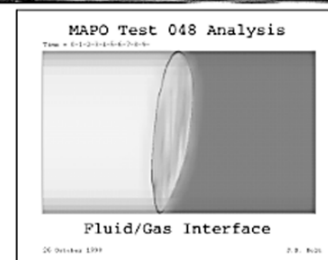
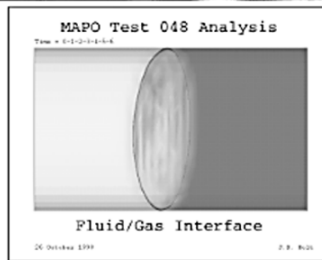
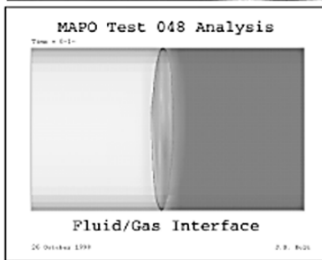
Test 48, shown in figure 15, employed a higher concentration of ferromagnetic solution to increase the magnetic influence on the fluid. The mixture ratio selected was 30 parts water to 1 part ferromagnetic solution (30:1). The test tank was initially positioned in an upright orientation with fluid settled against the bottom of the tank, shown in the image frame at 1.5 sec. Release and transition into the low-g environment were again performed smoothly and completed in 9.5 sec, shown in the image frames at 6 and 9.5 sec. The low-g float interval lasted  $\approx 11.5$  sec as illustrated in the image frames at 14, 18, and 21 sec. The fluid has a slight initial slosh (generated during the package release) which moved slowly back and forth along the tank walls, coating a portion of the tank surface. At 21.5 sec the test package was intercepted and the test concluded.

Results produced by the CFD model again show good correspondence with the test data and predicted that the fluid would remain settled against the bottom (magnet end) of the tank. The model fluid surface shape tracks the test data fairly well to the 14 sec image frame where the fluid coating effect begins to obscure the view of the fluid. It is noted that at 14 sec the model fluid surface prediction deviated from experimental data. The model shows the fluid climbing up more along the tank side wall rather than the back wall. The model coated surface sequence gave a good overall representation of what was visible in the test tank throughout the entire test interval.

Coated Surface



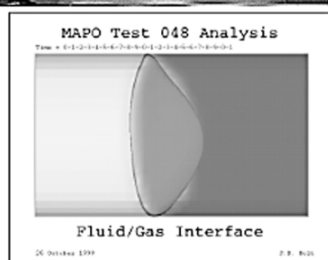
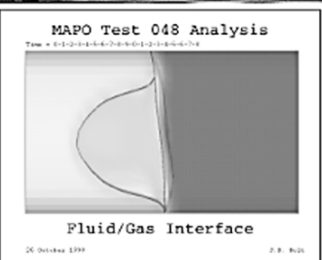
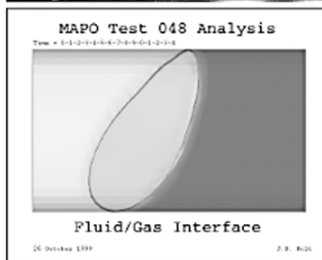
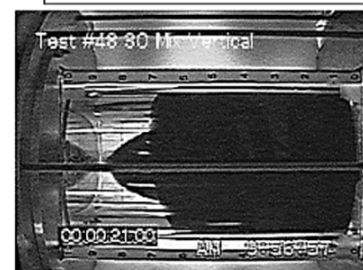
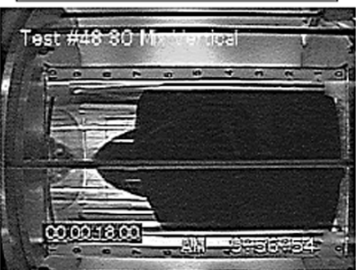
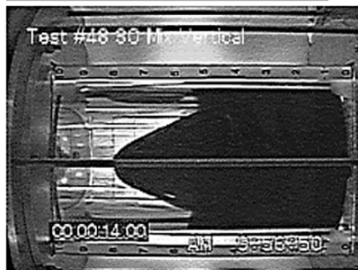
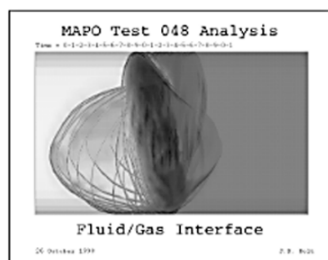
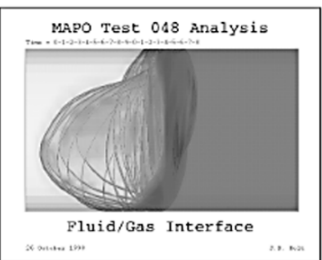
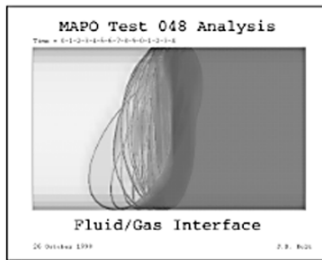
Fluid Surface



Time=1.5 sec

Time=6 sec

Time=9.5 sec



Time=14 sec

Time=18 sec

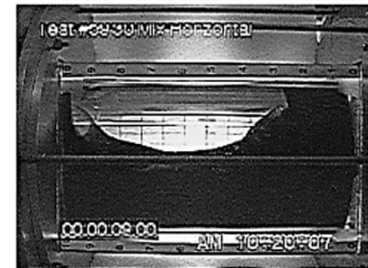
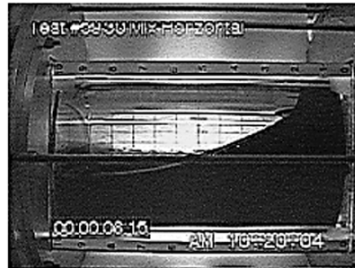
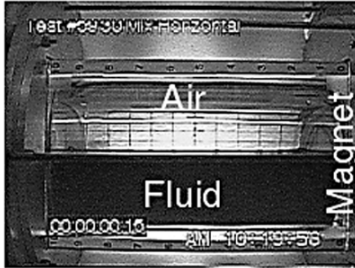
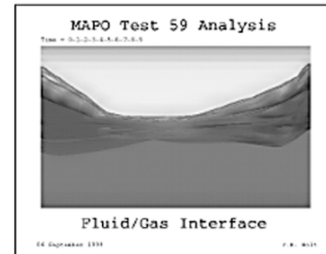
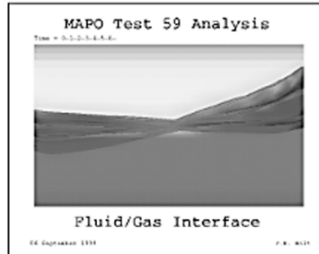
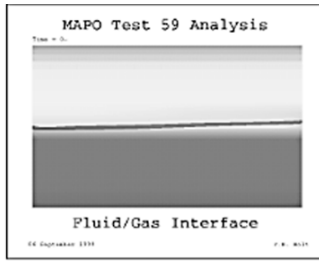
Time=21 sec

Figure 15. Mixture 30:1 test 48 image frames at 1.5, 6, 9.5, 14, 18, and 21 sec.

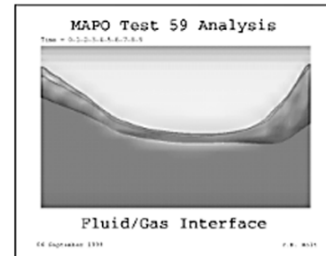
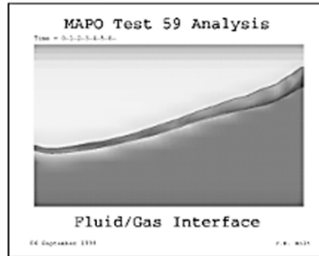
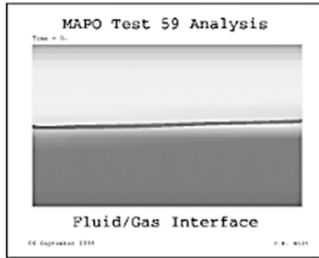
Test 59, illustrated in figure 16, was also performed with a water to ferromagnetic solution mixture ratio of 30:1. For this test, the tank was oriented on its side, creating a horizontal fluid interface contacting both the top and bottom ends of the tank as shown in the image frame at 0.5 sec. As expected, the fluid moved toward the bottom of the tank (magnet side) when the low-g environment was introduced. The release and transition into the low-g environment generated fluid slosh and was completed within  $\approx 11$  sec as shown in the image frames at 6.5 and 9 sec. The low-g float interval lasted  $\approx 12$  sec and is illustrated in the image frames at 13, 17, and 22 sec. The initial slosh moved slowly back and forth between the tank ends, coating almost the complete tank surface. However, a small region of the tank air space was left uncoated and visible, indicating that the fluid has moved toward the magnet end of the test tank. At 23.5 sec the test package was intercepted and the test concluded.

The CFD model shows excellent correspondence with the visible test data, predicting bulk fluid motion toward the magnet end of the tank where it settles. The model fluid surface shape tracks the test data very well to the 13-sec image frame where again the fluid coating effect begins to obscure the view. The model also predicts that as the bulk fluid settles, a small portion separates, remaining attached to the top end of the tank, caught in a corner where surface tension forces are large. The image sequence illustrated by the model coated surface shows excellent correspondence with the experimental data, capturing an evolution of the uncoated visible area in the tank air space almost identical to the pattern recorded in the test data.

Coated Surface



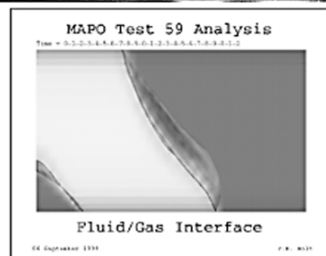
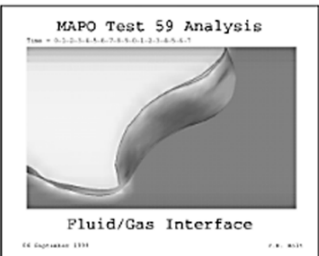
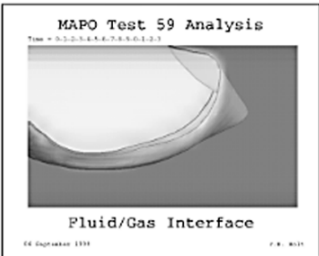
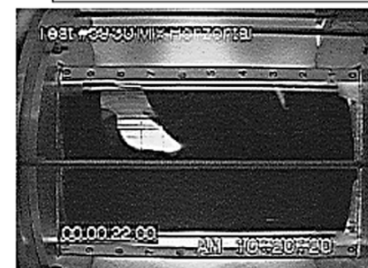
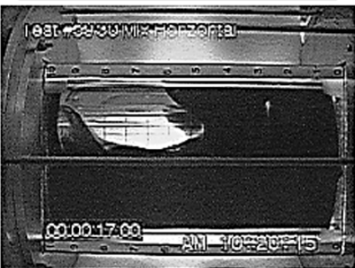
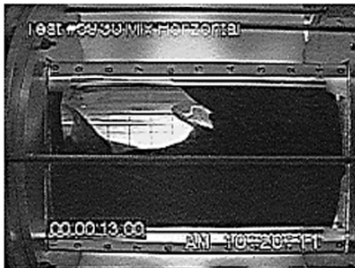
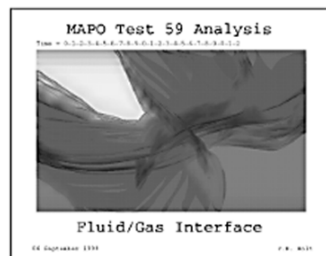
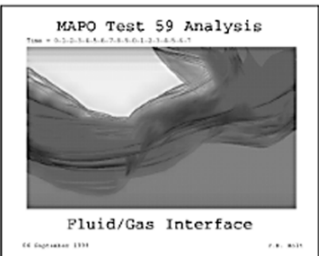
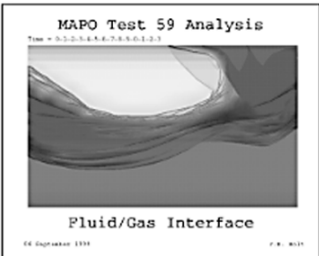
Fluid Surface



Time=0.5 sec

Time=6.5 sec

Time=9 sec



Time=13 sec

Time=17 sec

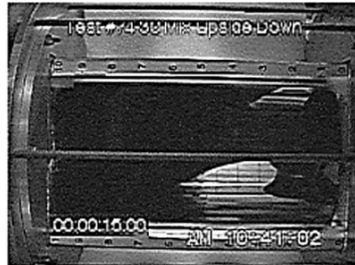
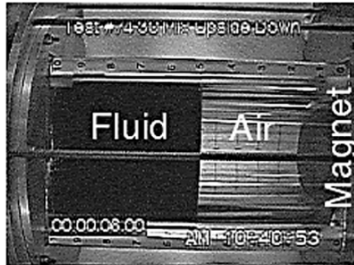
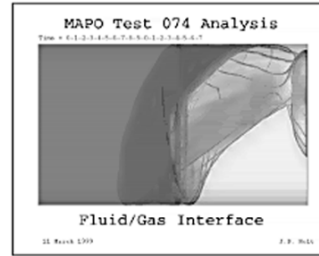
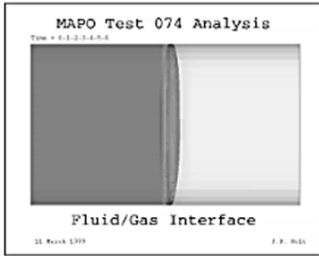
Time=22 sec

Figure 16. Mixture 30:1 test 59 image frames at 0.5, 6.5, 9, 13, 17, and 22.

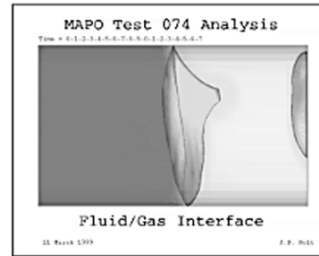
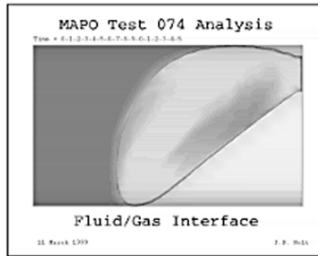
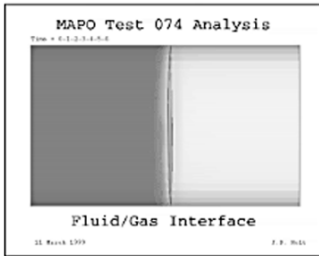
Figure 17 illustrates the results of test 74, also performed with a water to ferromagnetic solution mixture ratio of 30:1. For this test the tank was initially oriented upside down, positioning the fluid against the top of the tank, as shown in the image frame at 6 sec. The upside-down test was anticipated to be the most difficult due to the combination of slosh and magnetic attraction which would result in rapid coating of the tank walls obscuring fluid motion. The release and transition into the low-g environment generated some fluid slosh and was completed within  $\approx 13$  sec. The low-g float interval lasted  $\approx 14$  sec; however, it was interrupted at  $\approx 19.5$  sec with several bumps before resuming its free float. The first portion of this free float, illustrated in the image frames at 15 and 17 sec, shows the fluid slosh captured by the magnet and drawn down the tank wall where it begins pooling on the bottom. The bump was then encountered at 19.5 sec, depicted in the image frame at 20 sec which shows the tank walls completely coated, eliminating further visibility into the tank. The remaining portion of the free float, illustrated by image frames at 23 and 26.5 sec, lasted  $\approx 7.5$  sec. At 27 sec the test package was intercepted and the test concluded.

The CFD results show good correspondence with the visible test data up to  $\approx 16$  sec, at which point the fluid coating effect begins to obscure the view. The model predicts the fluid pulling back toward the top of the tank in the image frame at 17 sec, leaving a small amount of fluid on the tank bottom just prior to the bump (at 20 sec). Overall the CFD model tends to lag the fluid response recorded in the experiment data. This was evident in the coated surface image sequence where the experimental data shows the tank walls being coated before the model does. After the bump (and free float reestablished), the model predicts that the magnet attracts the fluid toward the tank bottom, as illustrated in the image frames at 23 and 26.5 sec. However, this could not be visually verified.

Coated Surface



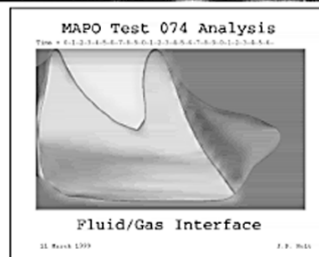
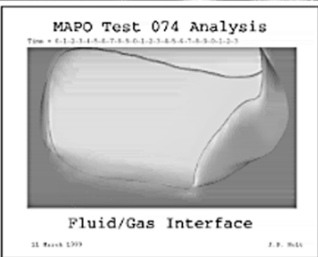
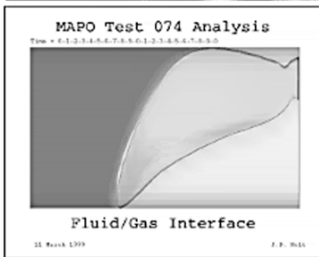
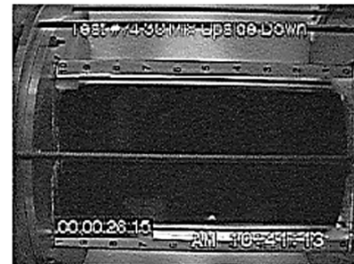
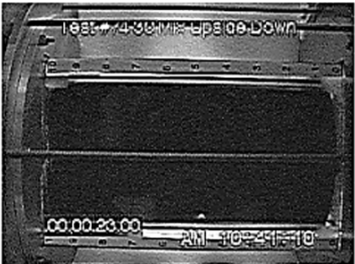
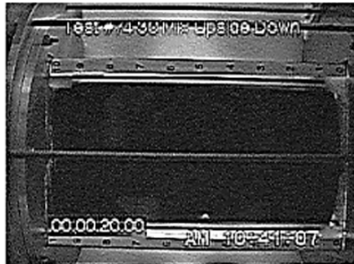
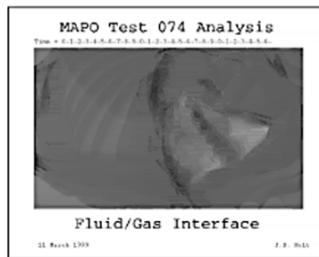
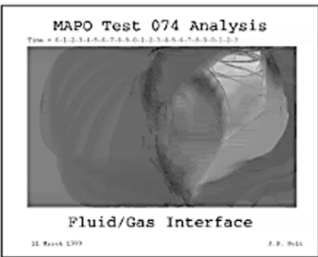
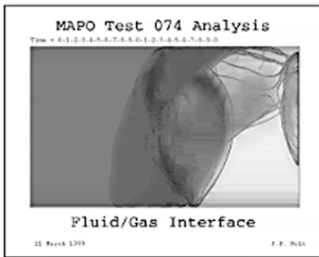
Fluid Surface



Time=6 sec

Time=15 sec

Time=17 sec



Time=20 sec

Time=23 sec

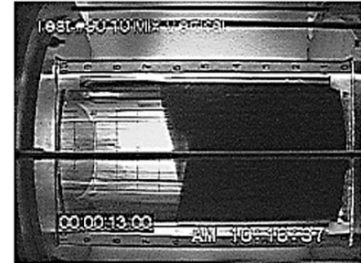
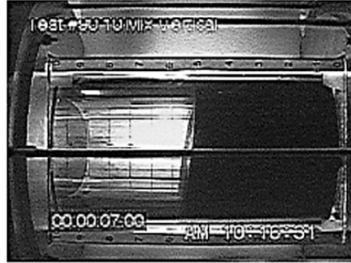
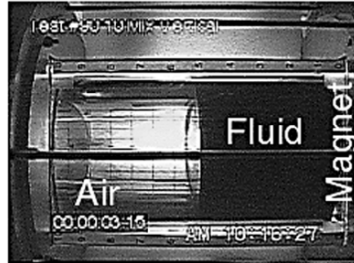
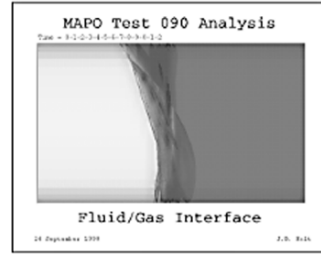
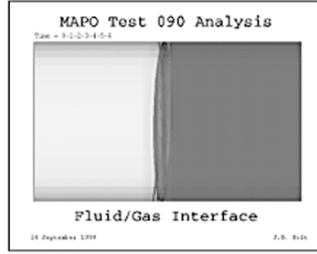
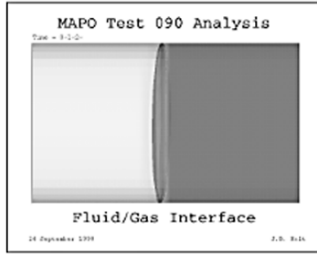
Time=26.5 sec

Figure 17. Mixture 30:1 test 74 image frames at 6, 15, 17, 20, 23 and 26.5 sec.

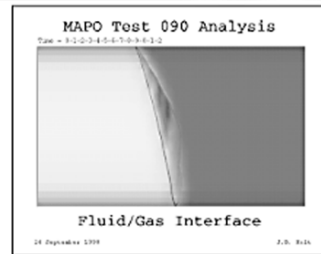
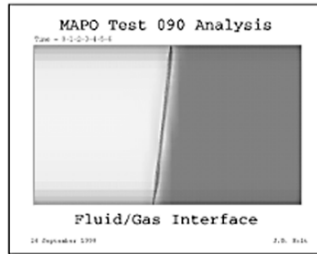
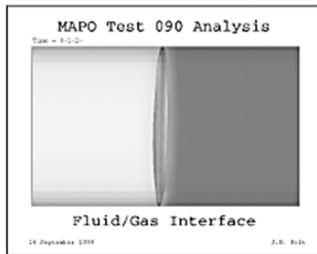
For test 90, the fluid magnetic strength was increased to its maximum level by adding additional ferromagnetic material which produced a mixture ratio of 10:1. This test is illustrated in the image sequence in figure 18 with the test tank placed in an upright position. This initial condition placed the fluid against the bottom (magnet) side of the tank as shown in the image frame at 3.5 sec. During the release and transition into the low-g environment ( $\approx 13$  sec), the package was agitated, producing some fluid slosh shown in the image frames at 7 and 13 sec. This wave moved slowly along the tank wall and penetrated the air space to a very limited extent as is illustrated by the free-float image frames taken at 16, 19, and 22.5 sec. The total low-g free float lasted  $\approx 9.5$  sec and was concluded at 22.5 sec when the test package was captured. During this test run, the fluid remained settled and nearly the entire tank wall (in the air space) was left uncoated.

The results produced by the CFD model showed excellent correspondence with the experimental test data. The model fluid surface shape tracks the data very well throughout the entire test with the fluid surface nearly visible at all times, since there is insufficient slosh to significantly coat the tank walls. During the low-g float the model shows the fluid settled firmly against the bottom (magnet) side of the tank (image frames at 16, 19, and 22.5 sec). The coated surface sequence shows the slight agitation about the liquid vapor interface generated by sloshing with an uncoated pattern that agrees favorably with the experimental data.

Coated Surface



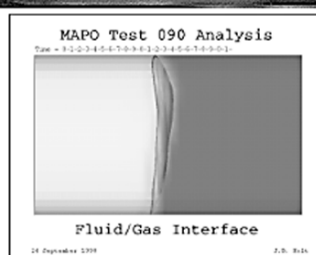
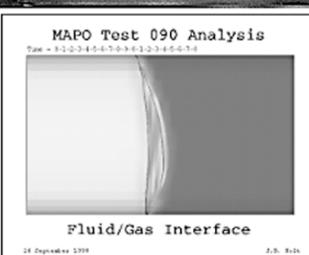
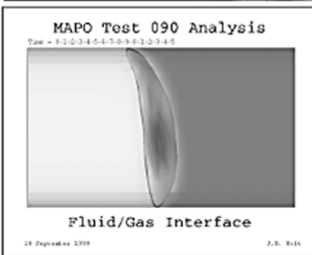
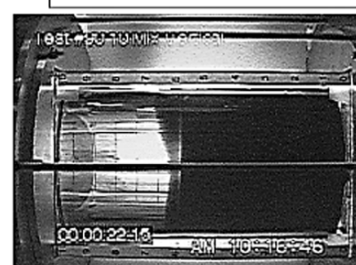
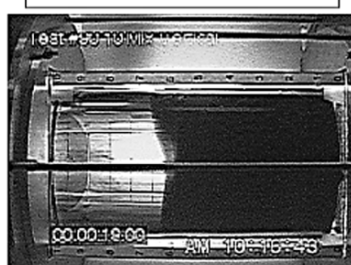
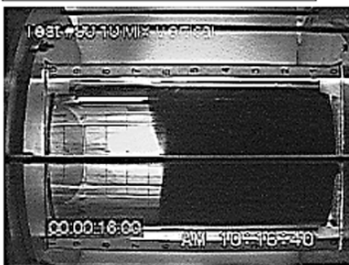
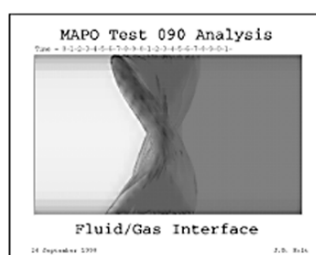
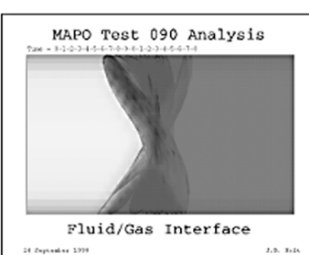
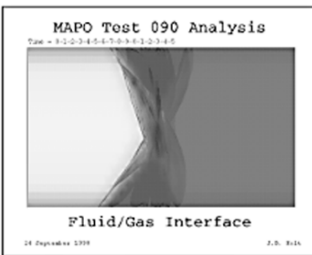
Fluid Surface



Time=3.5 sec

Time=7 sec

Time=13 sec



Time=16 sec

Time=19 sec

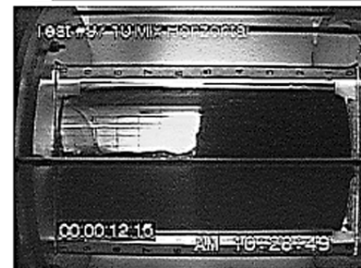
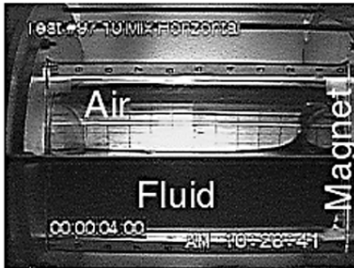
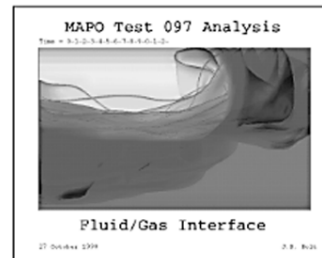
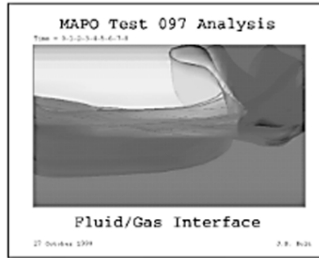
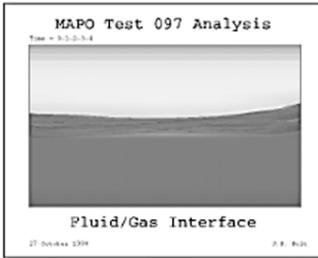
Time=22.5 sec

Figure 18. Mixture 10:1 test 90 image frames at 3.5, 7, 13, 16, 19, and 22.5 sec.

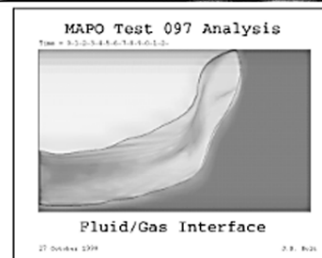
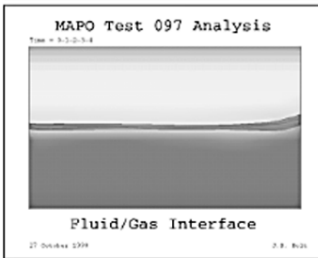
Figure 19 shows the results for test 97, which also used a water to ferromagnetic solution mixture ratio of 10:1. In this test the tank was oriented on its side, providing a horizontal fluid interface as the initial condition, shown in the image frame at 4 sec. The fluid moved very quickly toward the magnet (bottom of the tank) during the release and transition to low-g, as evident in the image frame at 8 sec. This transition period was completed at  $\approx 10$  sec and generated some fluid slosh. The low-g float interval lasted  $\approx 15$  sec as illustrated in the image frames at 12.5, 16.5, 20, and 25 sec. The slosh moved slowly between the tank ends, coating a portion of the tank surface in the region of the air space. However, a small portion of the tank air space was left uncoated, visibly indicating that the fluid had moved toward the magnet end of the test tank. At 25 sec, the test package was intercepted and the test concluded.

The CFD model shows excellent correspondence with the visible test data and predicts bulk fluid motion toward the magnet end of the tank where it pools. The model fluid surface shape tracks the test data well to the  $\approx 16$ -sec image frame where again the fluid coating effect obscures the view. The model shows that most of the fluid has settled by 25 sec with some fluid still left along the tank wall; however, this cannot be visually verified. The image sequence illustrated by the model coated surface also shows excellent correspondence with the experimental data.

Coated Surface



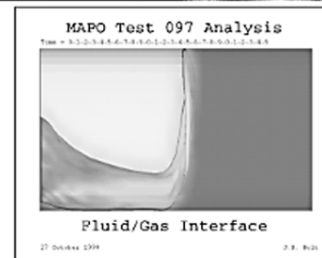
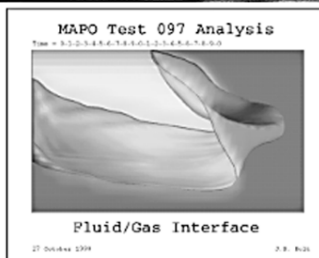
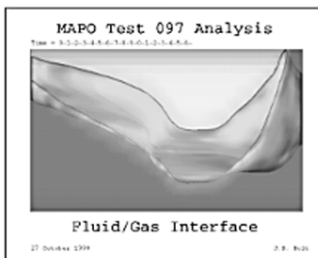
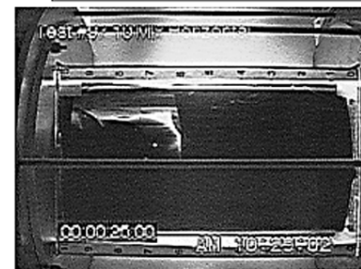
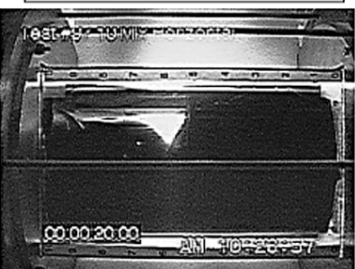
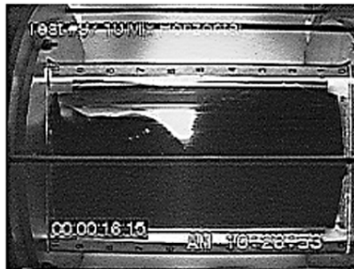
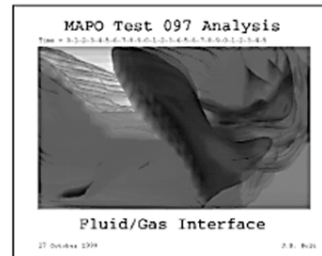
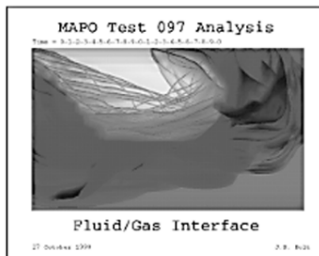
Fluid Surface



Time=4 sec

Time=8 sec

Time=12.5 sec



Time=16.5 sec

Time=20 sec

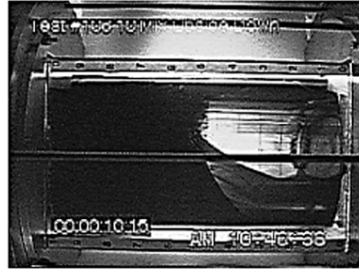
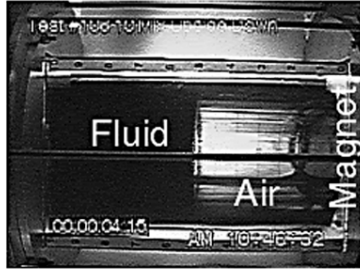
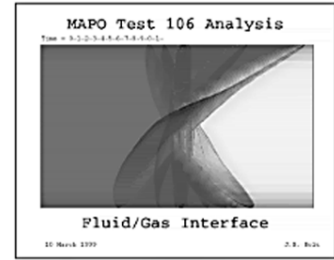
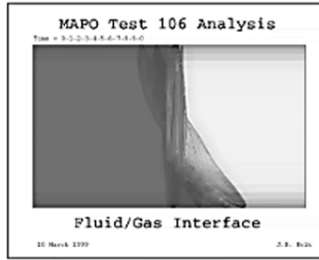
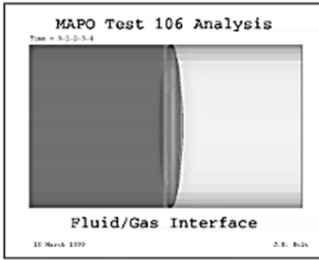
Time=25 sec

Figure 19. Mixture 10:1 test 97 image frames at 4, 8, 12.5, 16.5, 20, and 25 sec.

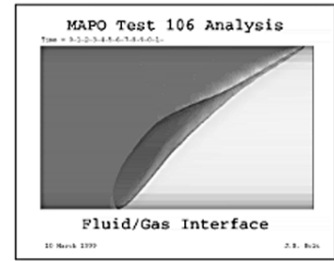
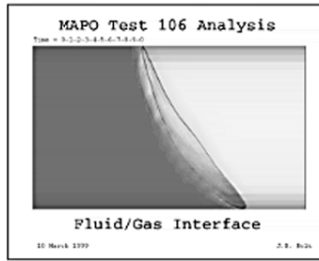
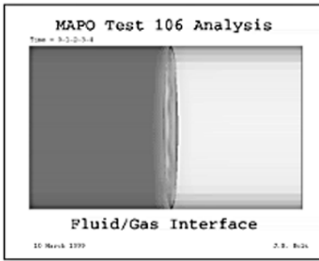
Figure 20 illustrates the results for test 106, also performed with a water to ferromagnetic solution mixture ratio of 10:1. The tank was initially placed upside down, positioning the fluid against the top of the tank, as shown in the image frame at 4.5 sec. Again the upside-down orientation was anticipated to be the most difficult since the slosh coupled with the magnetic attraction would tend to rapidly coat the tank walls, prohibiting observation. The release and transition into the low-g environment took  $\approx 11.5$  sec and generated some fluid agitation. The image frames at 10.5 and 12 sec show the back-and-forth motion of the fluid slosh and pooling on the bottom as the magnet captures the fluid. The low-g float interval lasted  $\approx 7$  sec, as illustrated in the image frames at 13.5, 16, and 18.5 sec. These image frames show the tank walls completely coated with fluid (which occurred at 13 sec), making direct observation impossible. At 19 sec, the test package was bumped, terminating the test.

For this test, like that in test 74, the CFD results tended to lag the motion that was recorded in the experiment. The slosh waves are shown in image frames at 10.5 and 12 sec; however, these results do not predict the fluid touching or pooling on the tank bottom to the extent of the experimental data. The model predictions for the free-float interval, image frames at 13.5, 16, and 18.5 sec, show some of the fluid being pulled along the wall and collecting at the bottom; however, there is no experimental data for verification. The model also predicted that a small portion of the tank wall remained clear and visible throughout the float, however this was not observed in the experimental results.

Coated Surface



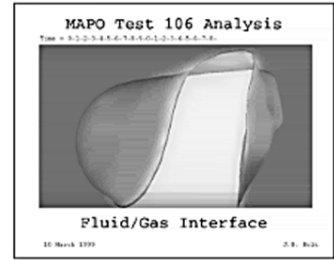
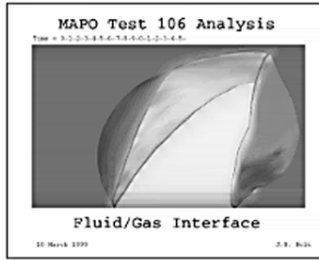
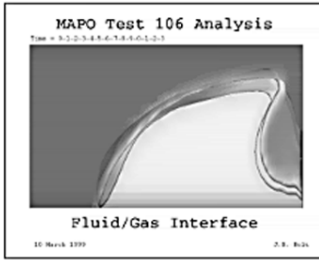
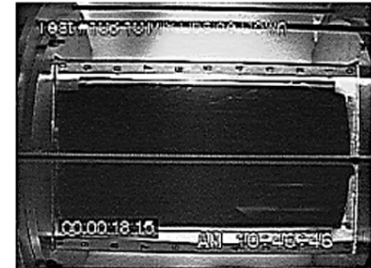
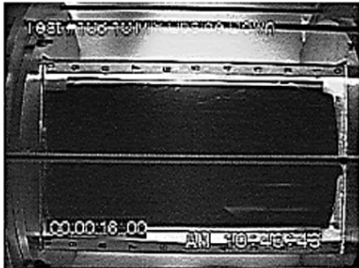
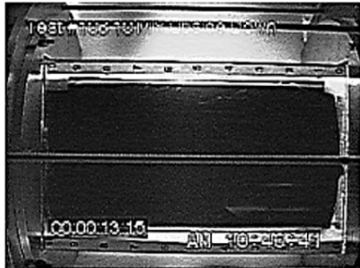
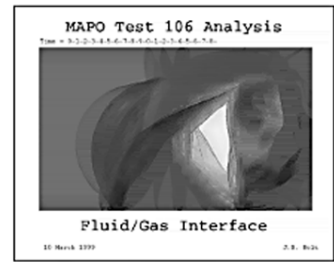
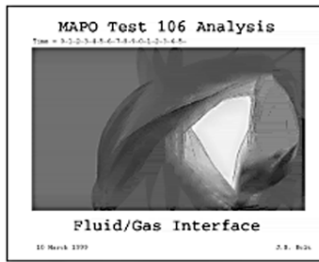
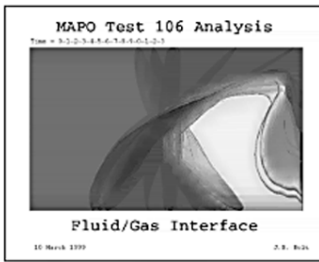
Fluid Surface



Time=4.5 sec

Time=10.5 sec

Time=12 sec



Time=13.5 sec

Time=16 sec

Time=18.5 sec

Figure 20. Mixture 10:1 test 106 image frames at 4.5, 10.5, 12, 13.5, 16, and 18.5 sec.

#### 4.4 Discussion

The results presented in section 4.3 showed that the CFD model was very successful in tracking the fluid motion across a range of test conditions. These initial tests have built confidence in the ability of the CFD model and its potential for use in modeling other fluids such as LO<sub>2</sub>. However, it was evident that the use of ferromagnetic solutions limited the quantity and quality of the data recorded because the solution would coat the tank walls, prohibiting continuous and precise viewing of the fluid motion. Also, the test environment aboard the KC-135 was highly variable, full of unpredictable movements and vibrations resulting in significant agitation during the package release phase, creating significant fluid slosh. Often the agitation was sufficient to coat the tank and effectively terminate the test before the low-g float even began. Because of this wide range of conditions imposed on the test package, it was useful to compare the relationship between the forces which acted on the test fluid. These forces included surface tension, acceleration, and magnetic attraction. The first of these relationships, the ratio of acceleration to surface tension forces, is characterized by the bond number ( $Bo$ )<sup>15</sup> and can be written as

$$Bo = \rho R^2 a / \sigma \quad , \quad (4)$$

where

- $\rho$  = fluid density
- $R$  = tank radius
- $a$  = acceleration
- $\sigma$  = fluid surface tension.

Using the fluid properties for the ferromagnetic solution, the  $Bo$  was calculated for a range of accelerations, as plotted in figure 21. For the ferromagnetic mixture test cases performed, the acceleration ratio or “g level” during the free-float portion of the test ranged from  $\approx 2.6 \times 10^{-5} g$  to 0.001 g, corresponding to  $Bo$ 's of 0.04 and 1.5, respectively. This range of  $Bo$  was sufficiently low, indicating surface tension to be the dominant controlling factor (not acceleration) for the nine tests examined. Again, these low  $Bo$ 's only apply to the low-g float period of the test and not during the lift-off, transition, and capture when the local accelerations are large and nonuniform. The large accelerations introduced fluid motion in the form of slosh that persisted into the low-g (low  $Bo$ ) float interval and shortened many tests by coating the tank walls preventing visibility. A calculation was made for LO<sub>2</sub>, also plotted in figure 21, which shows that the  $Bo$  would be higher when tested in the same free-floating environment. LO<sub>2</sub> has a higher density and lower surface tension as compared to the ferromagnetic mixture, hence the  $Bo$  values ranged from 0.1 to 6, indicating that acceleration would play a more significant role.

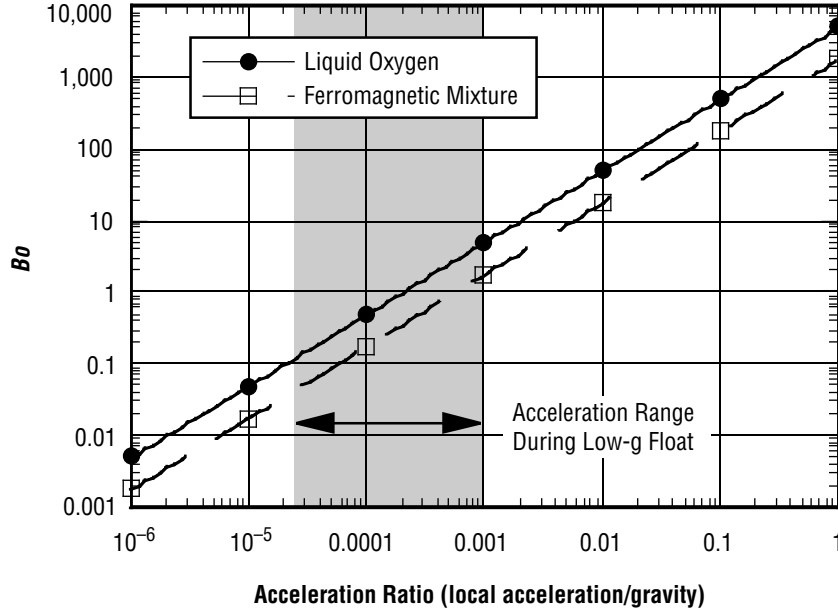


Figure 21.  $B_o$  for  $LO_2$  and ferromagnetic solution.

The traditional  $B_o$ , described above, provided a means of estimating when local acceleration forces are low enough that surface tension would dominate. This condition was clearly satisfied for the tests performed, as seen in the nonmagnetic water tests 5 and 23 described in the previous section. The second relationship of interest is the ratio of magnetic body force (exerted on a volume of fluid) to its surface tension and is termed the magnetic bond number ( $B_{omag}$ ). The expression for the magnetic body force on a volume basis can be written as follows (simplified for the magnetic field gradient along the length of the tank)

$$F_m = \mu_o \chi H dH/dl \quad , \quad (5)$$

- $\mu_o$  = permeability of free space
- $\chi$  = magnetic susceptibility
- $H$  = magnetic intensity
- $dH/dl$  = Gradient of magnetic intensity along tank length.

Formulating the  $B_{omag}$  in a fashion similar to the  $B_o$  results in the following expression,

$$B_{omag} = (\mu_o \chi H dH/dl) R^2 / \sigma \quad . \quad (6)$$

It is obvious from this expression that as the magnetic field varies throughout the tank, so does the  $B_{omag}$  with the highest value of  $B_{omag}$  near the magnet. Therefore, a situation can exist where magnetic forces dominate near the magnet, and surface tension dominates far from the magnet. Figure 22 illustrates the  $B_{omag}$  values for each of the three ferromagnetic mixture ratios (10:1, 30:1, and 133:1) tested. The figure also includes horizontal lines representing various gravity levels at corresponding  $B_o$ 's.

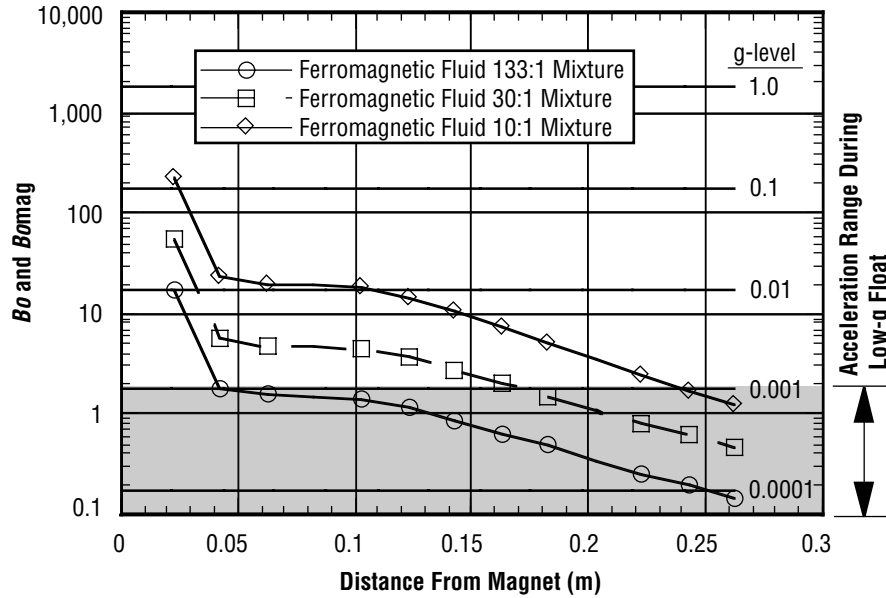


Figure 22.  $Bo$  and  $Bomag$  for ferromagnetic solutions.

This family of curves in figure 22 illustrates the various mixture ratios that were selected in an attempt to cover a wide range of  $Bomag$  without knowing precisely what level of acceleration would be achieved during the free float. The values of  $Bomag$  varied significantly across the tank, ranging from 20 to 0.15 for the 133:1 mixture, 50 to 0.5 for the 30:1 mixture, and 200 to 1 for the 10:1 mixture. Figure 22 also shows that high concentration ratios would tend to be more stable against variations in acceleration and provide a larger range of fluid motion. For test 30 (ratio of 133:1) the  $Bomag$  ranged from nearly unity at the liquid vapor interface to 20 near the magnet. This resulted in a condition where the influence of all forces was approximately equal near the center of the tank and the magnetic forces dominated in the region near the magnet end of the tank. In tests 48, 59, and 74 (ratio of 30:1) the  $Bomag$  ranged from  $\approx 3$  at the tank center to 50 near the magnet. The effects of the magnetic attraction were plainly visible in test 59 (horizontal orientation) as the fluid was pulled up the bottom of the tank, accumulating against the magnet. With the upside-down condition, test 74, the  $Bomag$  at the end of the tank away from the magnet was 0.5, indicating that surface tension dominated. However, the fluid interface for this test experienced rapidly changing  $Bomag$  values (range of 3 to 50) as it moved toward the magnet. The fluid would move rapidly along the walls and would tend to coat the test tank very rapidly as was seen in the experimental data. Tests 90, 97, and 106 with the highest concentration ratio of 10:1 produced  $Bomag$  values of 200 near the magnet, 10 at the center of the tank, and approximately unity at the top of the tank. Test 97 (horizontal orientation) showed very clearly the attractive nature of the magnetic field which provided excellent settling. The upside-down case, test 106, behaved similar to that in test 74, but in an accelerated fashion. In test 106, the range of  $Bomag$  was large enough that during the transition period the fluid slosh was strongly attracted by the magnet, resulting in rapid coating of the tank wall, even before complete free float was established.

With the initial success of the CFD model, it was decided that a number of computational simulations with  $LO_2$  would be performed. Using the properties of  $LO_2$  and the same tank geometry (as used in the experimental testing), a family of curves similar to that for the ferromagnetic mixtures

was constructed as illustrated in figure 23. However, since the magnetic properties of  $\text{LO}_2$  could not be changed (like the ferromagnetic mixture ratio) the applied magnet field was varied. Values of 2 times ( $2\times$ ) and 6 times ( $6\times$ ) the baseline ( $1\times$ ) magnetic field were used to produce the family of curves illustrated.

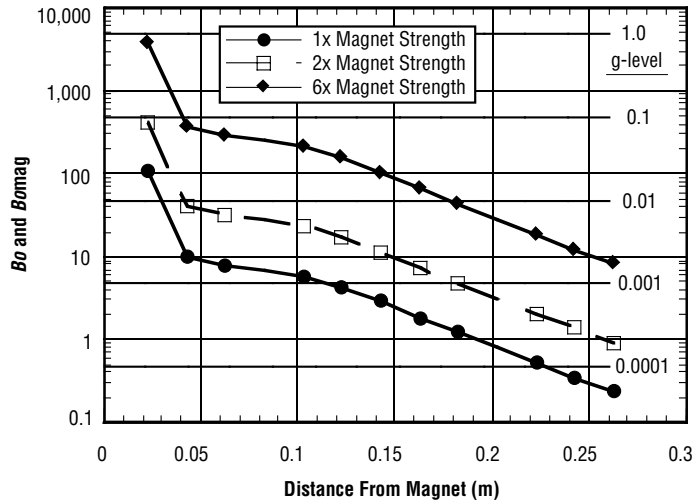


Figure 23.  $B_o$  and  $B_{omag}$  for  $\text{LO}_2$ .

In comparing the  $1\times$  or baseline case to the ferromagnetic solution curves in figure 22, the 30:1 mixture ratio approximates  $\text{LO}_2$  fairly well. Near the magnet (highest field) the  $\text{LO}_2$  has a  $B_{omag}$  value higher than the 30:1 mixture. At the center of the tank, the  $\text{LO}_2$  and 30:1 mixture have approximately the same  $B_{omag}$  and at the opposite side of the tank (lowest field) the  $\text{LO}_2$  has a  $B_{omag}$  value lower than the 30:1 mixture. This trend was expected since the magnetic susceptibility for the ferromagnetic mixture is not a constant but varies with applied magnetic field (see app. C). The additional curves for the  $2\times$  and  $6\times$  magnetic fields were used to assess the range of fluid motion achievable using stronger magnets. The approximate ranges of  $B_{omag}$  across the tank for the  $2\times$  and  $6\times$  cases were 400 to 1 and 3,700 to 10, respectively.

The CFD model, used in the ferromagnetic simulations, was then used to predict the motion of  $\text{LO}_2$  for each magnetic field strength using two initial fluid orientations. The first orientation assumed a zero-g initial condition which developed a surface tension dominant equilibrium state, where the liquid totally surrounded the vapor space, creating a bubble at the center of the tank. The results of this simulation are illustrated in the image sequence depicted in figure 24.

The magnet was “switched on” at the beginning of the simulation and the fluid position moved with time. For the baseline ( $1\times$ ) sequence, the fluid at the bottom of the tank (near the magnet) is pulled slightly as seen by the change in shape of the vapor bubble, which becomes more conical (loses its roundness) and elongates near the centerline of the tank. The vapor elongation results from the ring-shaped design of the magnet (a hole through the center) that creates a weaker field at the centerline of the tank. Hence, the fluid was pulled outward toward the bottom corners of the tank (stronger field region) and vapor is allowed to accumulate along the centerline. For the baseline magnet case, it is obvious that there is insufficient magnetic field strength to effect the fluid in the top third of the tank where the  $B_{omag}$  is  $\approx 2$  at the liquid vapor interface nearest the magnet. However, near the bottom (where the interface does move slightly) the range of  $B_{omag}$  is 6 to 10.

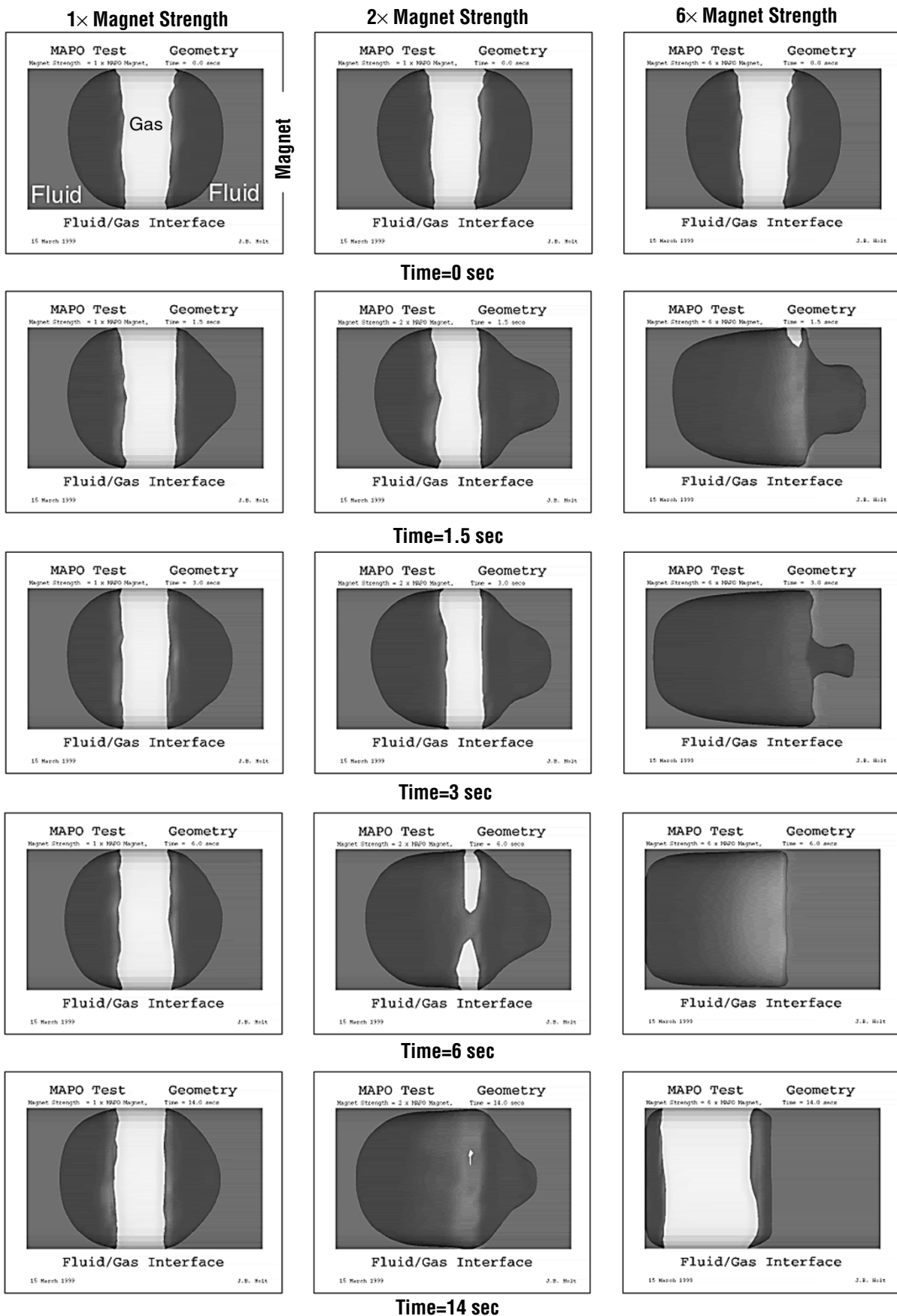


Figure 24. LO<sub>2</sub> motion simulation No. 1 for 1x, 2x, and 6x baseline magnetic field.

For the 2× baseline sequence, the motion of the spherical interface near the magnet is quite evident, with a *Bomag* range of 20 to 40. The vapor at the bottom of the tank again elongates along the centerline toward the magnet as fluid is pulled outward. The LO<sub>2</sub> at the top of the tank (*Bomag* of ≈7 at the liquid vapor interface nearest the magnet) is slowly pulled down along the tank walls until it meets the LO<sub>2</sub> in the bottom of the tank, as demonstrated in the image frame at 6 sec. Once connected, this bridge allows the fluid to flow slowly from the top region toward the magnet as illustrated in the image frame at 14 sec. As seen in this image frame, the spherical vapor interface near the top of the tank has moved upward (closer to the top of the tank) while the elongated vapor pocket at the centerline tends to flatten somewhat as fluid fills in the lower end of the tank. If additional simulation time were provided, it is anticipated that a majority of the fluid would be transferred to the magnet end of the test tank.

For the case with 6×, the baseline magnetic field strength, the LO<sub>2</sub> settling process is fairly rapid. The image frame at 1.5 sec shows that the LO<sub>2</sub> at the top has already flowed down along the tank walls and met the LO<sub>2</sub> in the bottom. The *Bomag* for the fluid in the top of the tank at the liquid vapor interface was ≈60. Within 6 sec the bulk of the fluid has been transferred from the upper region (LO<sub>2</sub> still coats the tank walls) and a nearly flat fluid interface established. At the conclusion of the simulation, 14-sec image frame, the transfer of fluid from the top of tank has been completed and the walls are clear. However, a small amount of LO<sub>2</sub> remains attached to the sharp corner formed between the tank wall and top cover. This was expected since surface tension forces would be quite large due to the small curvature around the perimeter.

A second LO<sub>2</sub> simulation was performed with an initial horizontal fluid condition (similar to that used during the tests) and the results are illustrated in figure 25. As with the previous simulation the magnet was “switched on” at time equal zero sec.

The same three levels of magnetic field were used, namely 1×, 2×, and 6× the baseline, each producing various degrees of fluid motion. As with the previous simulation, the 6× magnetic field rapidly settles the fluid against the bottom of the tank. This rapid movement results in a slosh wave moving back up the opposite wall toward the top of the tank, as seen in the image frames at 1.5 and 3 sec. The fluid surrounds the vapor space creating a short-lived bubble. By the end of the 14-sec simulation, essentially all the fluid (minus a small amount trapped in the top corner of the tank) has been settled firmly against the magnet. The 2× baseline case also generated a slosh wave during the settling process which traps the vapor space, as seen in the image frame at 6 sec. At the end of the simulation, this bubble has been pushed to the top of the tank with a majority of the LO<sub>2</sub> positioned against the bottom of the tank. If additional simulation time were allowed, it is expected that most of this fluid would be pulled along the walls toward the bottom, leaving only a small portion clinging to the corners on top. Comparing these 2× results to the first LO<sub>2</sub> simulation, shown in figure 24, the effect of the fluid bridge created by the horizontal orientation allowed, more LO<sub>2</sub> to be transferred to the magnet side of the tank during the simulation interval. This effect was expected since the bridge allows fluid to be freely entrained and not restricted by a creeping interface dominated by surface tension (as was the case in the first LO<sub>2</sub> simulation).

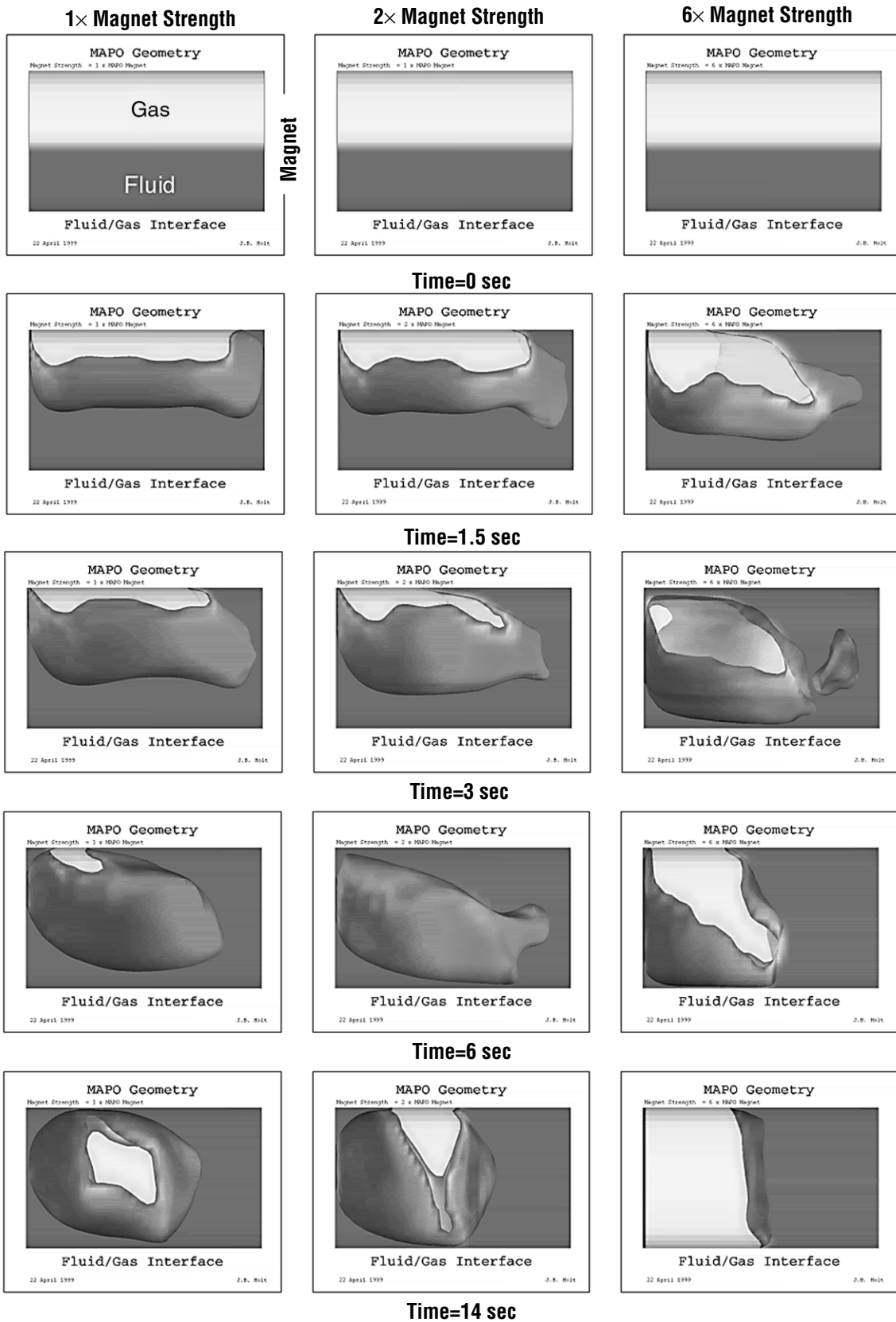


Figure 25.  $\text{LO}_2$  motion simulation No. 2 for 1x, 2x, and 6x baseline magnetic field.

The results for the horizontal 1× baseline simulation are very similar to those of the 2× case. The fluid surrounded the vapor space, trapping it, and creating a bubble that positioned itself against the top of the tank. With additional simulation time, some of the LO<sub>2</sub> would be pulled downward from around the bubble along the fluid bridge. However, due to the low value of  $B_{omag}$  at the top of the tank, this quantity would be small. Again, comparing these results to the 1× case shown in figure 24, the horizontal fluid bridge allowed for a significant transfer of fluid toward the magnet. This bridge was not present with the fluid in a detached configuration such as the first simulation where the magnet had no real effect.

Based on the results of these two LO<sub>2</sub> simulations, it appears that a larger amount of fluid motion and positioning can be achieved if a liquid bridge exists between regions of low and high magnetic field. This condition could greatly enhance the performance of existing liquid acquisition devices and channels which attempt to maintain fluid bridges (to tank outlets) through the use of surface tension. Strategic placement of small magnets within the liquid acquisition devices or tank could provide the necessary magnetic field gradients to keep these devices supplied with fluid, reducing potential for failure due to dry out or adverse accelerations.

## 5. CONCLUSIONS

The use of water-based ferromagnetic material and the KC-135 provided a good method for quickly obtaining low-cost, nonhazardous experimental data regarding the effect of magnetic fields on fluids. However, due to the dark opaque nature of the ferromagnetic mixture, fluid motion was many times obscured after the test tank walls became coated. Hence, considerable care was required in the handling and release techniques used to free float the test package. The combination of difficult fluid visualization and unpredictable aircraft motion required that a large number of tests be performed, from which only nine were acceptable for further investigation. This program should be viewed as a first step, and follow-on activities in paramagnetic fluid behavior should employ LO<sub>2</sub>, eliminating uncertainties associated with fluid visibility.

The CFD model (CFX-4 by AEA Technologies), modified to include magnetic body forces, performed very well overall in simulating the nine experimental tests. The model required no special case-by-case “tweaking” and was given input which included fluid properties, magnetic field distribution, and test package acceleration profile (with an assumed accelerometer cutoff of 0.001 g). The most difficult test cases to model were the upside-down orientation in which the fluid was attracted across the tank toward the magnet. The CFD model tended to lag the experimental data, potentially due to the more rapid fluid motion introduced by this orientation than with the water tests on which the time step for all CFD simulations was based. With the initial success of the CFD model, several simulations with LO<sub>2</sub> were performed for various magnetic field strengths and initial fluid orientations. These results showed that although the 1× baseline magnet was not strong enough to move the LO<sub>2</sub> from the opposite side, by doubling the magnetic field, the liquid could be resettled given sufficient time. Based on this result, a *Bomag* of ≈10 would be required to initiate and maintain LO<sub>2</sub> flow for settling in a zero-g environment. These simulations also showed that an alternative to an increased magnetic field is the creation of a fluid bridge between areas of low and high field strength. This bridge allows fluid to be pulled toward the magnet without the resistive effects of surface tension.

Based on this initial work, magnetic fields appear to provide a promising means of controlling fluids either independently or by augmenting existing propellant management hardware. The CFD model developed during this activity is a first step in this process, providing a means to evaluate the use of magnetic fields in conjunction with other fluids, hardware devices and tank geometries which more closely represent systems of interest. However, as a final verification of the CFD model’s ability, additional test data should be collected and analyzed using LO<sub>2</sub> as the test fluid.

## APPENDIX A—DETAILED DRAWING SET FOR TEST PACKAGE HARDWARE

Table 2 provides a list of drawings that were developed and used during the fabrication and assembly of the MAPO test hardware. Figures 26–37 show various MAPO components.

Table 2. Drawing list

Drawing Number	Drawing Description
SHT-1	MAPO assembly
SHT-2	MAPO frame layout
SHT-3	MAPO frame layout
SHT-3a	MAPO frame layout
SHT-4	MAPO test tank assembly
SHT-4a	MAPO test tank assembly
SHT-4b	MAPO test tank assembly
SHT-4c	MAPO test tank assembly
SHT-4d	MAPO test tank assembly
SHT-4e	MAPO test tank assembly
SHT-5	MAPO hand rail assembly
SHT-6	MAPO camera assembly

**Notes:**

- |  |  |       |     |       |     |       |     |        |       |         |       |
|--|--|-------|-----|-------|-----|-------|-----|--------|-------|---------|-------|
| <p>(1) MAPO test hardware secured to KC-135 aircraft floor using three cargo straps (two straps from side to side, one strap from front to back in flight direction). Cargo straps and related tie-down hardware provided by aircraft.</p> <p>(2) Package Envelope:   Width   16 in.<br/>                                           Height  16 in.<br/>                                           Length 47.5 in.<br/>                                           Weight 150 lb</p> | <p>(3) Torques (unlubricated in.-lb):</p> <table style="width: 100%; border: none;"> <tr> <td style="width: 50%;">No. 4</td> <td>3-4</td> </tr> <tr> <td>No. 6</td> <td>6-7</td> </tr> <tr> <td>No. 8</td> <td>8-9</td> </tr> <tr> <td>No. 10</td> <td>15-18</td> </tr> <tr> <td>No. 1/4</td> <td>40-42</td> </tr> </table> <p>(4) Tolerance <math>\pm 0.01</math></p> | No. 4 | 3-4 | No. 6 | 6-7 | No. 8 | 8-9 | No. 10 | 15-18 | No. 1/4 | 40-42 |
| No. 4  | 3-4  |       |     |       |     |       |     |        |       |         |       |
| No. 6  | 6-7  |       |     |       |     |       |     |        |       |         |       |
| No. 8  | 8-9  |       |     |       |     |       |     |        |       |         |       |
| No. 10   | 15-18  |       |     |       |     |       |     |        |       |         |       |
| No. 1/4  | 40-42  |       |     |       |     |       |     |        |       |         |       |

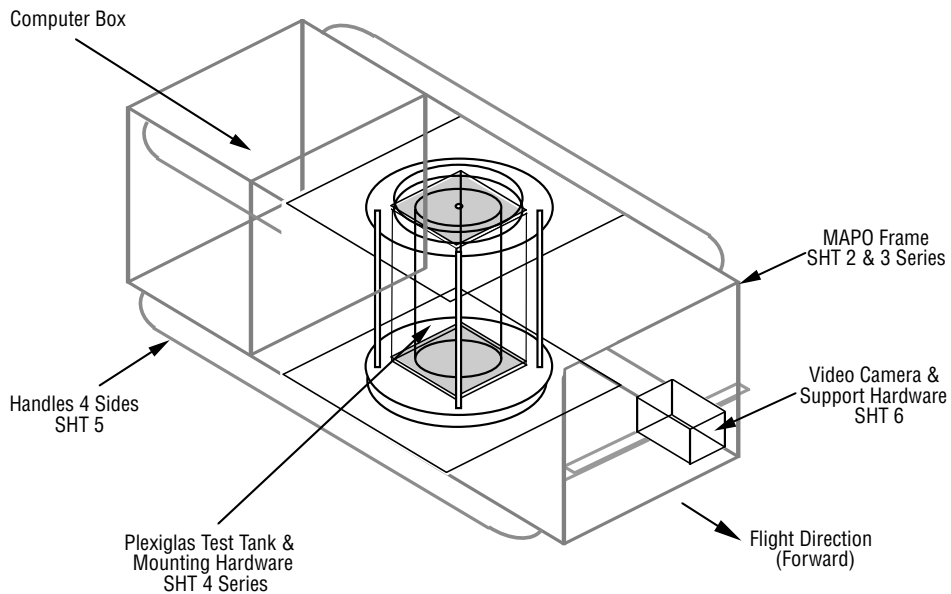
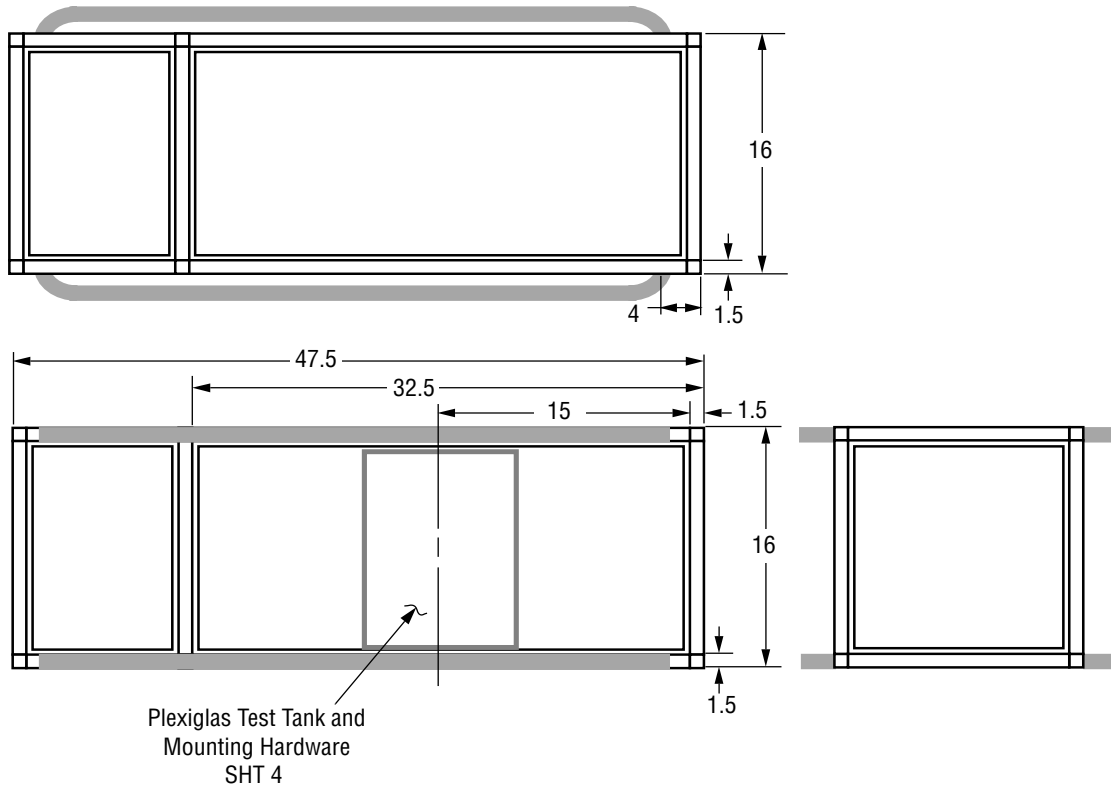
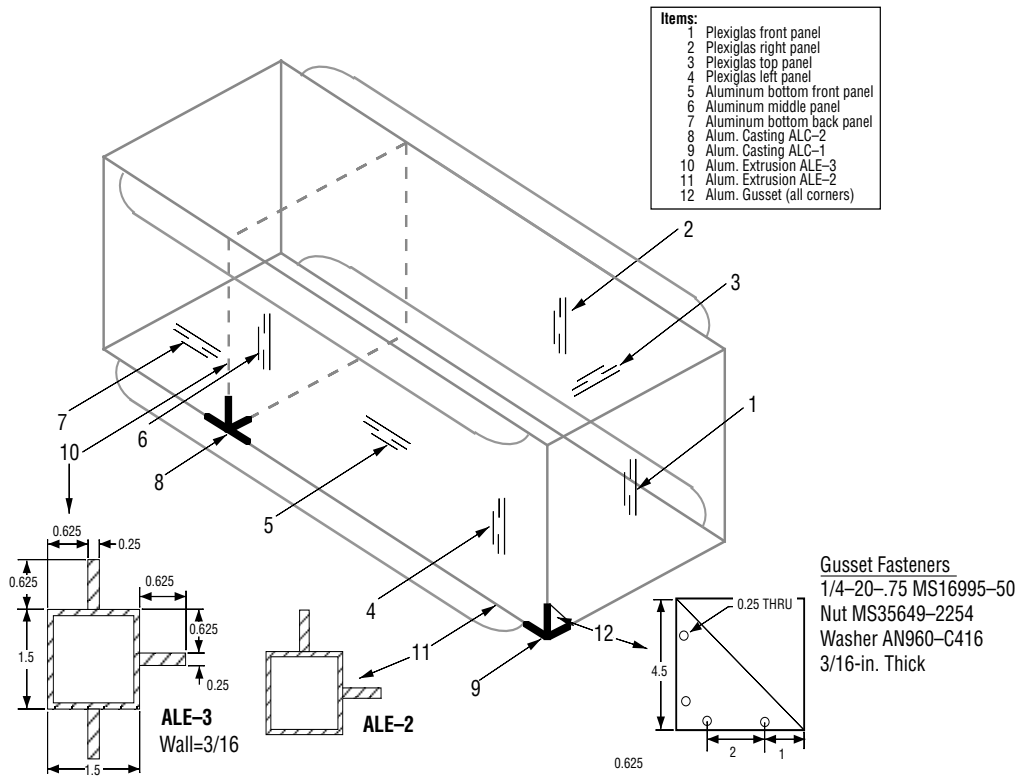


Figure 26. MAPO assembly sheet 1.



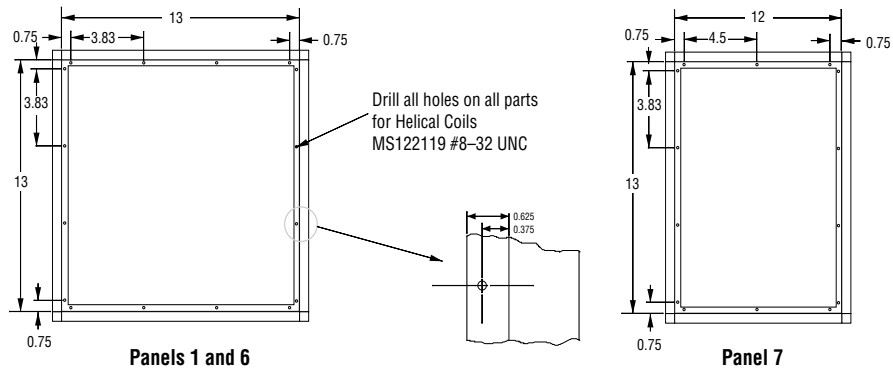
Note: All dimensions are in inches

Figure 27. MAPO frame layout sheet 2.



Note: All dimensions are in inches

Figure 28. MAPO frame layout sheet 3.



**Notes**

- (1) Space holes as equally as possible along ribs per given dimensions
- (2) Drill holes for Helical Coils MS122119 #8-32 UNC
- (3) Use cap screw fasteners MS16997-32 #8-32UNC/3A [5305-00-978-9370]
- (4) Washer AN960-C8 [5310-00-685-3744]
- (5) Match drill fastener holes into Plexiglas/Aluminum panels
- (6) Panels 1, 2, 3, and 4 are Plexiglas Type-G with a 1/10-in. thickness
- (7) Panels 5, 6, and 7 are Aluminum 6061-T6 with 1/16-in. to 1/10-in. thickness
- (8) Cut all Plexiglas and aluminum panels 0.125 in. less than window dimensions. See table below:

Panel 1	12.875 x 12.875
Panel 2,3,4&5	12.875 x 30.875
Panel 6	12.875 x 12.875
Panel 7	12.875 x 11.875

Note: All dimensions are in inches

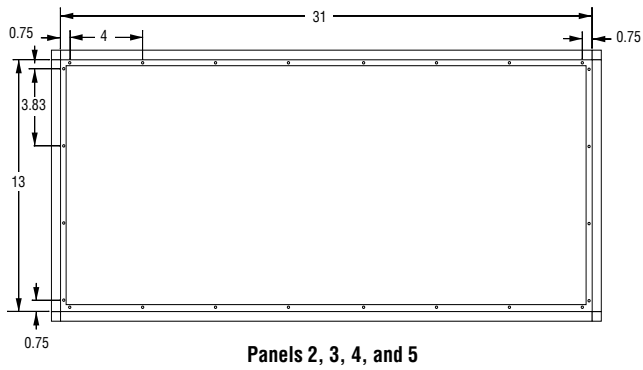
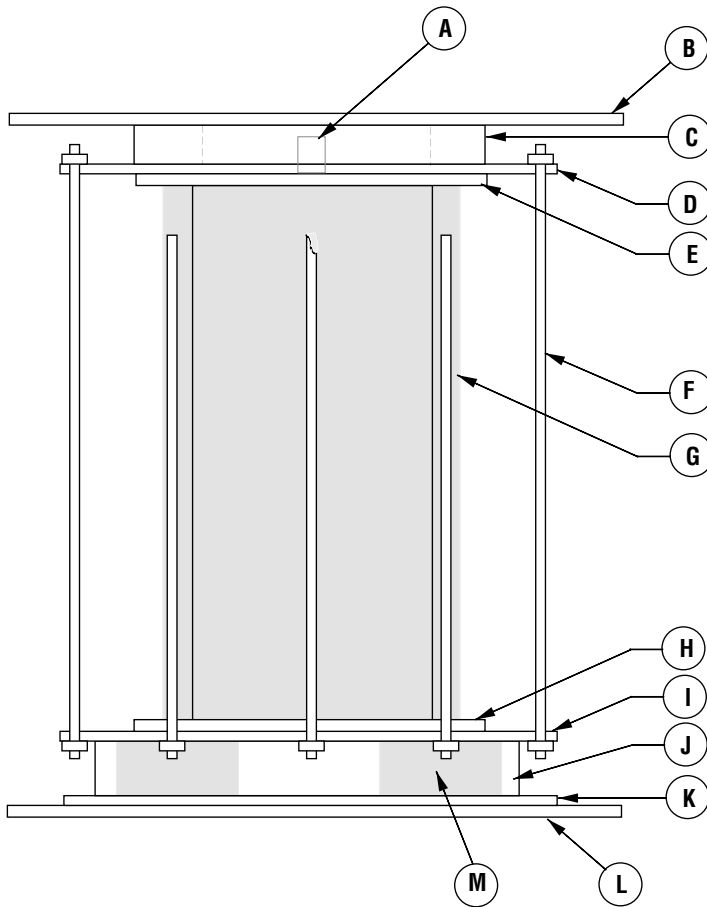


Figure 29. MAPO frame layout sheet 3a.

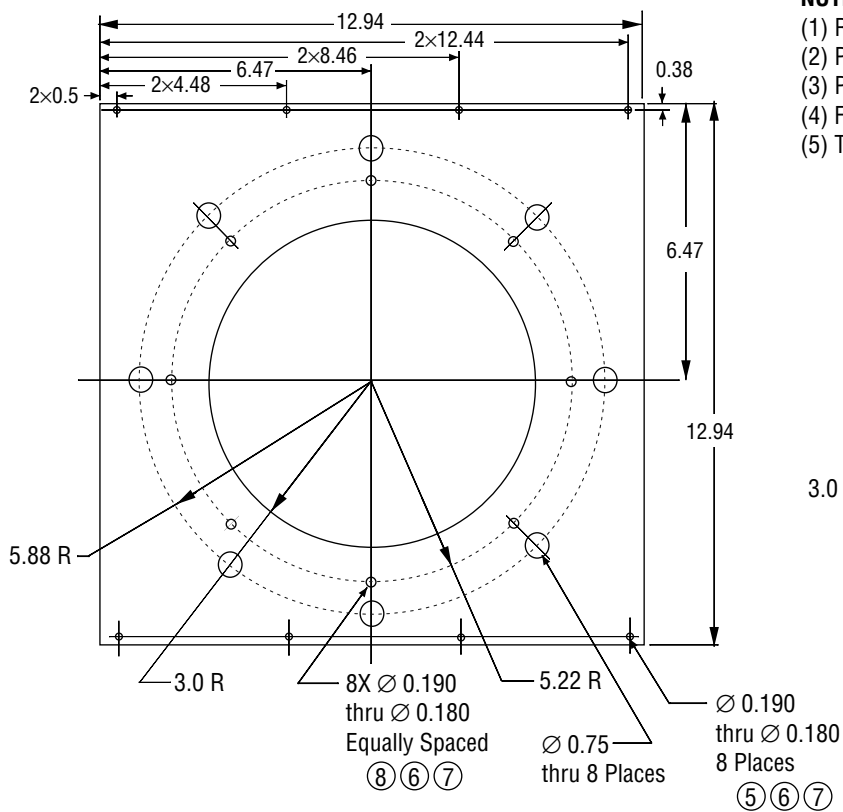


### TEST TANK ASSEMBLY

- (A) 3/8 in. AN Bulkhead Fitting With O-Ring
- (B) Upper Support Plate
- (C) Support Spacer Plate
- (D) Tank Upper Cover Plate
- (E) Tank Upper Alignment Plate
- (F) Tank Cover Plate Connecting Rods  
-X8 Threaded Rods  
-S.S. 0.25-20 UNC by 12.7 in.
- (G) Plexiglas Test Tank
- (H) Tank Lower Alignment Plate
- (I) Tank Lower Cover Plate
- (J) Magnet Container Side Wall
- (K) Magnet Container Bottom Plate
- (L) Lower Support Plate
- (M) 10-in.-Diameter Ring Magnet

- ① MS16995-50 1/4-20 UNC/2A 0.75 LG  
[5310-00-988-7614]
- ② NA960-416 1/4 WASHER  
[5310-00-515-7449]
- ③ MS35649-2254 1/4-20UNC-2B NUT  
[5310-00-930-5966]
- ④ MS35190 #6-32 UNC/2A 0.5 LG SCREW  
[5305-00-059-4533]
- ⑤ MS35190 #10-24 UNC/2A 1.0 LG COUNTER SUNK  
[5305-00-957-6269]
- ⑥ NAS1587-2 #10 WASHER  
[5310-00-059-5291]
- ⑦ MS35649-204 #10-24 UNC/2B NUT  
[5310-01-262-7899]
- ⑧ MS35190 #10-24 UNC/2A 1.5 LG COUNTER SUNK  
[5305-00-957-6269]
- ⑨ MS35190 #6-32 UNC/2A 0.75 LG  
[5305-00-958-5450]
- ⑩ AN960-C6 #6 WASHER  
[5310-00-531-9514]
- ⓕ ASTM-A193-B8 1/4-20UNC/2A 12.75 LG  
(Torque to 15-30 in-#)

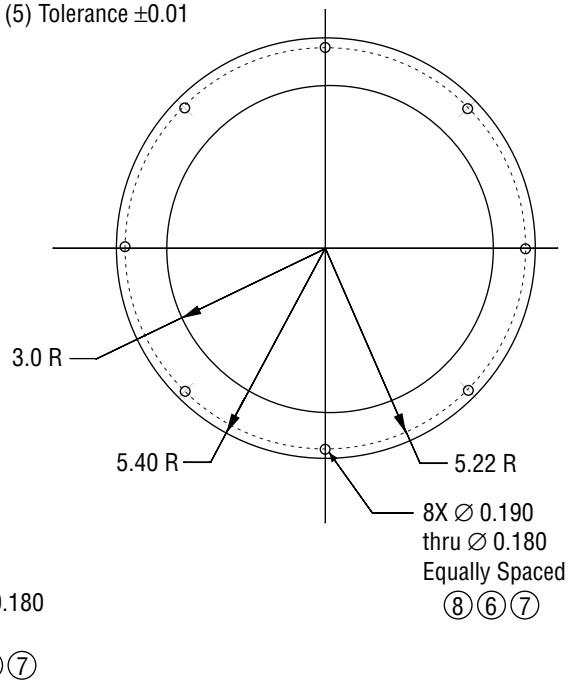
Figure 30. MAPO test tank assembly sheet 4.



**PART B**  
1 Part Required

**NOTES:**

- (1) Remove all Burrs and Break Sharp Edges
- (2) Part B Mat 0.25-in. Thick 6061-T6 Alum Plate
- (3) Part C Mat 0.25-in. Thick 6061-T6 Alum Plate
- (4) Fasteners See Sheet 4
- (5) Tolerance  $\pm 0.01$



**PART C**  
1 Part Required

Note: All dimensions are in inches

Figure 31. MAPO test tank assembly sheet 4a.

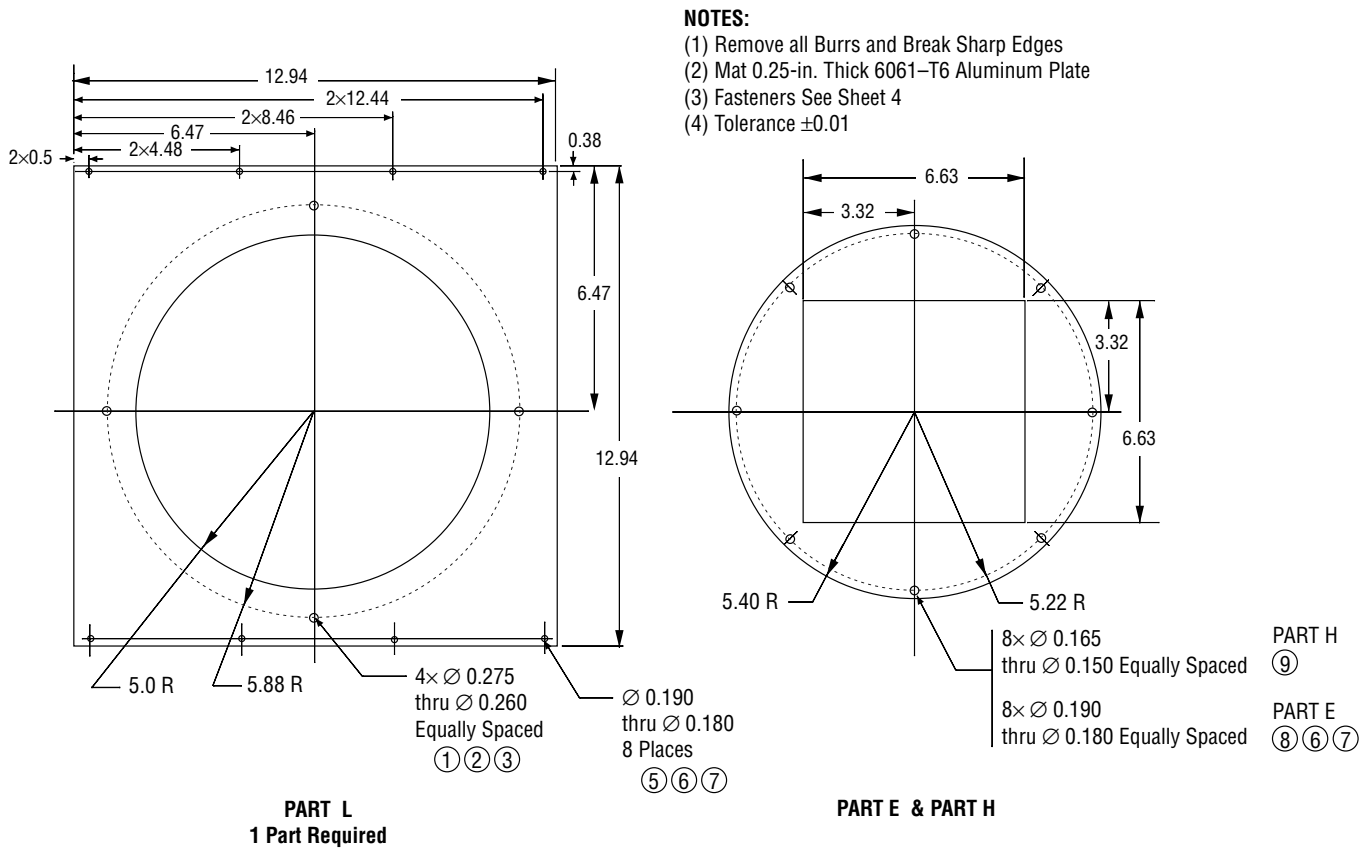
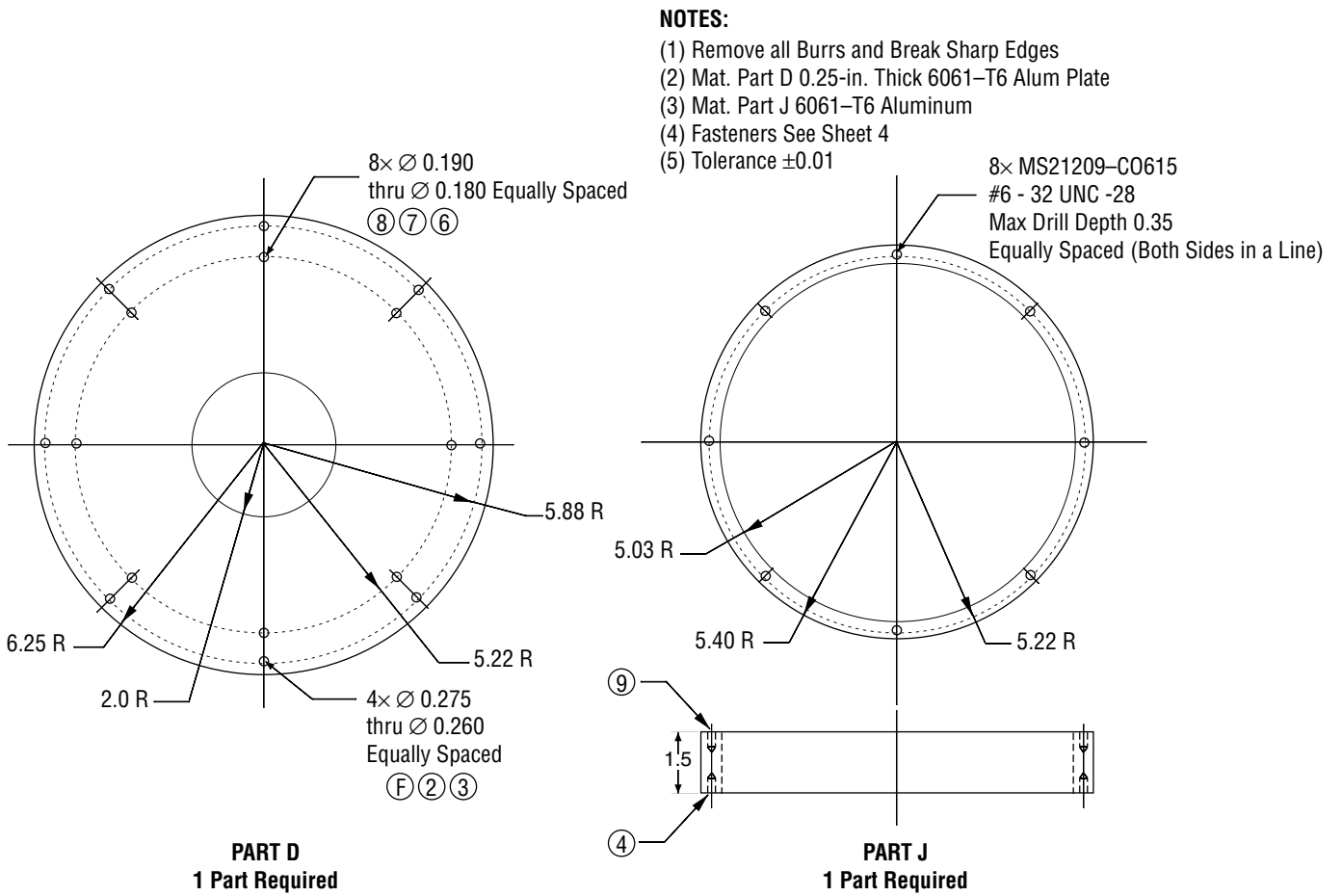
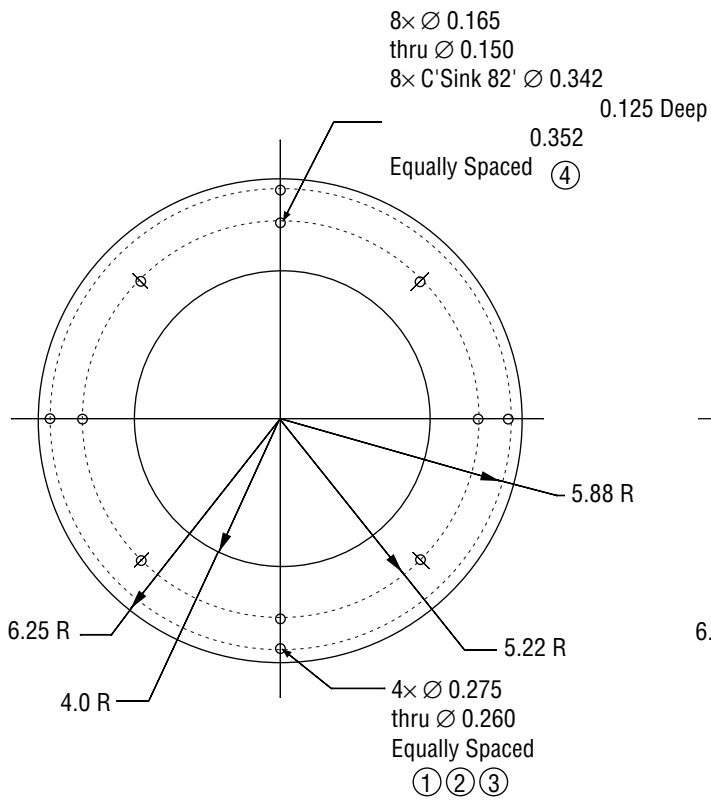


Figure 32. MAPO test tank assembly sheet 4b.

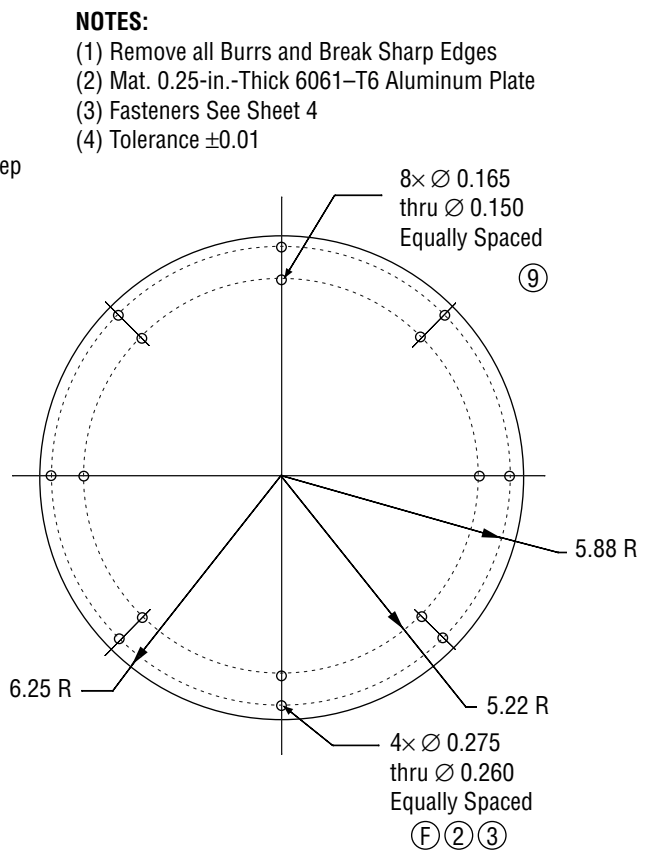


Note: All dimensions are in inches

Figure 33. MAPO test tank assembly sheet 4c.



**PART K**  
1 Part Required

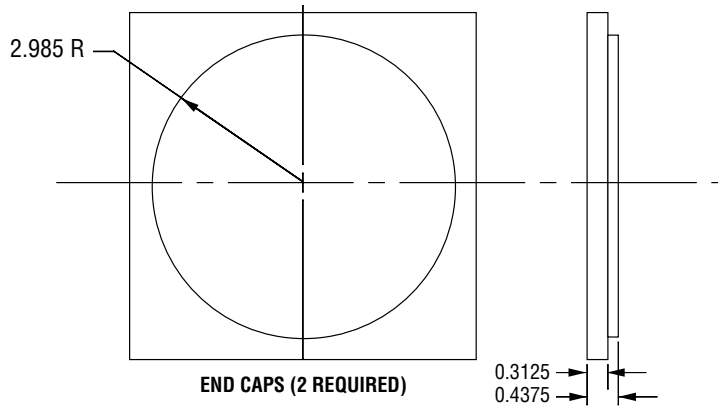


**PART I**  
1 Part Required

- NOTES:**
- (1) Remove all Burrs and Break Sharp Edges
  - (2) Mat. 0.25-in.-Thick 6061-T6 Aluminum Plate
  - (3) Fasteners See Sheet 4
  - (4) Tolerance  $\pm 0.01$

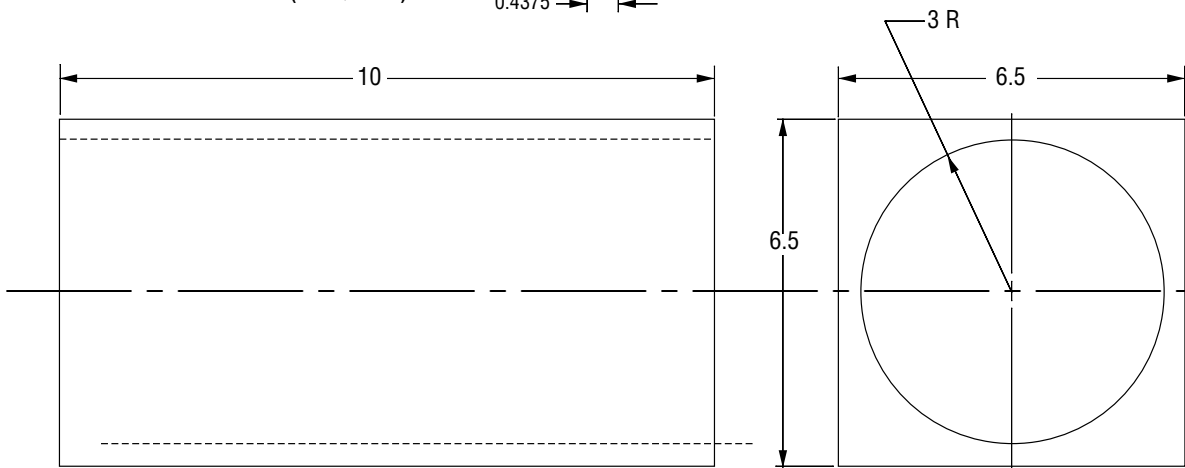
Note: All dimensions are in inches

Figure 34. MAPO test tank assembly sheet 4d.



**NOTES:**

- (1) Remove all Burrs and Break Sharp Edges
- (2) Material Type G-Plexiglas
- (3) Bottom Cap Adheasively Bonded to the Cylindrical Section
- (4) Top Cap is Removable
- (5) O-Ring Gasket with 6-in. ID and 1/16-in. Rope



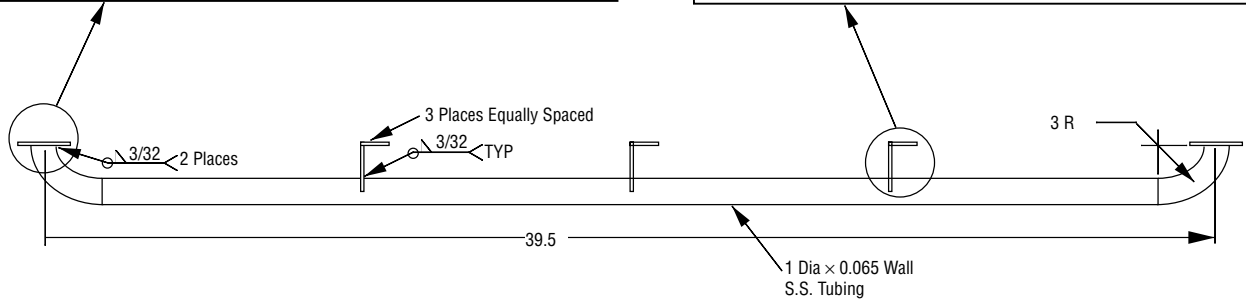
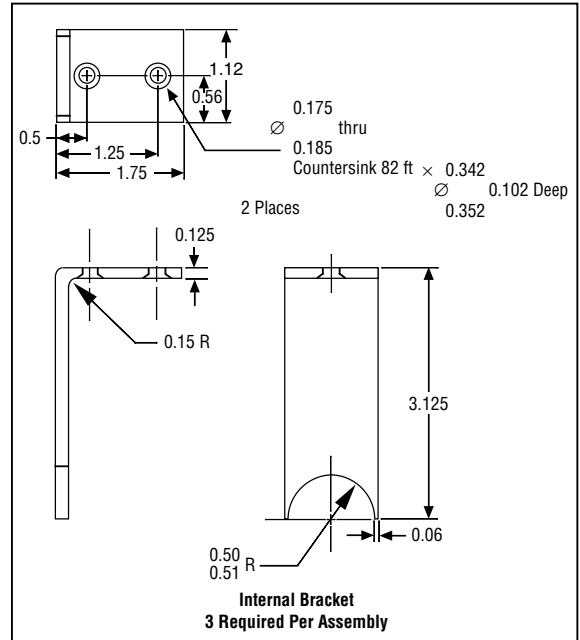
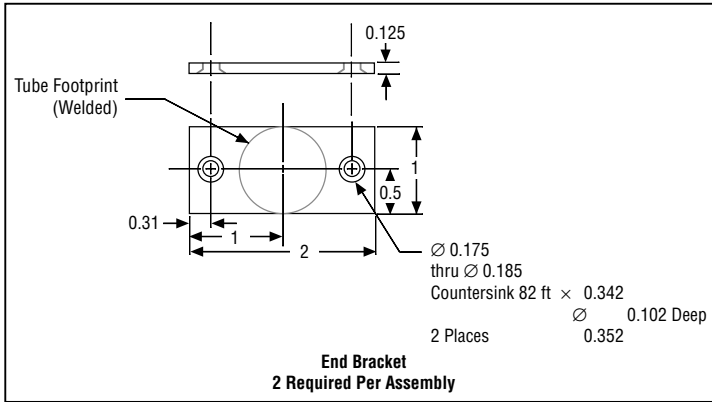
Note: All dimensions are in inches

Figure 35. MAPO test tank assembly sheet 4e.

Total 4 Assemblies Required

**Notes:**

- (1) Remove all Burrs and Break Sharp Edges
- (2) Material 304 Stainless Steel
- (3) Fasteners MS35109-261 #8 Screw [5305-00-957-6646]  
MS21644N08 #8 Nut [5310-00-811-3494]
- (4) Tolerance  $\pm 0.01$



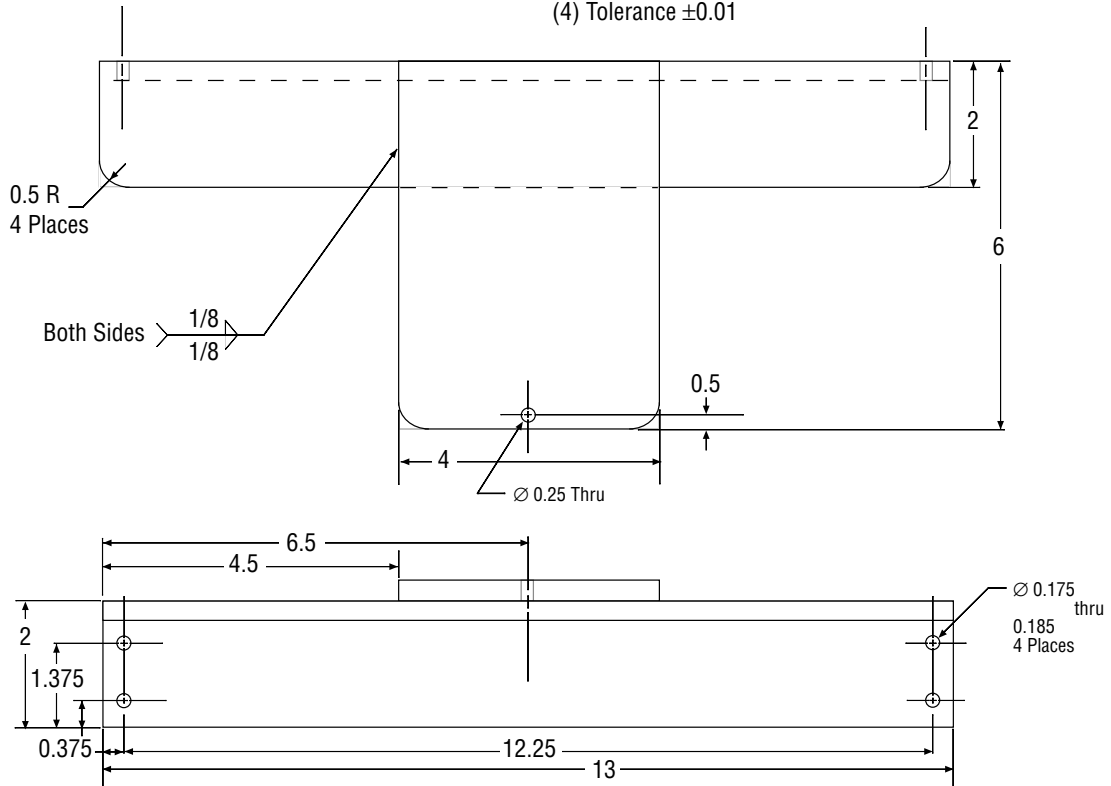
Note: All dimensions are in inches

Figure 36. MAPO hand rail assembly sheet 5.

Total 1 Assembly Required

**Notes:**

- (1) Remove all Burrs and Break Sharp Edges
- (2) Material 2x2x0.25 Aluminum Angle  
0.25-in.-Thick Aluminum Plate
- (3) Fasteners MS51957 #8 Screw [5305-00-054-6672]  
MS21644N08 #8 Nut [5310-00-811-3494]
- (4) Tolerance  $\pm 0.01$



Note: All dimensions are in inches

Figure 37. MAPO camera assembly sheet 6.

## APPENDIX B—MAGNETIC FIELD MEASUREMENTS OVER TEST TANK VOLUME

To control the motion of ferromagnetic mixtures used during low-g testing, it was necessary to impose a magnetic field throughout the test tank. This field was provided by a nonmovable, permanent magnet located at the bottom of the tank. The magnet selected, was a rare Earth-type ring magnet with a thickness of 1.5 in. and inner and outer diameters of 4 and 10 in., respectively. It has a maximum magnetic field strength of 6,000 G at the magnet surface and a total weight of 25 lb. Figure 38 illustrates the general shape of this magnet.

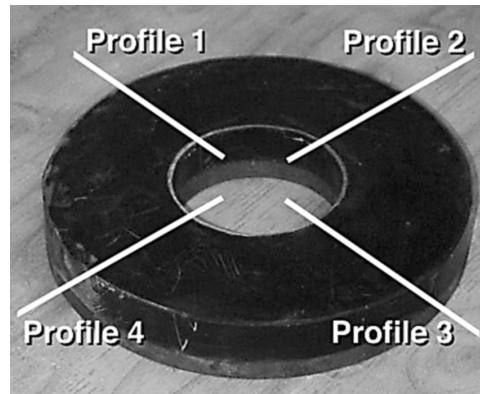


Figure 38. Test magnet.

To correctly model the magnetic body forces acting on the fluid inside the test tank, the magnetic field within the internal volume of the test tank must be known. For the ring magnet configuration, the magnetic field would be axisymmetric about the z-axis (directed along the centerline of the magnet) as shown in figure 39. To assess the magnetic field deviation around the magnet, measurements were taken at four profiles located at 90° intervals as shown in figure 38. These measurements were then used to produce an average magnetic field description that was used in computer modeling.

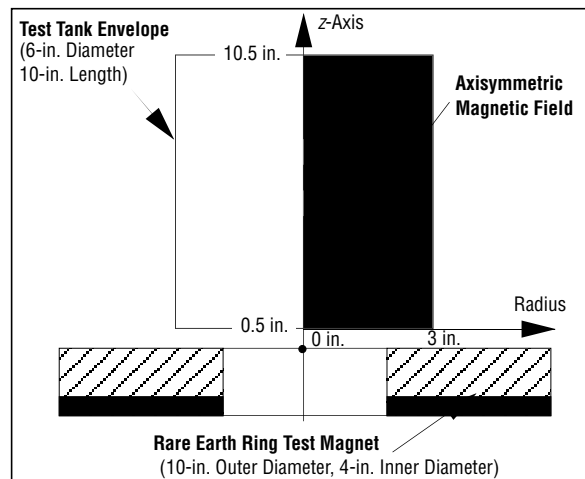


Figure 39. Magnet and tank layout.

Specific measurements were taken using a 0.7874-in. grid interval with the origin at  $R=0$  and  $z=0.5$  in. This 0.5-in. offset in height, corresponds to the position of the tank bottom relative to the top of the magnet. All magnetic field measurements were taken using a Lake Shore model 450 Gaussmeter which was placed at each grid point and oriented to achieve maximum magnetic field. These field values along with the accompanying direction were then recorded for each profile and are tabulated in table 3. The averaged data generated from the profiles is documented in table 4.

An additional concern was the minimum safe distance for placement of computers and magnetic storage media. To determine this distance, a floppy disk, which was considered to be the most sensitive storage media, was selected for testing. The disk was loaded with data files, then placed at a measured distance from the magnet and held for 60 sec. The files and disk structure were then checked for corruption. This process was repeated (moving the disk closer to the magnet) until corruption occurred. Using this approach, it was determined that the point of failure corresponded to a field strength of 240 G. The minimum safe distance was then selected at a position with 1/10 of the corrupting field strength or 24 G. (This provides a margin of safety without impacting the hardware layout, which corresponds to a distance of  $\approx 13$  in. from the magnet.)

Table 3. Magnetic field measurements—four intervals.

Grid Location (in.)		Profile 1		Profile 2		Profile 3		Profile 4	
R-Location (in.)	z-Location (in.)	Mag. Field (G)	Direction (deg)						
0.0	0.5	596.7	266	615.3	273	626.8	277	619.3	271
0.0	1.2874	100.1	253	97.7	281	128.1	313	110.5	248
0.0	2.0748	182.1	115	175.5	96	181.3	93	164.4	97
0.0	2.8622	258.5	96	262.4	88	258.4	91	257	94
0.0	3.6496	255	97	260	93	258.2	90	254.7	94
0.0	4.437	224.5	97	228.7	95	227.3	90	226.7	93
0.0	5.2244	188.3	97	191.7	96	191	85	190.3	95
0.0	6.0118	154.6	95	157.5	96	157	85	155.5	90
0.0	6.7992	126.8	96	128.5	90	128.7	85	128.4	93
0.0	7.5866	103.8	98	105.1	93	105.2	86	105.34	89
0.0	8.374	85.3	102	86.6	93	86.3	85	86.3	93
0.0	9.1614	70.8	95	71.6	93	71.5	87	71.6	96
0.0	9.9488	58.9	96	59.5	96	59.8	90	59.6	95
0.0	10.7362	49.4	95	49.9	90	50.2	92	50.3	93
0.7874	0.5	616.1	293	702.6	300	727	306	685	297
0.7874	1.2874	107	355	221.4	359	242.3	359	186.5	342
0.7874	2.0748	208.5	94	246.7	88	259.4	64	216.3	87
0.7874	2.8622	265.3	101	285.7	93	290.4	88	269.8	87
0.7874	3.6496	254.3	100	269	95	271.2	90	260.7	96
0.7874	4.437	221.6	103	231.2	92	233.7	95	227.3	99
0.7874	5.2244	184.7	106	192	97	193.5	92	190.6	95
0.7874	6.0118	152.1	103	157.3	100	158.7	96	155.6	104
0.7874	6.7992	124.4	104	128.2	102	129.2	97	127.6	99
0.7874	7.5866	101.8	111	104.6	99	105.6	96	104.3	95
0.7874	8.374	84.1	106	85.9	95	86.2	88	85.8	96
0.7874	9.1614	69.7	105	71	101	71.6	92	71.1	91
0.7874	9.9488	58.1	102	59.2	95	59.8	98	59.5	95
0.7874	10.7362	48.9	99	49.8	93	50	98	50	95
1.5748	0.5	649.6	321	852	322	861.6	338	835.9	328
1.5748	1.2874	258.9	45	425.7	40	413.5	37	372.1	41
1.5748	2.0748	298.4	89	375.2	72	376.4	77	338.7	81
1.5748	2.8622	296.6	104	340.1	91	341.3	90	318.2	94
1.5748	3.6496	261.9	110	287.1	101	291.3	92	278	102
1.5748	4.437	220	113	236.6	98	240	100	232.3	102
1.5748	5.2244	181.3	111	192.5	100	195.1	101	190	102
1.5748	6.0118	147.9	109	155.3	99	158.2	98	154.2	102
1.5748	6.7992	120.9	107	126.2	105	128.2	97	125.8	103
1.5748	7.5866	99.1	109	102.5	96	104.4	108	102.9	102
1.5748	8.374	81.6	108	84.3	107	85.7	100	84.4	103
1.5748	9.1614	67.6	103	69.8	103	70.9	98	69.9	103
1.5748	9.9488	56.7	109	58.1	103	59.4	99	58.6	97
1.5748	10.7362	47.9	110	49	102	49.8	99	49.3	98

Note: The direction indicator is taken positive as counter-clockwise starting from the right directed horizontal.

Table 3. Magnetic field measurements four intervals (Continued).

Grid Location (in.)		Profile 1		Profile 2		Profile 3		Profile 4	
R-Location (in.)	z-Location (in.)	Mag. Field (G)	Direction (deg)						
2.3622	0.5	698.8	25	1109.9	37	1021.9	26	1015.1	19
2.3622	1.2874	484.9	82	694.4	77	652.4	73	616.4	71
2.3622	2.0748	403.4	103	515.4	91	499.3	92	474.1	91
2.3622	2.8622	333	115	394.4	96	392.4	102	373.8	98
2.3622	3.6496	268.5	110	306.1	103	307.9	99	296.6	105
2.3622	4.437	216.6	125	240.6	109	243.8	110	235.6	103
2.3622	5.2244	175.3	118	190.2	107	193.6	102	187.9	104
2.3622	6.0118	141.8	118	152.1	110	155.5	101	151.5	103
2.3622	6.7992	115.7	115	122.5	105	125.4	104	121.9	107
2.3622	7.5866	94.6	115	99.5	101	101.8	103	99.7	102
2.3622	8.374	78.3	112	81.9	108	83.4	100	81.6	100
2.3622	9.1614	65.2	111	67.7	108	69.1	103	68.2	105
2.3622	9.9488	54.7	112	56.5	107	57.6	102	57	107
2.3622	10.7362	46.2	108	47.6	104	48.5	96	47.9	1
3.1496	0.5	1214.2	93	1642.4	83	1454.4	85	1416.8	76
3.1496	1.2874	705.4	114	944	100	874.1	100	865.1	100
3.1496	2.0748	479.3	121	610.6	102	886.8	107	572.9	113
3.1496	2.8622	350.1	125	425.9	108	419.8	108	407.5	114
3.1496	3.6496	266.7	118	311.3	114	312.5	122	303.4	113
3.1496	4.437	208.7	124	236.4	116	240.1	114	232.8	112
3.1496	5.2244	166.6	125	184.1	116	187.5	110	182.1	113
3.1496	6.0118	133.5	125	145.9	114	149.1	110	144.7	109
3.1496	6.7992	108.6	122	117.2	110	119.8	109	117.1	111
3.1496	7.5866	89.4	121	95.1	112	97.8	107	95.3	108
3.1496	8.374	74	118	78.2	115	80.1	109	78.4	110
3.1496	9.1614	61.9	121	64.8	105	66.5	116	65.3	106
3.1496	9.9488	52.1	119	54.2	114	55.5	103	54.7	110
3.1496	10.7362	44.2	118	45.8	110	46.8	107	46.2	109

Note: The direction indicator is taken positive as counter-clockwise starting from the right directed horizontal.

Table 4. Average magnetic field measurement.

Grid Location (in.)		Average Magnetic Field Properties	
R-Location (in.)	z-Location (in.)	Mag. Field (G)	Direction (deg)
0.0	0.5	614.525	271.75
0.0	1.2874	109.1	273.75
0.0	2.0748	175.825	100.25
0.0	2.8622	259.075	92.25
0.0	3.6496	256.975	93.5
0.0	4.437	226.8	93.75
0.0	5.2244	190.325	93.25
0.0	6.0118	156.15	91.5
0.0	6.7992	128.1	91
0.0	7.5866	104.86	91.5
0.0	8.374	86.125	93.25
0.0	9.1614	71.375	92.75
0.0	9.9488	59.45	94.25
0.0	10.7362	49.95	92.5
0.7874	0.5	682.675	299
0.7874	1.2874	189.3	353.7
0.7874	2.0748	232.725	83.25
0.7874	2.8622	277.8	92.25
0.7874	3.6496	263.8	95.25
0.7874	4.437	228.45	97.25
0.7874	5.2244	190.2	97.5
0.7874	6.0118	155.925	100.75
0.7874	6.7992	127.35	100.5
0.7874	7.5866	104.075	100.25
0.7874	8.374	85.5	96.25
0.7874	9.1614	70.85	97.25
0.7874	9.9488	59.15	97.5
0.7874	10.7362	49.675	96.25
1.5748	0.5	799.775	327.25
1.5748	1.2874	367.55	40.75
1.5748	2.0748	347.175	79.75
1.5748	2.8622	324.05	94.75
1.5748	3.6496	279.575	101.25
1.5748	4.437	232.225	103.25
1.5748	5.2244	189.725	103.5
1.5748	6.0118	153.9	102
1.5748	6.7992	125.275	103
1.5748	7.5866	102.225	103.75
1.5748	8.374	84	104.5
1.5748	9.1614	69.55	101.75
1.5748	9.9488	58.2	102
1.5748	10.7362	49	102.25

Grid Location (in.)		Average Magnetic Field Properties	
R-location (in.)	z-location (in.)	Mag. Field (G)	Direction (deg)
2.3622	0.5	961.425	26.75
2.3622	1.2874	612.025	75.75
2.3622	2.0748	473.05	94.25
2.3622	2.8622	373.4	102.75
2.3622	3.6496	294.775	104.25
2.3622	4.437	234.15	111.75
2.3622	5.2244	186.75	107.75
2.3622	6.0118	150.225	108
2.3622	6.7992	121.375	107.75
2.3622	7.5866	98.9	105.25
2.3622	8.374	81.3	105
2.3622	9.1614	67.55	106.75
2.3622	9.9488	56.45	107
2.3622	10.7362	47.55	103.25
3.1496	0.5	1431.95	84.25
3.1496	1.2874	847.15	103.5
3.1496	2.0748	637.4	110.75
3.1496	2.8622	400.825	113.75
3.1496	3.6496	298.475	116.75
3.1496	4.437	229.5	116.5
3.1496	5.2244	180.075	116
3.1496	6.0118	143.3	114.5
3.1496	6.7992	115.675	113
3.1496	7.5866	94.4	112
3.1496	8.374	77.675	113
3.1496	9.1614	64.625	112
3.1496	9.9488	54.125	111.5
3.1496	10.7362	45.75	111

Note: The direction indicator is taken positive as counter-clockwise starting from the right directed horizontal.

## APPENDIX C—MAGNETIZATION MEASUREMENTS OF WATER-BASED MAGNETIC FLUID

To accurately model the motion of a paramagnetic or ferromagnetic fluid subject to a magnetic field, the fluid's magnetic susceptibility ( $\chi$ ) must be known. The susceptibility is defined as the slope of the magnetization versus applied field curve, and for a paramagnetic material such as  $\text{LO}_2$  it is a constant. In the case of the MAPO experiment, a ferromagnetic fluid was used as a simulant to ease safety and handling concerns; however, ferromagnetic fluids have a significant nonlinear response in magnetization with varying applied field. Due to this response, it is possible to mix a ferromagnetic solution to match the susceptibility of a paramagnetic fluid, such as  $\text{LO}_2$ , at only one given applied field (i.e., distance from the magnet). This mixture then behaves weaker than  $\text{LO}_2$  as the applied field increases (i.e., mixture moved toward the magnet) and stronger than  $\text{LO}_2$  as the applied field is decreased (i.e., mixture moved away from the magnet). The magnetic field within the MAPO tank was measured and found to range from  $\approx 1,400$  G near the bottom (magnet end of the tank) to 45 G at the top end (opposite the magnet). Based on this range of magnetic field, a series of diluted ferromagnetic solutions were mixed and tested (using an alternating-gradient magnetometer<sup>16</sup>) for the range of susceptibilities.

The ferromagnetic solution, purchased from the Ferrofluidics Corporation, is a water-based material designated EMG-805 with a saturation magnetization of 200 G at room temperature. This material was diluted and tested for magnetic susceptibility, or rather ferro-susceptibility termed ferro- $\chi$  (so as not to be confused with the traditional interpretation of susceptibility as a constant), using the following procedure. It should also be noted that there are uncertainties with these values associated with the unknown effect of the sample's viscosity (since the measurement approach required using high-frequency oscillations).

Step 1: An alternating-gradient magnetometer was calibrated with a known standard so that measurements taken with the ferromagnetic mixtures could be converted to a useful quantity. The standard chosen for this work was Neodymium Oxide ( $\text{Nd}_2\text{O}_3$ ).  $\text{Nd}_2\text{O}_3$ , a paramagnetic salt, has a magnetic susceptibility of  $30.3 \times 10^{-6}$  in the cgs system. Figure 40 illustrates the measured magnetization versus applied field curve with a linear approximation given by:

$$\text{Nd}_2\text{O}_3 \text{ Standard Magnetization (mV)} = 0.0050514 * \text{Applied Field (G)}.$$

The slope of this curve (0.0050514 mV/G) then corresponds to the known magnetic susceptibility  $\chi$  of  $30.3 \times 10^{-6}$  (cgs) for  $\text{Nd}_2\text{O}_3$ , yielding a relationship which can be used to evaluate an unknown material such as the ferromagnetic mixtures.

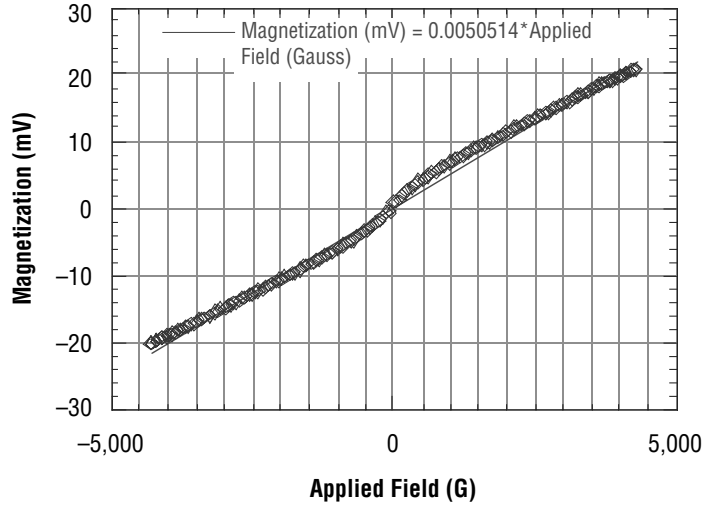


Figure 40. Magnetization of  $\text{Nd}_2\text{O}_3$  standard.

Step 2: Four diluted ferromagnetic solutions were mixed and tested using the same hardware setup and procedures that were established during calibration (step 1). These solutions, mixed on a volume basis, included water to ferromagnetic fluid ratios of: 170:1, 133:1, 83:1, and 30:1. The measured magnetization value for each mixture was then converted from a millivolt measurement to a cgs ferro-susceptibility through the use of the standard calibration curve (generated in step 1) at a given applied field strength by the following relationship:

$$\text{Ferro-}\chi \text{ of Mixture} = \frac{(\text{Measured Ferro Magnetization (mV)} * \chi_{\text{Nd}_2\text{O}_3})}{(\text{Nd}_2\text{O}_3 \text{ Standard Magnetization (mV)})}$$

This procedure produces the family of curves illustrated in figures 41–48. It is easily seen from these figures that the ferromagnetic mixture has a very nonlinear magnetization, unlike the paramagnetic  $\text{Nd}_2\text{O}_3$  shown in figure 40.

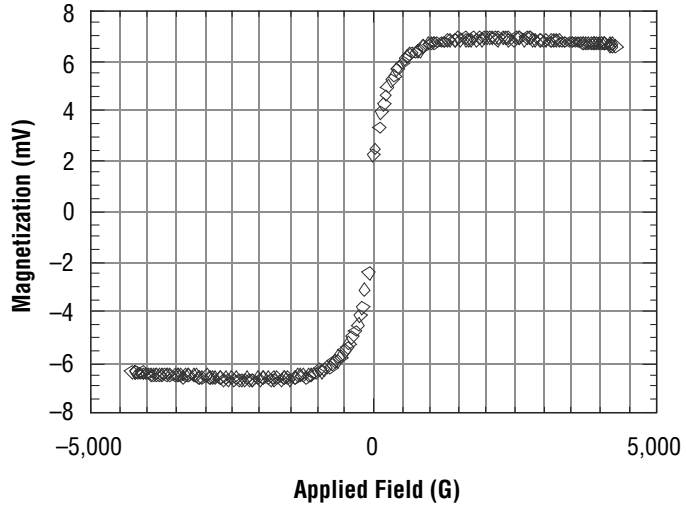


Figure 41. Magnetization of 170:1 ratio.

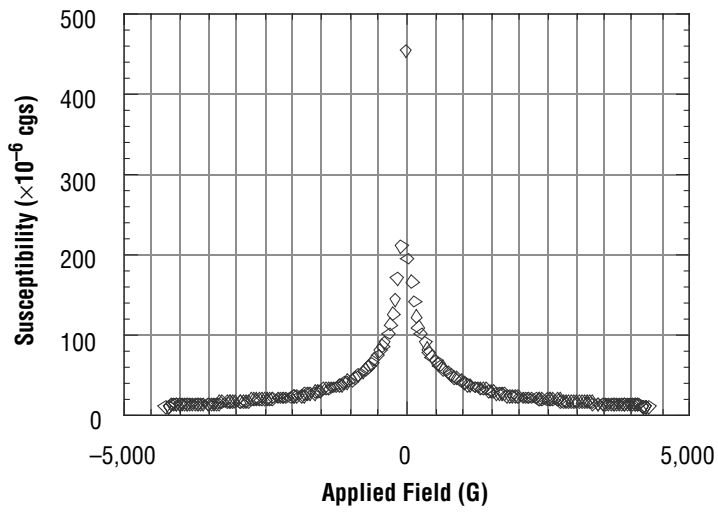


Figure 42. Ferro- $\chi$  of 170:1 ratio.

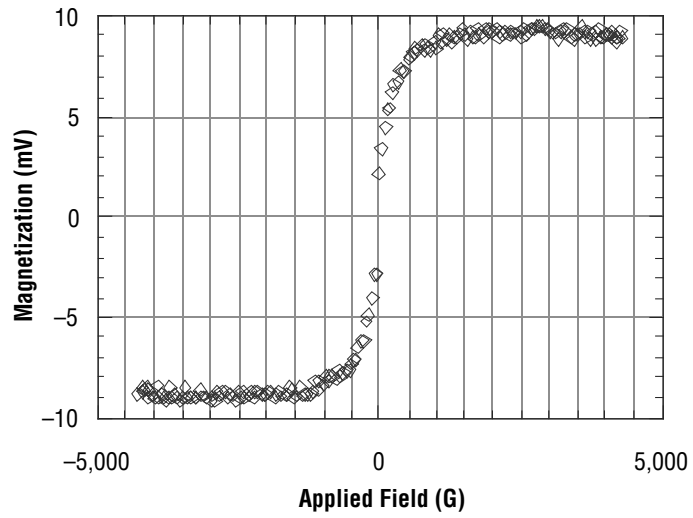


Figure 43. Magnetization of 133:1 ratio.

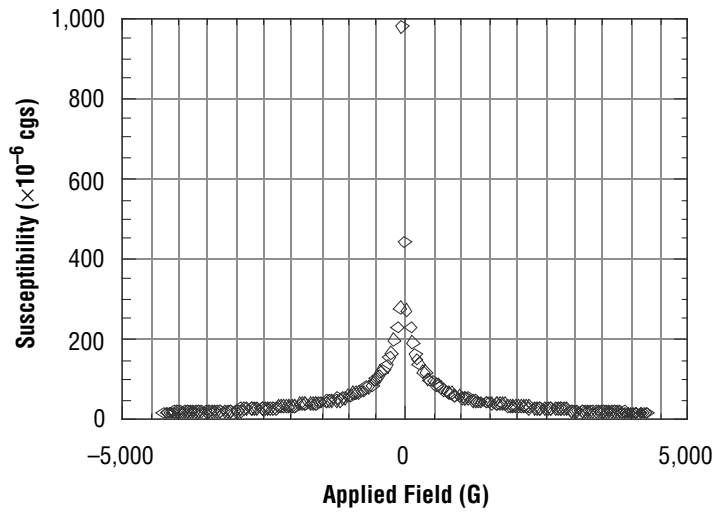


Figure 44. Ferro- $\chi$  of 133:1 ratio.

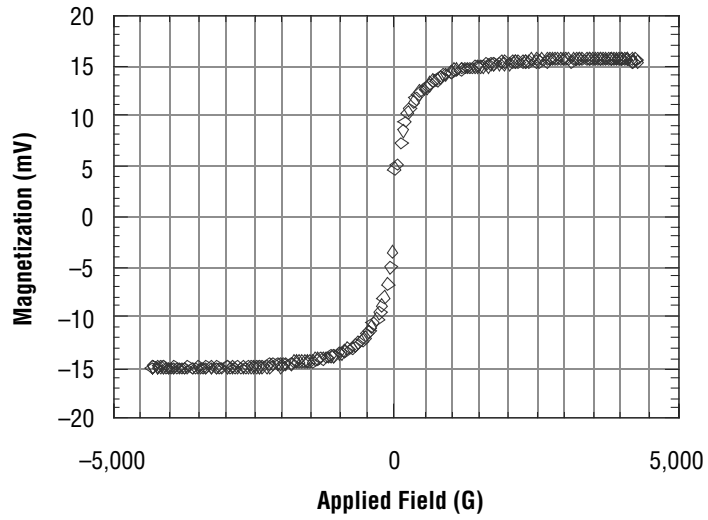


Figure 45. Magnetization of 83:1 ratio.

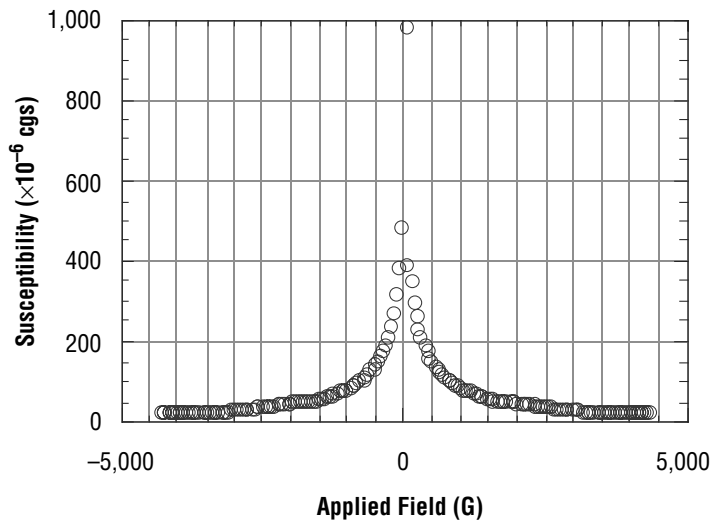


Figure 46. Ferro- $\chi$  of 83:1 ratio.

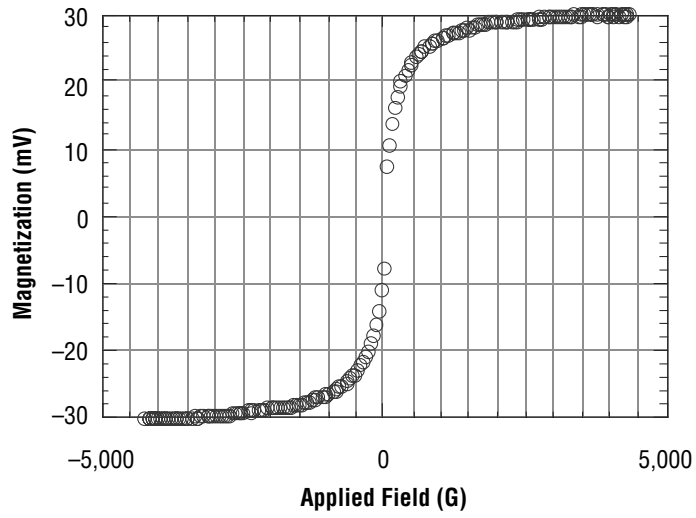


Figure 47. Magnetization of 30:1 ratio.

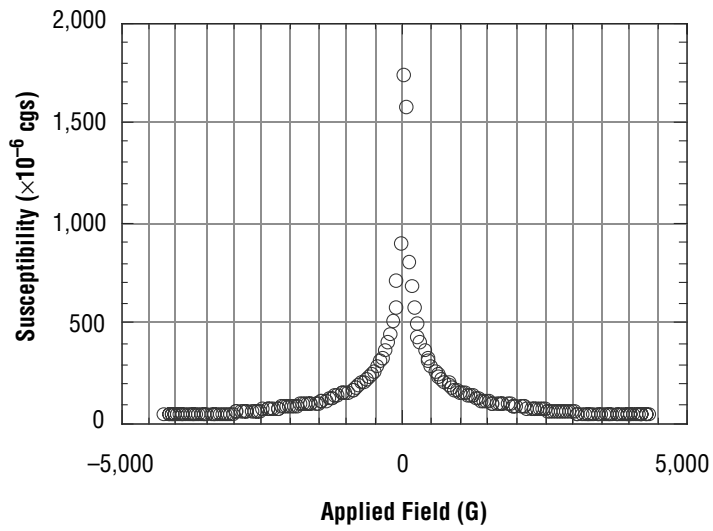


Figure 48. Ferro- $\chi$  of 30:1 ratio.

These data were used to select ferromagnetic mixtures for flight testing based on the desire to achieve or exceed the value of  $\text{LO}_2$  susceptibility ( $\approx 240 \times 10^{-6}$  (cgs) saturated at 1 atmosphere) near the center of the tank. Using this criteria, the 30:1 mixture was selected as the primary ratio to test, with 133:1 and 10:1 selected as bounding secondary ratios. Since the 10:1 ratio was not experimentally tested, its susceptibility curve was interpolated from the laboratory data measured for all concentrations. This interpolation, illustrated in figure 49, shows the magnetization response as a function of concentration ratio for seven levels of applied field. It should also be noted that the concentration mixture ratio of 1 was used to represent the pure ferromagnetic fluid.

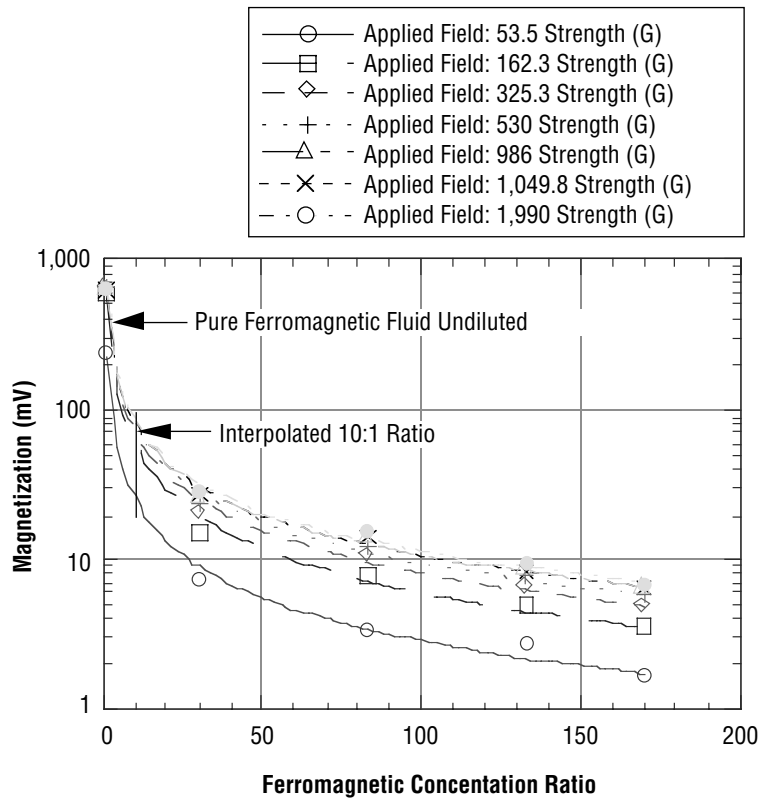


Figure 49. Magnetization versus concentration curve.

The interpolated data was further processed using the previously outlined steps to obtain magnetization and ferro-susceptibility curves for the 10:1 concentration illustrated in figures 50 and 51.

Tables 5, 6, and 7 provide the numerical data used to generate the plots for ferromagnetic mixture ratios of 133:1, 30:1, and 10:1. These data contain values for positive applied field only, the negative field data is nearly identical but with opposite sign.

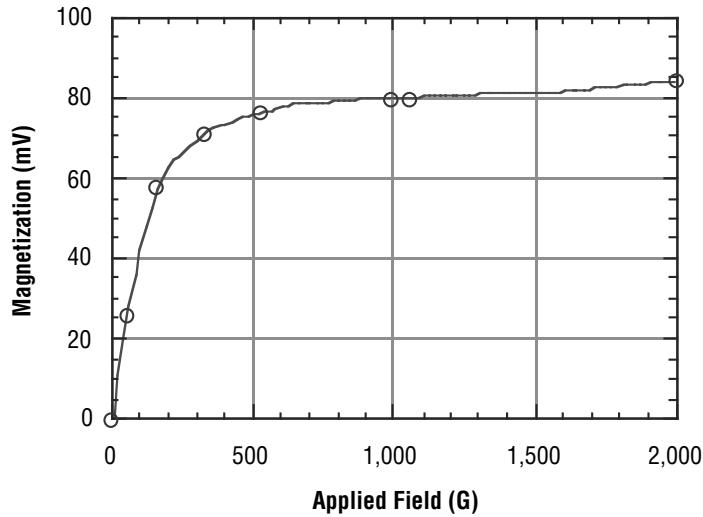


Figure 50. Magnetization of 10:1 ratio.

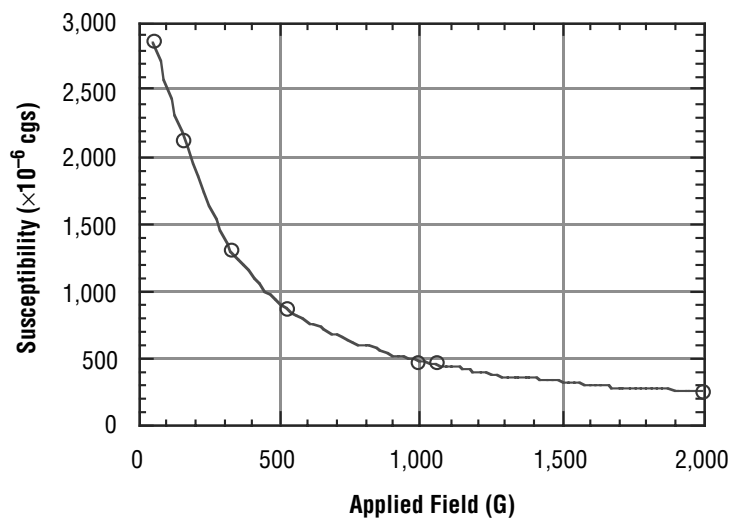


Figure 51. Ferro- $\chi$  of 10:1 ratio.

Table 5. Ferro- $\chi$  for a concentration ratio of 133:1.

Applied Field (G)	Magnetization (mV)	Ferro- $\chi$ (cgs) $\times 10^{-6}$
75	3.34	267.4
167	5.23	187.9
258	6.10	141.9
348	6.62	114.1
439	7.14	97.6
531	7.80	88.1
621	8.09	78.2
713	8.16	68.7
806	8.17	60.8
897	8.33	55.7
988	8.65	52.5
1,079	8.89	49.4
1,171	9.00	46.1
1,261	8.93	42.5
1,353	8.80	39.0
1,444	9.04	37.5
1,535	8.91	34.8
1,626	9.19	33.9
1,718	8.83	30.8
1,809	8.98	29.8
1,900	9.23	29.2
1,991	9.28	27.9
2,083	9.29	26.7
2,174	9.18	25.3
2,265	9.20	24.4
2,358	9.10	23.2
2,450	9.01	22.1
2,540	8.81	20.8
2,631	8.95	20.4
2,722	9.23	20.3
2,813	9.33	19.9
2,904	9.35	19.3
2,994	9.23	18.5
3,084	9.04	17.6
3,173	8.76	16.6
3,262	9.26	17.0
3,350	9.22	16.5
3,437	8.71	15.2
3,523	8.94	15.2
3,606	9.34	15.5
3,688	8.87	14.4
3,767	8.70	13.8
3,846	9.15	14.3
3,920	9.22	14.1
3,992	8.86	13.3
4,063	8.91	13.1
4,130	9.13	13.3
4,196	8.82	12.6
4,260	8.84	12.5
4,322	8.86	12.3

Table 6. Ferro- $\chi$  for a concentration ratio of 30:1.

Applied Field (G)	Magnetization (mV)	Ferro- $\chi$ (cgs) $\times 10^{-6}$
77	10.42	811.6
168	16.01	571.5
259	19.04	441.0
350	21.05	360.8
441	22.52	306.3
533	23.56	265.2
624	24.45	235.0
715	25.09	210.5
808	25.68	190.6
900	26.15	174.3
991	26.58	160.9
1,082	26.92	149.2
1,173	27.25	139.3
1,265	27.48	130.3
1,356	27.72	122.6
1,447	27.95	115.9
1,539	28.09	109.5
1,630	28.29	104.1
1,721	28.47	99.2
1,813	28.60	94.6
1,904	28.72	90.5
1,995	28.89	86.9
2,087	29.00	83.3
2,178	29.09	80.1
2,270	29.16	77.0
2,363	29.22	74.2
2,454	29.31	71.6
2,545	29.42	69.3
2,637	29.51	67.1
2,727	29.57	65.0
2,819	29.63	63.0
2,909	29.66	61.2
3,000	29.70	59.4
3,089	29.78	57.8
3,179	29.82	56.3
3,268	29.79	54.7
3,356	29.88	53.4
3,442	29.89	52.1
3,528	29.91	50.8
3,612	29.91	49.7
3,694	29.94	48.6
3,773	29.93	47.6
3,852	29.90	46.6
3,927	29.79	45.5
4,000	29.89	44.8
4,069	29.87	44.0
4,138	29.82	43.2
4,203	29.89	42.7
4,267	29.89	42.0
4,329	29.88	41.4

Table 7. Ferro- $\chi$  for a concentration ratio of 10:1.

<b>Applied Field (G)</b>	<b>Magnetization (mV)</b>	<b>Ferro-<math>\chi</math> (cgs)<math>\times 10^{-6}</math></b>
53.5	25.5	2,859
162.3	57.4	2,121.4
325.3	70.8	1,305.5
530	76.2	862.4
986	79.9	486.1
1,049	80.1	457.5
1,990	83.3	250.2

## **APPENDIX D—ACCELEROMETER EXPERIMENTAL DATA**

Tables 8–16 provide tabulated experimental data for tests 5, 23, 30, 48, 59, 74, 90, 97, and 106. Raw data were recorded at 128 samples per second and then averaged, post test, to 4 samples per second for use in computer models. The data were also corrected for accelerometer zero offset by adding or subtracting each channel bias value. These bias values were calculated as an average acceleration over the most quiescent interval of free float; however, the values varied very little as expected. The time stamp offset between the video and acceleration data is also listed for each test. This time offset value must be added to the accelerometer times listed below to match the video time index.

Table 8. MAPO test number 5 data.

Test File:	MAPOTEST.005					
Test Date:	Tue, 12-10-1996					
No. Channels:	3					
Sam/sec:	128 Average	32 pt centered				
Start:	10:17:50:25	End: 10:18:30:29				
Low-g Range	start	10:18 (10 sec)				
	end	10:18:09 (19 sec)				
Accelerometer Bias Average Interval	(14 to 18 sec)					
Bias Values	<i>x</i>	-0.0079				
(g's)	<i>y</i>	-0.0095				
	<i>z</i>	-0.0116				
Time Stamp Offset Between Data and Video	1 sec					
Time	<i>x</i> (g's)	<i>x</i> Corrected (g's)	<i>y</i> (g's)	<i>y</i> Corrected (g's)	<i>z</i> (g's)	<i>z</i> Corrected (g's)
0.125	-1.04E-01	-9.62E-02	-8.70E-03	7.67E-04	1.49E+00	1.50E+00
0.375	-1.11E-01	-1.04E-01	-3.26E-03	6.20E-03	1.53E+00	1.54E+00
0.625	-9.56E-02	-8.78E-02	-1.51E-02	-5.68E-03	1.57E+00	1.59E+00
0.875	-1.06E-01	-9.85E-02	1.94E-02	2.89E-02	1.53E+00	1.54E+00
1.125	-1.14E-01	-1.06E-01	1.97E-02	2.92E-02	1.50E+00	1.51E+00
1.375	-1.27E-01	-1.19E-01	8.46E-03	1.79E-02	1.47E+00	1.48E+00
1.625	-1.25E-01	-1.17E-01	1.65E-02	2.59E-02	1.44E+00	1.45E+00
1.875	-1.28E-01	-1.20E-01	6.67E-03	1.61E-02	1.48E+00	1.49E+00
2.125	-1.13E-01	-1.05E-01	-1.52E-02	-5.75E-03	1.49E+00	1.50E+00
2.375	-1.38E-01	-1.30E-01	-6.29E-03	3.17E-03	1.44E+00	1.45E+00
2.625	-1.57E-01	-1.49E-01	2.06E-02	3.01E-02	1.44E+00	1.45E+00
2.875	-1.55E-01	-1.47E-01	3.35E-02	4.30E-02	1.51E+00	1.52E+00
3.125	-1.29E-01	-1.21E-01	2.80E-02	3.75E-02	1.49E+00	1.50E+00
3.375	-1.40E-01	-1.32E-01	2.55E-02	3.50E-02	1.32E+00	1.33E+00
3.625	-1.28E-01	-1.20E-01	3.20E-02	4.15E-02	1.09E+00	1.10E+00
3.875	-7.66E-02	-6.87E-02	-1.79E-03	7.68E-03	9.53E-01	9.65E-01
4.125	-6.36E-02	-5.57E-02	-9.34E-04	8.53E-03	6.89E-01	7.01E-01
4.375	-4.01E-02	-3.22E-02	-2.41E-02	-1.47E-02	4.96E-01	5.08E-01
4.625	-5.16E-02	-4.37E-02	-1.87E-02	-9.25E-03	3.37E-01	3.48E-01
4.875	-3.89E-02	-3.11E-02	3.96E-03	1.34E-02	2.79E-01	2.90E-01
5.125	-4.00E-02	-3.21E-02	1.23E-02	2.18E-02	2.54E-01	2.66E-01
5.375	-2.65E-02	-1.86E-02	1.86E-02	2.81E-02	2.25E-01	2.36E-01
5.625	-2.76E-02	-1.98E-02	1.48E-02	2.43E-02	1.93E-01	2.04E-01
5.875	-2.24E-02	-1.45E-02	1.46E-02	2.41E-02	1.56E-01	1.67E-01
6.125	-2.36E-02	-1.58E-02	1.16E-02	2.11E-02	1.21E-01	1.32E-01
6.375	-2.13E-02	-1.35E-02	3.88E-03	1.33E-02	8.79E-02	9.94E-02
6.625	-1.86E-02	-1.07E-02	-1.79E-03	7.68E-03	6.89E-02	8.04E-02
6.875	-1.37E-02	-5.85E-03	-1.43E-02	-4.82E-03	6.90E-02	8.06E-02
7.125	-1.51E-02	-7.24E-03	-1.53E-02	-5.83E-03	6.27E-02	7.43E-02
7.375	-2.00E-02	-1.22E-02	-1.79E-02	-8.39E-03	5.08E-02	6.23E-02
7.625	-1.71E-02	-9.23E-03	-2.01E-02	-1.06E-02	4.93E-02	6.08E-02
7.875	-1.67E-02	-8.85E-03	-2.03E-02	-1.09E-02	4.70E-02	5.85E-02
8.125	-9.18E-03	-1.32E-03	-1.90E-02	-9.56E-03	3.25E-02	4.41E-02
8.375	-1.20E-02	-4.16E-03	-1.58E-02	-6.30E-03	3.15E-02	4.30E-02
8.625	-1.40E-02	-6.16E-03	-9.40E-03	6.85E-05	3.01E-02	4.17E-02
8.875	-1.56E-02	-7.70E-03	-1.89E-02	-9.48E-03	-2.97E-03	8.58E-03
9.125	-1.09E-02	-3.01E-03	-1.16E-02	-2.11E-03	-7.20E-03	4.35E-03
9.375	-1.11E-02	-3.24E-03	-5.59E-03	3.87E-03	-4.31E-03	7.24E-03
9.625	-9.49E-03	-1.63E-03	-4.82E-03	4.65E-03	-7.35E-03	4.20E-03
9.875	-9.56E-03	-1.70E-03	-6.14E-03	3.33E-03	-1.07E-02	8.60E-04
10.125	-1.31E-02	-5.24E-03	-2.88E-03	6.59E-03	-1.31E-02	-1.52E-03
10.375	-1.06E-02	-2.78E-03	-1.25E-03	8.22E-03	-1.18E-02	-2.53E-04
10.625	-1.66E-02	-8.70E-03	-2.80E-03	6.67E-03	-2.03E-02	-8.79E-03
10.875	-1.29E-02	-5.08E-03	1.78E-03	1.12E-02	-1.95E-02	-7.97E-03

Table 8. MAPO test number 5 data (Continued).

Time	x (g's)	x Corrected (g's)	y (g's)	y Corrected (g's)	z (g's)	z Corrected (g's)
11.125	-1.10E-02	-3.16E-03	4.35E-03	1.38E-02	-5.35E-03	6.21E-03
11.375	-1.36E-02	-5.78E-03	2.00E-02	2.94E-02	-2.00E-03	9.55E-03
11.625	-1.21E-02	-4.24E-03	1.86E-02	2.81E-02	-4.38E-03	7.17E-03
11.875	-1.30E-02	-5.16E-03	1.16E-02	2.10E-02	-1.46E-02	-3.00E-03
12.125	-9.18E-03	-1.32E-03	-1.01E-03	8.45E-03	-1.49E-02	-3.37E-03
12.375	-1.38E-02	-5.93E-03	1.22E-02	2.17E-02	-1.52E-02	-3.67E-03
12.625	-1.58E-02	-7.93E-03	4.97E-03	1.44E-02	-2.14E-02	-9.83E-03
12.875	-1.85E-02	-1.06E-02	-8.85E-03	6.12E-04	-2.77E-02	-1.61E-02
13.125	-1.79E-02	-1.01E-02	-1.13E-02	-1.79E-03	-2.35E-02	-1.19E-02
13.375	-1.51E-02	-7.24E-03	-1.01E-03	8.45E-03	-2.35E-02	-1.20E-02
13.625	-1.47E-02	-6.85E-03	-4.58E-03	4.88E-03	-1.86E-02	-7.01E-03
13.875	-1.42E-02	-6.39E-03	-2.72E-03	6.75E-03	-1.02E-02	1.31E-03
14.125	-1.09E-02	-3.01E-03	-1.11E-02	-1.64E-03	-1.09E-02	6.38E-04
14.375	-1.05E-02	-2.63E-03	-8.08E-03	1.39E-03	-1.13E-02	2.66E-04
14.625	-6.64E-03	1.22E-03	-1.00E-02	-5.53E-04	-9.80E-03	1.75E-03
14.875	-7.72E-03	1.40E-04	-1.03E-02	-8.63E-04	-1.13E-02	2.66E-04
15.125	-6.87E-03	9.85E-04	-9.01E-03	4.57E-04	-1.26E-02	-1.07E-03
15.375	-7.03E-03	8.32E-04	-9.86E-03	-3.97E-04	-1.09E-02	6.38E-04
15.625	-6.95E-03	9.08E-04	-9.32E-03	1.46E-04	-1.09E-02	6.38E-04
15.875	-8.18E-03	-3.21E-04	-9.79E-03	-3.20E-04	-1.20E-02	-4.76E-04
16.125	-6.95E-03	9.08E-04	-1.05E-02	-1.02E-03	-8.69E-03	2.86E-03
16.375	-6.41E-03	1.45E-03	-9.94E-03	-4.75E-04	-1.04E-02	1.16E-03
16.625	-7.64E-03	2.17E-04	-8.08E-03	1.39E-03	-1.32E-02	-1.66E-03
16.875	-9.41E-03	-1.55E-03	-9.24E-03	2.24E-04	-1.37E-02	-2.11E-03
17.125	-7.87E-03	-1.36E-05	-7.30E-03	2.16E-03	-1.31E-02	-1.52E-03
17.375	-8.64E-03	-7.82E-04	-8.93E-03	5.34E-04	-1.19E-02	-3.28E-04
17.625	-7.41E-03	4.47E-04	-1.03E-02	-8.63E-04	-1.25E-02	-9.96E-04
17.875	-6.64E-03	1.22E-03	-9.63E-03	-1.64E-04	-1.25E-02	-9.96E-04
18.125	-7.87E-03	-1.36E-05	-9.47E-03	-9.13E-06	-1.06E-02	9.35E-04
18.375	-5.57E-03	2.29E-03	-8.54E-03	9.23E-04	-1.24E-02	-8.47E-04
18.625	-8.64E-03	-7.82E-04	-9.32E-03	1.46E-04	-1.31E-02	-1.59E-03
18.875	-8.64E-03	-7.82E-04	-1.11E-02	-1.64E-03	-1.02E-02	1.38E-03
19.125	-4.38E-02	-3.59E-02	-5.67E-02	-4.72E-02	2.08E-02	3.23E-02
19.375	-8.36E-02	-7.57E-02	-6.63E-02	-5.68E-02	4.24E-02	5.39E-02
19.625	-1.14E-02	-3.55E-03	-5.83E-03	3.64E-03	-1.72E-02	-5.67E-03
19.875	-1.16E-02	-3.70E-03	-1.26E-02	-3.11E-03	-1.81E-02	-6.56E-03
20.125	-6.41E-03	1.45E-03	-3.16E-02	-2.21E-02	-2.89E-02	-1.73E-02
20.375	-1.53E-02	-7.47E-03	-5.09E-02	-4.15E-02	-4.68E-02	-3.52E-02
20.625	-1.57E-02	-7.85E-03	-3.85E-02	-2.90E-02	-4.95E-02	-3.80E-02
20.875	-9.33E-03	-1.47E-03	-1.64E-02	-6.92E-03	-2.93E-02	-1.78E-02
21.125	-1.65E-02	-8.62E-03	-9.79E-03	-3.20E-04	-1.30E-02	-1.44E-03
21.375	-9.72E-03	-1.86E-03	1.30E-02	2.24E-02	-3.86E-03	7.69E-03
21.625	-6.95E-03	9.08E-04	4.63E-04	9.93E-03	-1.37E-02	-2.18E-03
21.875	-7.26E-03	6.01E-04	-1.18E-02	-2.34E-03	-1.42E-02	-2.63E-03
22.125	-1.16E-02	-3.70E-03	-3.34E-03	6.12E-03	-1.21E-02	-5.50E-04
22.375	-7.18E-03	6.78E-04	-8.85E-03	6.12E-04	-1.25E-02	-9.96E-04
22.625	-9.41E-03	-1.55E-03	-9.16E-03	3.01E-04	-1.22E-02	-6.24E-04
22.875	-8.41E-03	-5.51E-04	-9.86E-03	-3.97E-04	-1.16E-02	-3.06E-05
23.125	-5.18E-03	2.68E-03	-8.47E-03	1.00E-03	-1.95E-02	-7.97E-03
23.375	-9.56E-03	-1.70E-03	-3.88E-03	5.58E-03	-1.83E-02	-6.71E-03
23.625	-1.41E-02	-6.24E-03	-4.60E-02	-3.66E-02	-1.72E-02	-5.67E-03
23.875	-1.42E-03	6.44E-03	-1.08E-02	-1.33E-03	-1.41E-02	-2.55E-03
24.125	-6.41E-03	1.45E-03	-1.03E-02	-8.63E-04	-1.56E-02	-4.04E-03
24.375	6.34E-03	1.42E-02	-1.86E-02	-9.09E-03	-6.90E-03	4.65E-03
24.625	8.11E-03	1.60E-02	-1.58E-02	-6.38E-03	-2.08E-03	9.47E-03
24.875	1.50E-03	9.36E-03	-1.51E-02	-5.60E-03	-2.67E-02	-1.52E-02
25.125	9.42E-03	1.73E-02	1.33E-02	2.27E-02	-5.84E-02	-4.69E-02
25.375	1.21E-02	2.00E-02	3.34E-03	1.28E-02	-5.30E-02	-4.15E-02

Table 8. MAPO test number 5 data (Continued).

Time	x (g's)	x Corrected (g's)	y (g's)	y Corrected (g's)	z (g's)	z Corrected (g's)
25.625	3.35E-03	1.12E-02	-1.48E-02	-5.29E-03	-1.39E-02	-2.33E-03
25.875	-2.72E-03	5.13E-03	-3.11E-03	6.36E-03	-1.16E-02	-3.06E-05
26.125	-2.64E-02	-1.85E-02	-3.86E-02	-2.91E-02	2.02E-02	3.17E-02
26.375	-3.94E-02	-3.15E-02	1.27E-02	2.21E-02	4.37E-02	5.53E-02
26.625	-5.72E-03	2.14E-03	2.73E-01	2.82E-01	3.37E-01	3.49E-01
26.875	-1.07E-01	-9.89E-02	3.14E-01	3.23E-01	4.37E-01	4.49E-01
27.125	7.89E-02	8.67E-02	3.58E-01	3.68E-01	4.55E-01	4.67E-01
27.375	-6.64E-03	1.22E-03	3.84E-01	3.93E-01	4.52E-01	4.64E-01
27.625	1.23E-02	2.01E-02	3.40E-01	3.50E-01	4.96E-01	5.07E-01
27.875	-7.41E-03	4.47E-04	2.06E-01	2.15E-01	6.21E-01	6.32E-01
28.125	1.27E-03	9.13E-03	1.67E-01	1.77E-01	6.04E-01	6.16E-01
28.375	-1.88E-04	7.67E-03	3.65E-03	1.31E-02	6.38E-01	6.49E-01
28.625	5.04E-03	1.29E-02	-1.65E-02	-7.07E-03	6.48E-01	6.60E-01
28.875	2.96E-03	1.08E-02	-3.42E-02	-2.48E-02	6.70E-01	6.81E-01
29.125	-6.57E-03	1.29E-03	-1.47E-02	-5.21E-03	7.17E-01	7.29E-01
29.375	-1.51E-02	-7.24E-03	-2.06E-02	-1.11E-02	7.91E-01	8.02E-01
29.625	-2.06E-02	-1.28E-02	-2.11E-02	-1.17E-02	8.92E-01	9.03E-01
29.875	-2.24E-02	-1.45E-02	-1.10E-02	-1.56E-03	9.86E-01	9.98E-01
30.125	-2.13E-02	-1.35E-02	-7.69E-03	1.78E-03	1.05E+00	1.07E+00
30.375	-3.06E-02	-2.28E-02	3.18E-03	1.26E-02	1.11E+00	1.12E+00
30.625	-3.17E-02	-2.38E-02	1.14E-02	2.09E-02	1.15E+00	1.16E+00
30.875	-2.72E-02	-1.93E-02	1.80E-02	2.75E-02	1.19E+00	1.20E+00
31.125	-2.67E-02	-1.88E-02	2.14E-02	3.09E-02	1.21E+00	1.22E+00
31.375	-2.35E-02	-1.57E-02	1.93E-02	2.88E-02	1.17E+00	1.18E+00
31.625	-1.60E-02	-8.16E-03	2.29E-02	3.24E-02	1.12E+00	1.13E+00
31.875	-8.03E-03	-1.67E-04	1.90E-02	2.85E-02	1.09E+00	1.10E+00
32.125	-1.30E-02	-5.16E-03	-1.58E-04	9.31E-03	1.12E+00	1.13E+00
32.375	-1.66E-02	-8.70E-03	-9.24E-03	2.24E-04	1.12E+00	1.13E+00
32.625	-1.17E-02	-3.86E-03	-5.98E-03	3.48E-03	1.06E+00	1.07E+00
32.875	-4.64E-03	3.21E-03	2.64E-03	1.21E-02	1.03E+00	1.05E+00
33.125	3.58E-03	1.14E-02	3.85E-04	9.85E-03	1.03E+00	1.04E+00
33.375	2.19E-03	1.01E-02	5.51E-03	1.50E-02	1.03E+00	1.04E+00
33.625	4.50E-03	1.24E-02	1.09E-02	2.04E-02	1.06E+00	1.07E+00
33.875	2.66E-03	1.05E-02	1.20E-02	2.15E-02	1.12E+00	1.13E+00
34.125	5.04E-04	8.36E-03	9.94E-03	1.94E-02	1.21E+00	1.23E+00
34.375	-1.11E-02	-3.24E-03	4.11E-03	1.36E-02	1.30E+00	1.31E+00
34.625	-1.25E-02	-4.62E-03	-1.06E-02	-1.10E-03	1.36E+00	1.37E+00
34.875	-1.59E-02	-8.00E-03	-4.66E-03	4.80E-03	1.43E+00	1.44E+00
35.125	-1.13E-02	-3.47E-03	3.85E-04	9.85E-03	1.45E+00	1.46E+00
35.375	-1.19E-02	-4.01E-03	7.61E-03	1.71E-02	1.42E+00	1.44E+00
35.625	-4.95E-04	7.36E-03	1.37E-02	2.31E-02	1.38E+00	1.40E+00
35.875	1.00E-02	1.79E-02	9.70E-03	1.92E-02	1.34E+00	1.36E+00
36.125	1.02E-02	1.80E-02	6.96E-04	1.02E-02	1.33E+00	1.34E+00
36.375	1.19E-02	1.97E-02	-1.63E-03	7.83E-03	1.33E+00	1.34E+00
36.625	9.26E-03	1.71E-02	-1.56E-03	7.91E-03	1.34E+00	1.35E+00
36.875	1.16E-02	1.94E-02	-2.80E-03	6.67E-03	1.37E+00	1.38E+00
37.125	8.19E-03	1.60E-02	-4.51E-03	4.96E-03	1.40E+00	1.41E+00
37.375	8.88E-03	1.67E-02	-6.84E-03	2.63E-03	1.43E+00	1.44E+00
37.625	9.80E-03	1.77E-02	-1.11E-02	-1.64E-03	1.45E+00	1.46E+00
37.875	8.57E-03	1.64E-02	-2.49E-02	-1.55E-02	1.47E+00	1.48E+00
38.125	1.06E-02	1.84E-02	-1.74E-02	-7.93E-03	1.48E+00	1.49E+00
38.375	1.65E-02	2.43E-02	-1.20E-02	-2.57E-03	1.48E+00	1.49E+00
38.625	1.63E-02	2.42E-02	2.79E-03	1.23E-02	1.48E+00	1.49E+00
38.875	2.26E-02	3.05E-02	1.04E-02	1.99E-02	1.49E+00	1.50E+00
39.125	2.32E-02	3.10E-02	2.07E-02	3.02E-02	1.47E+00	1.49E+00
39.375	2.31E-02	3.10E-02	2.02E-02	2.96E-02	1.48E+00	1.49E+00
39.625	2.34E-02	3.13E-02	2.39E-02	3.34E-02	1.48E+00	1.49E+00
39.875	2.62E-02	3.41E-02	1.54E-02	2.49E-02	1.50E+00	1.51E+00

Table 9. MAPO test number 23 data.

Test File: MAPOTEST.023 Test Date: Tue, 12-10-1996 No. Channels: 3 Sam/sec: 128      Average      32 pt centered Start: 10:36:13:16    End: 10:36:53:20 Low-g Range start    10:36:24    (11 sec) end      10:36:37    (24 sec) Accelerometer Bias Average Interval (21 to 24 sec)						
Bias Values $x$ -0.0082 (g's) $y$ -0.0096 $z$ -0.0121						
Time Stamp Offset Between Data and Video      1 sec						
Time	$x$ (g's)	$x$ Corrected (g's)	$y$ (g's)	$y$ Corrected (g's)	$z$ (g's)	$z$ Corrected (g's)
0.125	-1.01E-01	-9.25E-02	1.75E+00	1.76E+00	3.72E-02	4.93E-02
0.375	-9.41E-02	-8.58E-02	1.82E+00	1.83E+00	-1.78E-03	1.03E-02
0.625	-1.01E-01	-9.28E-02	1.77E+00	1.78E+00	5.17E-02	6.38E-02
0.875	-9.35E-02	-8.52E-02	1.78E+00	1.79E+00	1.31E-02	2.52E-02
1.125	-9.61E-02	-8.78E-02	1.66E+00	1.67E+00	6.83E-02	8.04E-02
1.375	-9.48E-02	-8.65E-02	1.60E+00	1.61E+00	3.20E-02	4.41E-02
1.625	-7.13E-02	-6.31E-02	1.58E+00	1.59E+00	4.15E-02	5.36E-02
1.875	-9.68E-02	-8.85E-02	1.55E+00	1.56E+00	4.91E-02	6.13E-02
2.125	-8.57E-02	-7.75E-02	1.55E+00	1.56E+00	5.54E-02	6.75E-02
2.375	-9.09E-02	-8.26E-02	1.57E+00	1.58E+00	4.67E-02	5.88E-02
2.625	-9.65E-02	-8.83E-02	1.59E+00	1.60E+00	3.37E-02	4.58E-02
2.875	-9.65E-02	-8.82E-02	1.55E+00	1.56E+00	3.20E-02	4.41E-02
3.125	-9.78E-02	-8.95E-02	1.50E+00	1.51E+00	1.70E-02	2.91E-02
3.375	-9.81E-02	-8.98E-02	1.48E+00	1.49E+00	2.63E-02	3.84E-02
3.625	-8.99E-02	-8.16E-02	1.42E+00	1.43E+00	3.51E-02	4.72E-02
3.875	-8.55E-02	-7.72E-02	1.30E+00	1.31E+00	1.56E-02	2.77E-02
4.125	-8.86E-02	-8.04E-02	1.17E+00	1.18E+00	-1.35E-02	-1.39E-03
4.375	-6.33E-02	-5.50E-02	9.69E-01	9.79E-01	2.00E-03	1.41E-02
4.625	-3.97E-02	-3.14E-02	7.39E-01	7.48E-01	-9.35E-03	2.77E-03
4.875	-3.36E-02	-2.54E-02	5.32E-01	5.41E-01	1.03E-02	2.24E-02
5.125	-3.82E-02	-3.00E-02	3.85E-01	3.94E-01	-1.31E-02	-1.02E-03
5.375	-3.06E-02	-2.24E-02	2.88E-01	2.98E-01	-1.31E-02	-9.47E-04
5.625	-3.65E-02	-2.83E-02	2.03E-01	2.12E-01	-5.64E-03	6.48E-03
5.875	-2.33E-02	-1.51E-02	1.60E-01	1.70E-01	-9.28E-03	2.84E-03
6.125	-1.82E-02	-9.93E-03	1.55E-01	1.65E-01	4.75E-03	1.69E-02
6.375	-2.00E-02	-1.18E-02	1.63E-01	1.72E-01	5.64E-03	1.78E-02
6.625	-1.43E-02	-6.09E-03	1.85E-01	1.95E-01	1.09E-02	2.30E-02
6.875	-1.34E-02	-5.17E-03	1.94E-01	2.04E-01	7.20E-03	1.93E-02
7.125	-1.56E-02	-7.32E-03	1.77E-01	1.86E-01	7.42E-05	1.22E-02
7.375	-1.38E-02	-5.55E-03	1.29E-01	1.39E-01	-7.05E-03	5.07E-03
7.625	-1.68E-02	-8.55E-03	6.60E-02	7.56E-02	-1.06E-02	1.50E-03
7.875	-1.42E-02	-5.94E-03	3.76E-02	4.72E-02	-9.65E-03	2.47E-03
8.125	-1.86E-02	-1.04E-02	3.59E-02	4.55E-02	-1.09E-02	1.21E-03
8.375	-1.41E-02	-5.86E-03	3.57E-02	4.53E-02	-8.83E-03	3.29E-03
8.625	-1.26E-02	-4.40E-03	4.47E-02	5.43E-02	-1.16E-02	5.38E-04
8.875	-1.32E-02	-4.94E-03	4.68E-02	5.64E-02	-9.95E-03	2.17E-03
9.125	-1.39E-02	-5.63E-03	4.89E-02	5.85E-02	-9.28E-03	2.84E-03
9.375	-1.29E-02	-4.63E-03	5.17E-02	6.13E-02	-1.52E-02	-3.10E-03
9.625	-1.13E-02	-3.09E-03	3.89E-02	4.85E-02	-1.31E-02	-1.02E-03
9.875	-1.16E-02	-3.40E-03	1.36E-02	2.32E-02	-1.92E-02	-7.11E-03
10.125	-1.02E-02	-1.94E-03	3.65E-03	1.33E-02	-1.76E-02	-5.48E-03
10.375	-1.21E-02	-3.86E-03	5.74E-03	1.54E-02	-1.90E-02	-6.89E-03
10.625	-1.11E-02	-2.86E-03	-8.04E-05	9.54E-03	-1.53E-02	-3.17E-03
10.875	-1.02E-02	-1.94E-03	-6.68E-03	2.94E-03	-1.34E-02	-1.32E-03

Table 9. MAPO test number 23 data (Continued).

Time	x (g's)	x Corrected (g's)	y (g's)	y Corrected (g's)	z (g's)	z Corrected (g's)
11.125	-1.29E-02	-4.63E-03	-1.88E-02	-9.17E-03	-7.28E-03	4.84E-03
11.375	-1.46E-02	-6.40E-03	-2.39E-02	-1.43E-02	-7.80E-03	4.32E-03
11.625	-1.79E-02	-9.62E-03	-3.14E-02	-2.18E-02	-6.53E-03	5.59E-03
11.875	-2.09E-02	-1.26E-02	1.18E-02	2.14E-02	-2.13E-02	-9.19E-03
12.125	-2.40E-02	-1.58E-02	2.40E-02	3.36E-02	-2.41E-02	-1.19E-02
12.375	-2.08E-02	-1.25E-02	8.46E-03	1.81E-02	-2.09E-02	-8.82E-03
12.625	-1.59E-02	-7.63E-03	-7.92E-03	1.70E-03	-1.08E-02	1.35E-03
12.875	-1.57E-02	-7.47E-03	-2.80E-03	6.82E-03	-1.60E-02	-3.84E-03
13.125	-1.46E-02	-6.32E-03	-6.99E-03	2.63E-03	-1.66E-02	-4.44E-03
13.375	-1.43E-02	-6.09E-03	-1.34E-02	-3.74E-03	-1.36E-02	-1.47E-03
13.625	-1.09E-02	-2.63E-03	-1.03E-02	-7.12E-04	-1.60E-02	-3.84E-03
13.875	-1.62E-02	-7.93E-03	-1.19E-02	-2.26E-03	-1.42E-02	-2.06E-03
14.125	-1.76E-02	-9.39E-03	-1.03E-02	-7.12E-04	-1.66E-02	-4.51E-03
14.375	-1.60E-02	-7.78E-03	-1.28E-02	-3.20E-03	-1.49E-02	-2.80E-03
14.625	-1.51E-02	-6.86E-03	-1.36E-02	-3.97E-03	-1.96E-02	-7.48E-03
14.875	-1.83E-02	-1.01E-02	-8.00E-03	1.62E-03	-2.33E-02	-1.12E-02
15.125	-2.02E-02	-1.20E-02	4.42E-03	1.40E-02	-2.34E-02	-1.13E-02
15.375	-2.00E-02	-1.18E-02	1.47E-03	1.11E-02	-2.41E-02	-1.19E-02
15.625	-1.60E-02	-7.78E-03	-6.84E-03	2.78E-03	-1.33E-02	-1.17E-03
15.875	-1.62E-02	-8.01E-03	-2.36E-04	9.38E-03	-1.45E-02	-2.36E-03
16.125	-1.51E-02	-6.86E-03	-1.20E-02	-2.42E-03	-1.79E-02	-5.77E-03
16.375	-7.33E-03	9.03E-04	-1.14E-02	-1.80E-03	-1.16E-02	5.38E-04
16.625	-7.41E-03	8.26E-04	-9.47E-03	1.42E-04	-1.08E-02	1.35E-03
16.875	-7.64E-03	5.95E-04	-1.06E-02	-1.02E-03	-1.02E-02	1.95E-03
17.125	-6.80E-03	1.44E-03	-9.09E-03	5.31E-04	-1.25E-02	-4.27E-04
17.375	-7.18E-03	1.06E-03	-7.61E-03	2.01E-03	-1.50E-02	-2.88E-03
17.625	-9.18E-03	-9.41E-04	-7.30E-03	2.32E-03	-1.48E-02	-2.65E-03
17.875	-7.41E-03	8.26E-04	-1.00E-02	-4.01E-04	-1.23E-02	-2.04E-04
18.125	-9.10E-03	-8.64E-04	-8.85E-03	7.63E-04	-1.34E-02	-1.32E-03
18.375	-1.02E-02	-1.94E-03	-8.00E-03	1.62E-03	-1.25E-02	-4.27E-04
18.625	-6.95E-03	1.29E-03	-1.01E-02	-4.79E-04	-1.22E-02	-5.57E-05
18.875	-8.18E-03	5.76E-05	-8.78E-03	8.41E-04	-1.47E-02	-2.58E-03
19.125	-8.41E-03	-1.73E-04	-8.31E-03	1.31E-03	-1.41E-02	-1.99E-03
19.375	-7.64E-03	5.95E-04	-9.94E-03	-3.23E-04	-1.16E-02	5.38E-04
19.625	-9.25E-03	-1.02E-03	-8.00E-03	1.62E-03	-1.42E-02	-2.06E-03
19.875	-7.72E-03	5.19E-04	-1.01E-02	-4.79E-04	-1.08E-02	1.28E-03
20.125	-6.41E-03	1.82E-03	-1.24E-02	-2.81E-03	-1.07E-02	1.43E-03
20.375	-6.64E-03	1.59E-03	-7.77E-03	1.85E-03	-1.26E-02	-5.01E-04
20.625	-5.95E-03	2.29E-03	-1.08E-02	-1.18E-03	-1.01E-02	2.02E-03
20.875	-7.72E-03	5.19E-04	-9.24E-03	3.75E-04	-1.23E-02	-2.04E-04
21.125	-7.10E-03	1.13E-03	-9.01E-03	6.08E-04	-1.25E-02	-3.53E-04
21.375	-7.95E-03	2.88E-04	-1.01E-02	-4.79E-04	-1.10E-02	1.13E-03
21.625	-7.87E-03	3.65E-04	-8.93E-03	6.86E-04	-1.34E-02	-1.24E-03
21.875	-6.80E-03	1.44E-03	-1.11E-02	-1.49E-03	-1.05E-02	1.58E-03
22.125	-9.79E-03	-1.56E-03	-1.07E-02	-1.10E-03	-1.23E-02	-2.04E-04
22.375	-8.87E-03	-6.34E-04	-8.62E-03	9.96E-04	-1.20E-02	1.67E-04
22.625	-6.80E-03	1.44E-03	-1.06E-02	-9.45E-04	-9.73E-03	2.39E-03
22.875	-9.49E-03	-1.25E-03	-8.93E-03	6.86E-04	-1.44E-02	-2.28E-03
23.125	-8.10E-03	1.34E-04	-1.00E-02	-4.01E-04	-1.11E-02	9.84E-04
23.375	-9.18E-03	-9.41E-04	-9.47E-03	1.42E-04	-1.25E-02	-4.27E-04
23.625	-8.18E-03	5.76E-05	-8.93E-03	6.86E-04	-1.31E-02	-1.02E-03
23.875	-8.72E-03	-4.80E-04	-9.01E-03	6.08E-04	-1.28E-02	-7.24E-04
24.125	-2.87E-02	-2.05E-02	8.23E-03	1.78E-02	-1.81E-02	-5.99E-03
24.375	-7.53E-02	-6.70E-02	3.36E-02	4.32E-02	-3.74E-02	-2.53E-02
24.625	-6.41E-02	-5.59E-02	2.65E-02	3.61E-02	-3.82E-02	-2.61E-02
24.875	-4.84E-02	-4.02E-02	1.18E-02	2.14E-02	-2.67E-02	-1.45E-02
25.125	-3.73E-02	-2.91E-02	1.16E-02	2.13E-02	-2.26E-02	-1.05E-02
25.375	-5.01E-02	-4.18E-02	2.56E-03	1.22E-02	-2.47E-02	-1.26E-02

Table 9. MAPO test number 23 data (Continued).

Time	x (g's)	x Corrected (g's)	y (g's)	y Corrected (g's)	z (g's)	z Corrected (g's)
25.625	-4.53E-02	-3.71E-02	-6.84E-03	2.78E-03	-2.80E-02	-1.59E-02
25.875	-3.30E-02	-2.48E-02	-1.69E-02	-7.31E-03	-2.23E-02	-1.02E-02
26.125	-3.24E-02	-2.41E-02	-8.54E-03	1.07E-03	-2.22E-02	-1.01E-02
26.375	-3.18E-02	-2.36E-02	3.08E-04	9.92E-03	-2.35E-02	-1.13E-02
26.625	-5.01E-02	-4.19E-02	-4.35E-02	-3.39E-02	-7.35E-03	4.77E-03
26.875	-4.15E-02	-3.33E-02	-2.80E-03	6.82E-03	-7.48E-02	-6.27E-02
27.125	-4.64E-03	3.59E-03	-3.88E-02	-2.92E-02	-1.01E-01	-8.90E-02
27.375	5.31E-02	6.14E-02	1.39E-03	1.10E-02	-1.31E-01	-1.19E-01
27.625	3.65E-03	1.19E-02	1.54E-02	2.51E-02	-4.75E-02	-3.54E-02
27.875	-1.09E-02	-2.63E-03	-1.58E-04	9.46E-03	6.06E-02	7.27E-02
28.125	-7.10E-03	1.13E-03	-9.33E-02	-8.37E-02	-5.10E-02	-3.89E-02
28.375	-1.65E-03	6.59E-03	-3.35E-02	-2.38E-02	8.92E-02	1.01E-01
28.625	2.70E-02	3.52E-02	7.65E-02	8.61E-02	2.12E-01	2.24E-01
28.875	1.13E-01	1.21E-01	2.84E-01	2.93E-01	1.88E-01	2.00E-01
29.125	2.19E-01	2.27E-01	2.57E-01	2.67E-01	1.07E-01	1.19E-01
29.375	3.65E-01	3.73E-01	3.88E-01	3.97E-01	9.99E-02	1.12E-01
29.625	3.45E-01	3.53E-01	5.26E-01	5.36E-01	1.96E-01	2.08E-01
29.875	-1.00E-02	-1.79E-03	5.38E-01	5.48E-01	7.71E-02	8.92E-02
30.125	-1.27E-01	-1.19E-01	7.64E-01	7.73E-01	2.02E-01	2.14E-01
30.375	2.57E-02	3.39E-02	6.08E-01	6.18E-01	8.96E-02	1.02E-01
30.625	-2.65E-04	7.97E-03	7.40E-01	7.50E-01	-3.48E-02	-2.27E-02
30.875	3.19E-03	1.14E-02	7.53E-01	7.62E-01	4.90E-03	1.70E-02
31.125	-6.03E-03	2.21E-03	7.98E-01	8.08E-01	-9.35E-03	2.77E-03
31.375	-6.87E-03	1.36E-03	8.26E-01	8.36E-01	-1.26E-03	1.09E-02
31.625	-1.36E-02	-5.40E-03	8.79E-01	8.89E-01	7.42E-05	1.22E-02
31.875	-9.41E-03	-1.17E-03	9.45E-01	9.54E-01	5.20E-03	1.73E-02
32.125	-1.09E-02	-2.63E-03	1.02E+00	1.03E+00	1.18E-02	2.39E-02
32.375	-1.85E-02	-1.02E-02	1.09E+00	1.10E+00	5.35E-03	1.75E-02
32.625	-2.19E-02	-1.37E-02	1.13E+00	1.14E+00	4.38E-03	1.65E-02
32.875	-2.19E-02	-1.37E-02	1.18E+00	1.19E+00	1.13E-02	2.34E-02
33.125	-1.92E-02	-1.09E-02	1.22E+00	1.23E+00	8.02E-03	2.01E-02
33.375	-2.06E-02	-1.24E-02	1.24E+00	1.25E+00	1.01E-02	2.22E-02
33.625	-2.35E-02	-1.53E-02	1.27E+00	1.27E+00	3.64E-03	1.58E-02
33.875	-2.58E-02	-1.75E-02	1.28E+00	1.29E+00	9.43E-03	2.15E-02
34.125	-2.39E-02	-1.57E-02	1.29E+00	1.30E+00	1.14E-02	2.36E-02
34.375	-2.45E-02	-1.62E-02	1.30E+00	1.31E+00	1.43E-02	2.64E-02
34.625	-2.38E-02	-1.55E-02	1.31E+00	1.32E+00	2.01E-02	3.22E-02
34.875	-2.78E-02	-1.95E-02	1.32E+00	1.33E+00	1.77E-02	2.99E-02
35.125	-1.65E-02	-8.24E-03	1.33E+00	1.34E+00	1.95E-02	3.16E-02
35.375	-1.67E-02	-8.47E-03	1.27E+00	1.28E+00	2.50E-02	3.71E-02
35.625	-8.87E-03	-6.34E-04	1.20E+00	1.21E+00	2.23E-02	3.45E-02
35.875	7.50E-03	1.57E-02	1.10E+00	1.11E+00	2.16E-02	3.37E-02
36.125	1.03E-02	1.85E-02	1.03E+00	1.04E+00	1.11E-02	2.33E-02
36.375	1.93E-02	2.75E-02	9.76E-01	9.86E-01	4.68E-03	1.68E-02
36.625	2.17E-02	2.99E-02	9.50E-01	9.60E-01	1.19E-03	1.33E-02
36.875	2.34E-02	3.16E-02	9.76E-01	9.85E-01	-1.78E-03	1.03E-02
37.125	2.35E-02	3.17E-02	1.02E+00	1.03E+00	1.26E-03	1.34E-02
37.375	2.16E-02	2.99E-02	1.05E+00	1.06E+00	-3.64E-03	8.48E-03
37.625	2.16E-02	2.98E-02	1.09E+00	1.10E+00	-1.35E-02	-1.39E-03
37.875	8.80E-03	1.70E-02	1.13E+00	1.14E+00	-2.23E-02	-1.02E-02
38.125	1.33E-02	2.16E-02	1.15E+00	1.16E+00	9.28E-03	2.14E-02
38.375	2.24E-02	3.06E-02	1.09E+00	1.10E+00	1.65E-01	1.77E-01
38.625	9.49E-03	1.77E-02	1.10E+00	1.11E+00	2.52E-01	2.64E-01
38.875	8.34E-03	1.66E-02	1.21E+00	1.22E+00	1.51E-01	1.63E-01
39.125	1.53E-02	2.36E-02	1.40E+00	1.41E+00	-2.49E-02	-1.28E-02
39.375	9.88E-03	1.81E-02	1.42E+00	1.43E+00	4.91E-02	6.13E-02
39.625	3.42E-03	1.17E-02	1.46E+00	1.47E+00	5.84E-02	7.05E-02
39.875	2.89E-03	1.11E-02	1.48E+00	1.49E+00	4.68E-02	5.89E-02

Table 10. MAPO test number 30 data.

Test File: MAPOTEST.030 Test Date: Tue, 12-10-1996 No. Channels: 3 Sam/sec: 128      Average      32 pt centered Start: 10:48:03:23      End: 10:48:43:28 Low-g Range start 10:48:10 (6 sec) end 10:48:15 (11 sec) Accelerometer Bias Average Interval (7 to 10 sec)						
Bias Values $x$ -0.0076 (g's) $y$ -0.0098 $z$ -0.0112						
Time Stamp Offset Between Data and Video      1 sec						
Time	$x$ (g's)	$x$ Corrected (g's)	$y$ (g's)	$y$ Corrected (g's)	$z$ (g's)	$z$ Corrected (g's)
0.125	-1.05E-01	-9.78E-02	5.04E-03	1.49E-02	5.34E-01	5.45E-01
0.375	-6.29E-02	-5.53E-02	3.26E-03	1.31E-02	4.13E-01	4.24E-01
0.625	-4.44E-02	-3.68E-02	-9.86E-03	-3.58E-05	3.24E-01	3.35E-01
0.875	-5.74E-02	-4.98E-02	-7.53E-03	2.29E-03	2.69E-01	2.80E-01
1.125	-4.66E-02	-3.90E-02	9.55E-03	1.94E-02	2.10E-01	2.22E-01
1.375	-4.97E-02	-4.21E-02	9.39E-03	1.92E-02	1.83E-01	1.94E-01
1.625	-4.54E-02	-3.78E-02	4.89E-03	1.47E-02	1.83E-01	1.94E-01
1.875	-3.98E-02	-3.22E-02	7.22E-03	1.70E-02	1.67E-01	1.78E-01
2.125	-3.56E-02	-2.80E-02	5.90E-03	1.57E-02	1.51E-01	1.62E-01
2.375	-2.97E-02	-2.21E-02	-1.10E-02	-1.12E-03	1.40E-01	1.51E-01
2.625	-2.53E-02	-1.77E-02	-8.47E-03	1.36E-03	1.31E-01	1.43E-01
2.875	-2.40E-02	-1.64E-02	-8.47E-03	1.36E-03	1.22E-01	1.34E-01
3.125	-2.19E-02	-1.42E-02	-1.43E-02	-4.46E-03	1.12E-01	1.23E-01
3.375	-2.01E-02	-1.25E-02	-7.07E-03	2.76E-03	9.52E-02	1.06E-01
3.625	-2.08E-02	-1.32E-02	-9.32E-03	5.08E-04	8.21E-02	9.33E-02
3.875	-1.83E-02	-1.07E-02	-1.37E-02	-3.92E-03	7.62E-02	8.75E-02
4.125	-1.87E-02	-1.11E-02	-1.68E-02	-6.95E-03	6.35E-02	7.48E-02
4.375	-1.46E-02	-6.94E-03	-1.39E-02	-4.07E-03	5.12E-02	6.25E-02
4.625	-1.79E-02	-1.02E-02	-5.28E-03	4.54E-03	4.08E-02	5.21E-02
4.875	-1.61E-02	-8.48E-03	-4.82E-03	5.01E-03	3.17E-02	4.29E-02
5.125	-1.76E-02	-1.00E-02	-8.08E-03	1.75E-03	1.83E-02	2.95E-02
5.375	-1.97E-02	-1.21E-02	-8.31E-03	1.52E-03	1.60E-02	2.72E-02
5.625	-2.00E-02	-1.24E-02	-1.24E-02	-2.60E-03	1.91E-02	3.03E-02
5.875	-2.10E-02	-1.34E-02	-1.76E-02	-7.80E-03	1.14E-02	2.27E-02
6.125	-2.01E-02	-1.25E-02	-1.16E-02	-1.74E-03	8.17E-04	1.20E-02
6.375	-1.58E-02	-8.17E-03	-1.32E-03	8.50E-03	1.34E-03	1.26E-02
6.625	-8.72E-03	-1.11E-03	-1.09E-02	-1.05E-03	-4.38E-03	6.85E-03
6.875	-6.18E-03	1.43E-03	-1.01E-02	-2.69E-04	-1.11E-02	9.71E-05
7.125	-6.95E-03	6.62E-04	-1.06E-02	-7.35E-04	-9.35E-03	1.88E-03
7.375	-7.87E-03	-2.60E-04	-8.08E-03	1.75E-03	-1.27E-02	-1.46E-03
7.625	-7.26E-03	3.55E-04	-1.13E-02	-1.43E-03	-8.17E-03	3.07E-03
7.875	-8.10E-03	-4.91E-04	-1.02E-02	-3.46E-04	-1.16E-02	-3.48E-04
8.125	-5.95E-03	1.66E-03	-1.18E-02	-1.98E-03	-8.98E-03	2.25E-03
8.375	-1.04E-02	-2.80E-03	-9.47E-03	3.52E-04	-1.15E-02	-2.74E-04
8.625	-8.03E-03	-4.14E-04	-1.03E-02	-5.02E-04	-1.18E-02	-5.71E-04
8.875	-5.95E-03	1.66E-03	-9.47E-03	3.52E-04	-1.22E-02	-1.02E-03
9.125	-8.56E-03	-9.52E-04	-9.79E-03	4.18E-05	-1.09E-02	3.20E-04
9.375	-7.64E-03	-2.96E-05	-8.54E-03	1.28E-03	-1.28E-02	-1.54E-03
9.625	-6.95E-03	6.62E-04	-9.86E-03	-3.58E-05	-1.13E-02	-5.14E-05
9.875	-8.49E-03	-8.75E-04	-8.85E-03	9.73E-04	-1.28E-02	-1.54E-03
10.125	-6.80E-03	8.16E-04	-9.55E-03	2.75E-04	-1.20E-02	-7.20E-04
10.375	-9.18E-03	-1.57E-03	-8.16E-03	1.67E-03	-1.28E-02	-1.61E-03
10.625	-1.33E-02	-5.72E-03	2.95E-03	1.28E-02	-6.61E-03	4.63E-03
10.875	-1.26E-02	-4.95E-03	1.39E-03	1.12E-02	-8.61E-03	2.62E-03

Table 10. MAPO test number 30 data (Continued).

Time	x (g's)	x Corrected (g's)	y (g's)	y Corrected (g's)	z (g's)	z Corrected (g's)
11.125	-1.42E-02	-6.56E-03	7.06E-03	1.69E-02	-6.46E-03	4.77E-03
11.375	-6.49E-02	-5.73E-02	-8.23E-03	1.59E-03	7.97E-02	9.09E-02
11.625	-1.19E-01	-1.12E-01	3.10E-02	4.08E-02	1.38E-01	1.49E-01
11.875	-1.49E-02	-7.33E-03	2.64E-03	1.25E-02	-1.28E-02	-1.54E-03
12.125	-7.64E-03	-2.96E-05	-7.84E-03	1.98E-03	-1.47E-02	-3.47E-03
12.375	-2.49E-02	-1.73E-02	1.89E-02	2.87E-02	-5.57E-03	5.67E-03
12.625	-4.95E-02	-4.19E-02	3.34E-02	4.32E-02	8.46E-03	1.97E-02
12.875	-5.84E-02	-5.08E-02	2.64E-02	3.62E-02	1.11E-02	2.23E-02
13.125	-4.13E-02	-3.37E-02	4.35E-03	1.42E-02	-6.61E-03	4.63E-03
13.375	-2.87E-02	-2.11E-02	1.08E-03	1.09E-02	-8.02E-03	3.22E-03
13.625	-1.16E-02	-3.95E-03	-7.07E-03	2.76E-03	-1.41E-02	-2.87E-03
13.875	-3.42E-03	4.20E-03	-1.02E-02	-3.46E-04	-1.47E-02	-3.47E-03
14.125	-3.49E-03	4.12E-03	-8.08E-03	1.75E-03	-1.47E-02	-3.47E-03
14.375	-1.31E-02	-5.48E-03	1.73E-02	2.71E-02	-1.08E-02	4.68E-04
14.625	-1.16E-02	-3.95E-03	1.20E-02	2.18E-02	-2.30E-03	8.93E-03
14.875	-6.18E-03	1.43E-03	-1.55E-02	-5.70E-03	-1.37E-02	-2.50E-03
15.125	-6.95E-03	6.62E-04	-2.39E-02	-1.41E-02	-1.59E-02	-4.65E-03
15.375	-5.57E-03	2.05E-03	-1.06E-02	-8.12E-04	-1.01E-02	1.14E-03
15.625	-1.38E-02	-6.18E-03	-7.38E-03	2.45E-03	-1.06E-02	6.17E-04
15.875	-2.28E-02	-1.52E-02	-1.15E-02	-1.67E-03	-1.05E-02	7.65E-04
16.125	-2.25E-02	-1.49E-02	-1.90E-02	-9.20E-03	-3.71E-04	1.09E-02
16.375	-2.59E-02	-1.83E-02	-1.74E-02	-7.57E-03	1.05E-02	2.17E-02
16.625	-1.93E-02	-1.17E-02	-3.27E-02	-2.29E-02	-6.68E-03	4.55E-03
16.875	-1.86E-02	-1.09E-02	-2.79E-02	-1.80E-02	-1.40E-02	-2.72E-03
17.125	-1.51E-02	-7.48E-03	-8.31E-03	1.52E-03	-1.08E-02	4.68E-04
17.375	-1.56E-02	-8.02E-03	-1.16E-02	-1.74E-03	-9.73E-03	1.51E-03
17.625	-1.64E-02	-8.79E-03	-1.08E-02	-9.68E-04	-9.65E-03	1.58E-03
17.875	-1.44E-02	-6.79E-03	-1.49E-02	-5.08E-03	-1.26E-02	-1.39E-03
18.125	-1.04E-02	-2.80E-03	-1.11E-02	-1.28E-03	-2.12E-02	-9.93E-03
18.375	-8.64E-03	-1.03E-03	-1.34E-02	-3.53E-03	-2.36E-02	-1.24E-02
18.625	-6.95E-03	6.62E-04	-8.47E-03	1.36E-03	-1.69E-02	-5.62E-03
18.875	-7.72E-03	-1.06E-04	-1.44E-02	-4.54E-03	-1.73E-02	-6.06E-03
19.125	-1.00E-02	-2.41E-03	-1.71E-02	-7.26E-03	-1.54E-02	-4.13E-03
19.375	-9.72E-03	-2.10E-03	-8.78E-03	1.05E-03	-1.61E-02	-4.88E-03
19.625	-1.42E-02	-6.64E-03	-1.21E-02	-2.29E-03	-1.49E-02	-3.69E-03
19.875	-1.20E-02	-4.41E-03	-2.76E-02	-1.77E-02	-1.40E-02	-2.72E-03
20.125	-1.49E-02	-7.33E-03	-1.58E-02	-5.94E-03	-1.17E-02	-4.23E-04
20.375	-1.49E-03	6.12E-03	-4.20E-03	5.63E-03	-1.36E-02	-2.35E-03
20.625	-2.88E-03	4.73E-03	-1.21E-02	-2.29E-03	-1.26E-02	-1.39E-03
20.875	-9.41E-03	-1.80E-03	-8.16E-03	1.67E-03	-8.61E-03	2.62E-03
21.125	-1.41E-02	-6.48E-03	-4.08E-02	-3.10E-02	-1.22E-02	-1.02E-03
21.375	-1.32E-02	-5.56E-03	-9.63E-03	1.97E-04	-3.19E-03	8.04E-03
21.625	-1.39E-02	-6.33E-03	-7.07E-03	2.76E-03	-1.04E-03	1.02E-02
21.875	-1.40E-02	-6.41E-03	2.33E-03	1.22E-02	1.27E-02	2.39E-02
22.125	-1.39E-02	-6.25E-03	6.91E-03	1.67E-02	1.51E-02	2.63E-02
22.375	-1.99E-02	-1.23E-02	1.67E-02	2.65E-02	2.40E-02	3.52E-02
22.625	-1.42E-02	-6.64E-03	1.39E-03	1.12E-02	1.08E-02	2.20E-02
22.875	-2.43E-02	-1.67E-02	8.28E-02	9.26E-02	2.37E-01	2.49E-01
23.125	-2.12E-02	-1.36E-02	-2.81E-02	-1.83E-02	2.13E-01	2.24E-01
23.375	4.54E-02	5.30E-02	1.50E-01	1.60E-01	2.95E-01	3.06E-01
23.625	2.41E-02	3.17E-02	5.79E-02	6.77E-02	4.06E-01	4.17E-01
23.875	-1.72E-01	-1.64E-01	1.65E-01	1.75E-01	4.65E-01	4.77E-01
24.125	-1.86E-02	-1.09E-02	1.24E-01	1.34E-01	7.22E-01	7.33E-01
24.375	-2.43E-01	-2.36E-01	-8.54E-02	-7.56E-02	1.74E-01	1.85E-01
24.625	2.57E-02	3.33E-02	-1.35E-02	-3.68E-03	8.51E-01	8.62E-01
24.875	-4.43E-02	-3.67E-02	4.84E-02	5.83E-02	6.31E-01	6.42E-01
25.125	-1.32E-01	-1.24E-01	-2.57E-02	-1.59E-02	5.67E-01	5.78E-01
25.375	-8.12E-02	-7.36E-02	6.40E-02	7.38E-02	5.45E-01	5.56E-01

Table 10. MAPO test number 30 data (Continued).

Time	x (g's)	x Corrected (g's)	y (g's)	y Corrected (g's)	z (g's)	z Corrected (g's)
25.625	-1.86E-02	-1.09E-02	-2.74E-02	-1.76E-02	5.90E-01	6.01E-01
25.875	-4.68E-02	-3.92E-02	-1.06E-02	-8.12E-04	5.62E-01	5.73E-01
26.125	8.58E-02	9.34E-02	1.44E-02	2.43E-02	6.39E-01	6.50E-01
26.375	3.18E-01	3.26E-01	-2.58E-02	-1.60E-02	7.20E-01	7.31E-01
26.625	1.30E-01	1.38E-01	-3.88E-03	5.94E-03	7.81E-01	7.92E-01
26.875	1.81E-03	9.42E-03	-1.46E-02	-4.77E-03	8.60E-01	8.71E-01
27.125	-8.64E-03	-1.03E-03	-1.79E-03	8.04E-03	9.51E-01	9.63E-01
27.375	-1.19E-02	-4.33E-03	3.41E-03	1.32E-02	1.01E+00	1.02E+00
27.625	-1.13E-02	-3.64E-03	3.96E-03	1.38E-02	1.07E+00	1.08E+00
27.875	-1.73E-02	-9.71E-03	9.94E-03	1.98E-02	1.12E+00	1.13E+00
28.125	-1.29E-02	-5.25E-03	9.00E-03	1.88E-02	1.17E+00	1.18E+00
28.375	-1.46E-02	-7.02E-03	6.67E-03	1.65E-02	1.20E+00	1.21E+00
28.625	-1.77E-02	-1.01E-02	5.12E-03	1.49E-02	1.24E+00	1.25E+00
28.875	-2.22E-02	-1.46E-02	3.96E-03	1.38E-02	1.28E+00	1.29E+00
29.125	-2.20E-02	-1.44E-02	6.44E-03	1.63E-02	1.31E+00	1.32E+00
29.375	-2.25E-02	-1.49E-02	7.14E-03	1.70E-02	1.34E+00	1.35E+00
29.625	-2.15E-02	-1.39E-02	-3.42E-03	6.41E-03	1.35E+00	1.36E+00
29.875	-2.02E-02	-1.26E-02	-5.36E-03	4.47E-03	1.30E+00	1.31E+00
30.125	-7.41E-03	2.01E-04	-8.57E-04	8.97E-03	1.24E+00	1.25E+00
30.375	6.50E-03	1.41E-02	1.52E-04	9.98E-03	1.18E+00	1.19E+00
30.625	6.19E-03	1.38E-02	5.43E-03	1.53E-02	1.13E+00	1.14E+00
30.875	9.49E-03	1.71E-02	7.92E-03	1.77E-02	1.11E+00	1.12E+00
31.125	1.83E-02	2.59E-02	4.50E-03	1.43E-02	1.10E+00	1.11E+00
31.375	1.13E-02	1.89E-02	6.44E-03	1.63E-02	1.11E+00	1.12E+00
31.625	1.14E-02	1.90E-02	3.49E-03	1.33E-02	1.11E+00	1.13E+00
31.875	1.80E-02	2.56E-02	-2.18E-03	7.65E-03	1.15E+00	1.16E+00
32.125	1.14E-02	1.90E-02	-1.69E-02	-7.10E-03	1.27E+00	1.28E+00
32.375	-6.95E-03	6.62E-04	-2.09E-02	-1.11E-02	1.38E+00	1.40E+00
32.625	-1.26E-03	6.35E-03	-1.62E-02	-6.32E-03	1.44E+00	1.45E+00
32.875	-2.19E-03	5.43E-03	-3.57E-03	6.25E-03	1.48E+00	1.49E+00
33.125	1.04E-03	8.65E-03	-1.01E-03	8.82E-03	1.50E+00	1.51E+00
33.375	6.88E-03	1.45E-02	7.53E-03	1.74E-02	1.48E+00	1.49E+00
33.625	6.57E-03	1.42E-02	6.44E-03	1.63E-02	1.45E+00	1.46E+00
33.875	1.43E-02	2.19E-02	5.98E-03	1.58E-02	1.43E+00	1.44E+00
34.125	1.79E-02	2.55E-02	1.35E-02	2.33E-02	1.42E+00	1.43E+00
34.375	2.13E-02	2.89E-02	1.24E-03	1.11E-02	1.43E+00	1.44E+00
34.625	2.34E-02	3.10E-02	1.61E-02	2.59E-02	1.43E+00	1.45E+00
34.875	2.47E-02	3.23E-02	-6.60E-03	3.23E-03	1.45E+00	1.46E+00
35.125	9.42E-03	1.70E-02	-2.43E-02	-1.45E-02	1.46E+00	1.47E+00
35.375	1.91E-02	2.67E-02	-1.82E-02	-8.42E-03	1.52E+00	1.54E+00
35.625	2.16E-02	2.92E-02	-2.63E-02	-1.65E-02	1.53E+00	1.54E+00
35.875	2.67E-02	3.43E-02	-2.19E-02	-1.21E-02	1.52E+00	1.53E+00
36.125	2.62E-02	3.39E-02	-9.01E-03	8.18E-04	1.54E+00	1.55E+00
36.375	3.47E-02	4.23E-02	-1.58E-02	-6.01E-03	1.53E+00	1.54E+00
36.625	3.12E-02	3.88E-02	-9.09E-03	7.41E-04	1.57E+00	1.58E+00
36.875	2.47E-02	3.23E-02	4.42E-03	1.42E-02	1.60E+00	1.61E+00
37.125	2.42E-02	3.18E-02	5.20E-03	1.50E-02	1.62E+00	1.63E+00
37.375	3.65E-02	4.42E-02	2.71E-03	1.25E-02	1.63E+00	1.64E+00
37.625	2.85E-02	3.62E-02	1.16E-02	2.15E-02	1.61E+00	1.62E+00
37.875	3.02E-02	3.79E-02	8.85E-03	1.87E-02	1.62E+00	1.63E+00
38.125	3.15E-02	3.91E-02	8.07E-03	1.79E-02	1.60E+00	1.61E+00
38.375	3.76E-02	4.52E-02	2.64E-03	1.25E-02	1.60E+00	1.62E+00
38.625	3.13E-02	3.89E-02	-4.51E-03	5.32E-03	1.62E+00	1.63E+00
38.875	2.82E-02	3.59E-02	-1.47E-02	-4.85E-03	1.61E+00	1.62E+00
39.125	2.80E-02	3.56E-02	-1.33E-02	-3.45E-03	1.63E+00	1.65E+00
39.375	1.83E-02	2.59E-02	-9.55E-03	2.75E-04	1.63E+00	1.65E+00
39.625	9.57E-03	1.72E-02	-2.64E-03	7.18E-03	1.65E+00	1.66E+00
39.875	2.04E-02	2.80E-02	-5.59E-03	4.23E-03	1.66E+00	1.67E+00

Table 11. MAPO test number 48 data.

Test File: MAPOTEST.048 Test Date: Wed, 12-11-1996 No. Channels: 3 Sam/sec: 128      Average      32 pt centered Start: 09:56:36:48      End: 09:57:16:74 Low-g Range start 9:56:41 (5 sec) end 9:56:57 (21 sec) Accelerometer Bias Average Interval (15 to 20 sec)  Bias Values $x$ -0.0078 (g's) $y$ -0.0098 $z$ -0.0119 Time Stamp Offset Between Data and Video      0 sec						
Time	$x$ (g's)	$x$ Corrected (g's)	$y$ (g's)	$y$ Corrected (g's)	$z$ (g's)	$z$ Corrected (g's)
0.125	-9.33E-02	-8.55E-02	9.94E-03	1.98E-02	6.88E-01	7.00E-01
0.375	-9.22E-02	-8.43E-02	3.05E-02	4.03E-02	5.52E-01	5.64E-01
0.625	-6.53E-02	-5.74E-02	-1.16E-02	-1.82E-03	5.27E-01	5.39E-01
0.875	-7.20E-02	-6.42E-02	1.43E-02	2.41E-02	4.72E-01	4.84E-01
1.125	-7.07E-02	-6.29E-02	2.71E-03	1.25E-02	4.75E-01	4.87E-01
1.375	-6.52E-02	-5.74E-02	1.06E-02	2.05E-02	4.62E-01	4.74E-01
1.625	-6.32E-02	-5.54E-02	1.50E-02	2.48E-02	4.23E-01	4.35E-01
1.875	-7.07E-02	-6.29E-02	-1.64E-02	-6.56E-03	4.28E-01	4.40E-01
2.125	-6.29E-02	-5.51E-02	2.44E-02	3.42E-02	3.40E-01	3.52E-01
2.375	-6.20E-02	-5.42E-02	-2.38E-02	-1.40E-02	3.37E-01	3.49E-01
2.625	-6.33E-02	-5.55E-02	6.18E-04	1.04E-02	2.80E-01	2.92E-01
2.875	-4.95E-02	-4.17E-02	-2.66E-02	-1.68E-02	2.63E-01	2.75E-01
3.125	-4.86E-02	-4.08E-02	-1.20E-02	-2.21E-03	2.27E-01	2.39E-01
3.375	-4.61E-02	-3.82E-02	-8.70E-03	1.13E-03	1.89E-01	2.01E-01
3.625	-4.63E-02	-3.85E-02	-9.55E-03	2.77E-04	1.59E-01	1.71E-01
3.875	-4.11E-02	-3.32E-02	-9.55E-03	2.77E-04	1.28E-01	1.40E-01
4.125	-3.56E-02	-2.78E-02	-1.00E-02	-1.89E-04	1.10E-01	1.22E-01
4.375	-2.88E-02	-2.10E-02	-1.07E-02	-8.87E-04	9.70E-02	1.09E-01
4.625	-2.38E-02	-1.60E-02	-8.16E-03	1.67E-03	8.32E-02	9.52E-02
4.875	-2.35E-02	-1.57E-02	-7.30E-03	2.53E-03	7.15E-02	8.34E-02
5.125	-2.28E-02	-1.50E-02	-7.22E-03	2.61E-03	6.25E-02	7.45E-02
5.375	-2.50E-02	-1.72E-02	-1.03E-02	-4.21E-04	4.47E-02	5.66E-02
5.625	-2.01E-02	-1.23E-02	-7.61E-03	2.22E-03	3.66E-02	4.85E-02
5.875	-2.14E-02	-1.36E-02	-1.05E-02	-6.54E-04	3.34E-02	4.54E-02
6.125	-1.99E-02	-1.20E-02	-9.55E-03	2.77E-04	3.71E-02	4.91E-02
6.375	-1.91E-02	-1.13E-02	-1.11E-02	-1.28E-03	4.09E-02	5.29E-02
6.625	-1.70E-02	-9.19E-03	-1.16E-02	-1.74E-03	3.82E-02	5.01E-02
6.875	-1.86E-02	-1.07E-02	-1.34E-02	-3.53E-03	3.62E-02	4.82E-02
7.125	-1.63E-02	-8.50E-03	-1.38E-02	-3.99E-03	3.21E-02	4.41E-02
7.375	-1.77E-02	-9.89E-03	-1.34E-02	-3.60E-03	2.95E-02	4.15E-02
7.625	-1.69E-02	-9.12E-03	-1.18E-02	-1.97E-03	2.40E-02	3.59E-02
7.875	-1.86E-02	-1.07E-02	-1.14E-02	-1.59E-03	2.02E-02	3.21E-02
8.125	-1.79E-02	-1.01E-02	-1.08E-02	-9.65E-04	1.59E-02	2.78E-02
8.375	-1.78E-02	-9.96E-03	-1.30E-02	-3.22E-03	1.69E-02	2.88E-02
8.625	-1.63E-02	-8.50E-03	-9.55E-03	2.77E-04	1.16E-02	2.35E-02
8.875	-1.36E-02	-5.81E-03	-9.86E-03	-3.33E-05	1.14E-02	2.33E-02
9.125	-1.53E-02	-7.50E-03	-3.57E-03	6.26E-03	9.95E-03	2.19E-02
9.375	-2.08E-02	-1.30E-02	-6.99E-03	2.84E-03	7.57E-03	1.95E-02
9.625	-1.66E-02	-8.73E-03	-7.92E-03	1.91E-03	7.87E-03	1.98E-02
9.875	-1.65E-02	-8.66E-03	-5.83E-03	4.00E-03	6.98E-03	1.89E-02
10.125	-1.52E-02	-7.35E-03	-7.30E-03	2.53E-03	5.05E-03	1.70E-02
10.375	-1.62E-02	-8.35E-03	-7.07E-03	2.76E-03	8.46E-03	2.04E-02
10.625	-1.70E-02	-9.19E-03	-6.84E-03	2.99E-03	6.68E-03	1.86E-02
10.875	-1.55E-02	-7.66E-03	-5.83E-03	4.00E-03	5.72E-03	1.77E-02

Table 11. MAPO test number 48 data (Continued).

Time	x (g's)	x Corrected (g's)	y (g's)	y Corrected (g's)	z (g's)	z Corrected (g's)
11.125	-1.40E-02	-6.20E-03	-7.15E-03	2.68E-03	8.91E-03	2.09E-02
11.375	-1.42E-02	-6.35E-03	-9.71E-03	1.22E-04	4.75E-03	1.67E-02
11.625	-1.42E-02	-6.35E-03	-8.85E-03	9.76E-04	5.35E-03	1.73E-02
11.875	-1.50E-02	-7.20E-03	-8.70E-03	1.13E-03	7.05E-03	1.90E-02
12.125	-1.02E-02	-2.36E-03	-7.07E-03	2.76E-03	-2.90E-03	9.05E-03
12.375	-1.46E-02	-6.81E-03	-5.36E-03	4.47E-03	-1.26E-03	1.07E-02
12.625	-1.29E-02	-5.12E-03	-4.66E-03	5.17E-03	-3.27E-03	8.68E-03
12.875	-1.62E-02	-8.43E-03	-3.50E-03	6.33E-03	-2.00E-03	9.94E-03
13.125	-1.03E-02	-2.43E-03	-1.08E-02	-9.65E-04	-2.75E-03	9.20E-03
13.375	-1.33E-02	-5.51E-03	-9.47E-03	3.55E-04	-7.28E-03	4.67E-03
13.625	-1.29E-02	-5.05E-03	-7.77E-03	2.06E-03	-1.04E-02	1.56E-03
13.875	-7.95E-03	-1.28E-04	-9.09E-03	7.43E-04	-1.07E-02	1.26E-03
14.125	-7.95E-03	-1.28E-04	-1.01E-02	-2.66E-04	-9.95E-03	2.00E-03
14.375	-8.33E-03	-5.12E-04	-9.16E-03	6.65E-04	-1.16E-02	3.68E-04
14.625	-7.72E-03	1.02E-04	-9.94E-03	-1.11E-04	-1.17E-02	2.19E-04
14.875	-6.72E-03	1.10E-03	-9.55E-03	2.77E-04	-1.28E-02	-8.94E-04
15.125	-9.02E-03	-1.20E-03	-8.16E-03	1.67E-03	-1.44E-02	-2.45E-03
15.375	-7.10E-03	7.17E-04	-9.55E-03	2.77E-04	-1.25E-02	-5.23E-04
15.625	-8.64E-03	-8.20E-04	-9.55E-03	2.77E-04	-1.11E-02	8.13E-04
15.875	-8.18E-03	-3.59E-04	-9.32E-03	5.10E-04	-1.24E-02	-4.49E-04
16.125	-5.34E-03	2.48E-03	-1.16E-02	-1.74E-03	-1.01E-02	1.85E-03
16.375	-8.95E-03	-1.13E-03	-9.09E-03	7.43E-04	-1.20E-02	-7.78E-05
16.625	-8.18E-03	-3.59E-04	-1.02E-02	-3.44E-04	-1.20E-02	-3.54E-06
16.875	-8.72E-03	-8.96E-04	-1.01E-02	-2.66E-04	-1.11E-02	8.13E-04
17.125	-7.72E-03	1.02E-04	-9.16E-03	6.65E-04	-1.20E-02	-3.54E-06
17.375	-6.33E-03	1.49E-03	-1.03E-02	-4.99E-04	-1.02E-02	1.70E-03
17.625	-8.18E-03	-3.59E-04	-1.07E-02	-8.87E-04	-1.19E-02	7.07E-05
17.875	-8.18E-03	-3.59E-04	-1.07E-02	-8.87E-04	-1.21E-02	-1.52E-04
18.125	-6.95E-03	8.71E-04	-9.55E-03	2.77E-04	-1.09E-02	1.04E-03
18.375	-7.72E-03	1.02E-04	-1.03E-02	-4.99E-04	-1.14E-02	5.90E-04
18.625	-8.41E-03	-5.89E-04	-9.94E-03	-1.11E-04	-1.11E-02	8.13E-04
18.875	-8.72E-03	-8.96E-04	-9.55E-03	2.77E-04	-1.21E-02	-1.52E-04
19.125	-8.33E-03	-5.12E-04	-9.55E-03	2.77E-04	-1.30E-02	-1.04E-03
19.375	-6.33E-03	1.49E-03	-9.86E-03	-3.33E-05	-1.18E-02	1.45E-04
19.625	-1.04E-02	-2.59E-03	-8.93E-03	8.98E-04	-1.47E-02	-2.75E-03
19.875	-5.80E-03	2.02E-03	-1.05E-02	-6.54E-04	-1.25E-02	-5.23E-04
20.125	-7.03E-03	7.94E-04	-9.79E-03	4.44E-05	-1.17E-02	2.93E-04
20.375	-7.18E-03	6.40E-04	-1.06E-02	-7.32E-04	-1.09E-02	1.04E-03
20.625	-6.49E-03	1.33E-03	-1.06E-02	-7.32E-04	-1.10E-02	9.62E-04
20.875	-3.40E-02	-2.62E-02	1.04E-02	2.02E-02	-4.45E-03	7.49E-03
21.125	-8.51E-02	-7.73E-02	4.33E-02	5.32E-02	3.12E-03	1.51E-02
21.375	-1.24E-01	-1.16E-01	4.37E-02	5.35E-02	-8.59E-02	-7.39E-02
21.625	-1.39E-01	-1.31E-01	-1.82E-02	-8.42E-03	-9.32E-02	-8.12E-02
21.875	-7.91E-02	-7.13E-02	2.67E-02	3.65E-02	1.28E-02	2.48E-02
22.125	-4.14E-02	-3.36E-02	1.18E-02	2.16E-02	-7.94E-03	4.01E-03
22.375	-4.57E-02	-3.79E-02	2.48E-03	1.23E-02	1.78E-03	1.37E-02
22.625	-3.71E-02	-2.93E-02	9.39E-03	1.92E-02	-8.91E-04	1.11E-02
22.875	-7.41E-03	4.10E-04	-4.97E-03	4.86E-03	-1.49E-02	-2.97E-03
23.125	-2.13E-02	-1.35E-02	7.30E-03	1.71E-02	-1.31E-02	-1.12E-03
23.375	-9.33E-03	-1.51E-03	5.59E-03	1.54E-02	-1.55E-02	-3.57E-03
23.625	1.45E-02	2.23E-02	1.70E-02	2.68E-02	-1.95E-02	-7.58E-03
23.875	2.16E-02	2.95E-02	-2.08E-02	-1.10E-02	-4.42E-02	-3.23E-02
24.125	5.45E-02	6.23E-02	-8.94E-02	-7.95E-02	-1.47E-01	-1.35E-01
24.375	-1.89E-02	-1.10E-02	-2.51E-02	-1.53E-02	-7.12E-02	-5.92E-02
24.625	-6.88E-02	-6.10E-02	-1.23E-02	-2.44E-03	-5.75E-02	-4.55E-02
24.875	-5.63E-02	-4.85E-02	-7.61E-03	2.22E-03	-2.93E-02	-1.74E-02
25.125	-1.59E-01	-1.52E-01	1.41E-01	1.51E-01	8.07E-02	9.26E-02
25.375	-6.62E-01	-6.55E-01	1.75E-01	1.85E-01	7.53E-01	7.65E-01

Table 11. MAPO test number 48 data (Continued).

Time	x (g's)	x Corrected (g's)	y (g's)	y Corrected (g's)	z (g's)	z Corrected (g's)
25.625	-1.05E-01	-9.71E-02	-1.12E-01	-1.02E-01	1.70E-01	1.82E-01
25.875	-1.18E-01	-1.10E-01	1.54E-02	2.53E-02	1.52E-01	1.64E-01
26.125	-1.66E-01	-1.58E-01	7.52E-02	8.51E-02	5.85E-01	5.97E-01
26.375	-3.43E-02	-2.65E-02	9.04E-02	1.00E-01	4.96E-01	5.08E-01
26.625	-7.83E-02	-7.05E-02	1.89E-01	1.99E-01	5.24E-01	5.36E-01
26.875	-1.53E-02	-7.50E-03	1.54E-01	1.64E-01	4.97E-01	5.09E-01
27.125	2.39E-02	3.18E-02	1.42E-01	1.52E-01	6.21E-01	6.33E-01
27.375	-2.52E-02	-1.74E-02	-1.58E-02	-6.01E-03	7.35E-01	7.47E-01
27.625	-1.31E-01	-1.23E-01	5.15E-02	6.13E-02	7.75E-01	7.86E-01
27.875	-9.62E-02	-8.84E-02	4.97E-02	5.95E-02	8.10E-01	8.22E-01
28.125	3.58E-02	4.37E-02	4.02E-02	5.00E-02	8.76E-01	8.88E-01
28.375	2.77E-01	2.85E-01	-1.43E-01	-1.33E-01	9.16E-01	9.28E-01
28.625	4.25E-02	5.04E-02	-4.04E-02	-3.05E-02	9.82E-01	9.94E-01
28.875	-1.78E-02	-9.96E-03	4.89E-03	1.47E-02	1.01E+00	1.03E+00
29.125	-1.76E-02	-9.73E-03	6.29E-03	1.61E-02	1.04E+00	1.06E+00
29.375	-1.72E-02	-9.43E-03	7.68E-03	1.75E-02	1.09E+00	1.10E+00
29.625	-2.37E-02	-1.59E-02	8.46E-03	1.83E-02	1.12E+00	1.13E+00
29.875	-2.13E-02	-1.35E-02	1.76E-02	2.75E-02	1.14E+00	1.15E+00
30.125	-2.13E-02	-1.35E-02	2.66E-02	3.64E-02	1.17E+00	1.18E+00
30.375	-2.23E-02	-1.45E-02	1.69E-02	2.68E-02	1.19E+00	1.20E+00
30.625	-2.17E-02	-1.39E-02	2.75E-02	3.73E-02	1.22E+00	1.23E+00
30.875	-2.94E-02	-2.16E-02	3.00E-02	3.98E-02	1.24E+00	1.25E+00
31.125	-1.51E-02	-7.27E-03	3.11E-02	4.10E-02	1.27E+00	1.28E+00
31.375	-1.87E-02	-1.09E-02	2.94E-02	3.93E-02	1.27E+00	1.29E+00
31.625	-1.88E-02	-1.10E-02	2.38E-02	3.37E-02	1.27E+00	1.29E+00
31.875	-2.41E-02	-1.63E-02	2.72E-02	3.70E-02	1.28E+00	1.29E+00
32.125	-2.21E-02	-1.43E-02	1.44E-02	2.42E-02	1.28E+00	1.29E+00
32.375	-2.19E-02	-1.41E-02	2.03E-02	3.02E-02	1.30E+00	1.31E+00
32.625	-1.92E-02	-1.13E-02	9.70E-03	1.95E-02	1.31E+00	1.32E+00
32.875	-2.61E-02	-1.83E-02	1.41E-02	2.40E-02	1.32E+00	1.33E+00
33.125	-2.32E-02	-1.54E-02	4.50E-03	1.43E-02	1.34E+00	1.35E+00
33.375	-2.62E-02	-1.84E-02	9.24E-03	1.91E-02	1.35E+00	1.36E+00
33.625	-3.00E-02	-2.22E-02	1.16E-03	1.10E-02	1.36E+00	1.38E+00
33.875	-3.47E-02	-2.69E-02	-1.79E-03	8.04E-03	1.37E+00	1.38E+00
34.125	-2.38E-02	-1.60E-02	-3.34E-03	6.49E-03	1.39E+00	1.40E+00
34.375	-2.32E-02	-1.54E-02	-2.36E-04	9.59E-03	1.42E+00	1.43E+00
34.625	-2.95E-02	-2.16E-02	1.02E-02	2.01E-02	1.43E+00	1.45E+00
34.875	-3.29E-02	-2.51E-02	1.12E-02	2.10E-02	1.44E+00	1.46E+00
35.125	-2.36E-02	-1.58E-02	1.34E-02	2.32E-02	1.43E+00	1.45E+00
35.375	-1.80E-02	-1.02E-02	1.51E-02	2.49E-02	1.41E+00	1.43E+00
35.625	-1.59E-02	-8.04E-03	5.90E-03	1.57E-02	1.38E+00	1.39E+00
35.875	-1.09E-02	-3.05E-03	2.69E-02	3.68E-02	1.34E+00	1.35E+00
36.125	-6.10E-03	1.72E-03	2.74E-02	3.72E-02	1.32E+00	1.33E+00
36.375	-8.33E-03	-5.12E-04	1.82E-02	2.80E-02	1.33E+00	1.34E+00
36.625	-1.24E-02	-4.58E-03	9.47E-03	1.93E-02	1.35E+00	1.37E+00
36.875	-1.59E-02	-8.12E-03	6.91E-03	1.67E-02	1.38E+00	1.40E+00
37.125	-7.64E-03	1.79E-04	4.89E-03	1.47E-02	1.42E+00	1.43E+00
37.375	-2.16E-02	-1.38E-02	5.04E-03	1.49E-02	1.42E+00	1.44E+00
37.625	-2.12E-02	-1.34E-02	8.51E-04	1.07E-02	1.44E+00	1.46E+00
37.875	-2.14E-02	-1.36E-02	4.63E-04	1.03E-02	1.45E+00	1.46E+00
38.125	-1.57E-02	-7.89E-03	-1.21E-02	-2.28E-03	1.45E+00	1.46E+00
38.375	-2.22E-02	-1.44E-02	4.89E-03	1.47E-02	1.45E+00	1.46E+00
38.625	-1.62E-02	-8.43E-03	5.04E-03	1.49E-02	1.46E+00	1.47E+00
38.875	-1.14E-02	-3.59E-03	1.92E-02	2.90E-02	1.43E+00	1.45E+00
39.125	-2.34E-03	5.48E-03	2.12E-02	3.10E-02	1.43E+00	1.44E+00
39.375	-6.03E-03	1.79E-03	2.97E-02	3.95E-02	1.42E+00	1.43E+00
39.625	-3.26E-03	4.56E-03	3.05E-02	4.03E-02	1.42E+00	1.43E+00
39.875	-4.18E-03	3.64E-03	2.42E-02	3.41E-02	1.42E+00	1.43E+00



Table 12. MAPO test number 59 data (Continued).

Time	x (g's)	x Corrected (g's)	y (g's)	y Corrected (g's)	z (g's)	z Corrected (g's)
11.125	-1.13E-02	-3.80E-03	-2.56E-03	7.00E-03	-1.37E-02	-2.00E-03
11.375	-7.79E-03	-2.65E-04	-7.84E-03	1.72E-03	-1.35E-02	-1.77E-03
11.625	-9.79E-03	-2.26E-03	-6.84E-03	2.73E-03	-1.32E-02	-1.48E-03
11.875	-9.64E-03	-2.11E-03	-9.01E-03	5.60E-04	-1.30E-02	-1.25E-03
12.125	-8.26E-03	-7.26E-04	-1.06E-02	-9.93E-04	-1.20E-02	-2.89E-04
12.375	-7.26E-03	2.73E-04	-1.05E-02	-9.16E-04	-1.24E-02	-6.60E-04
12.625	-1.15E-02	-3.95E-03	-7.69E-03	1.88E-03	-1.23E-02	-5.86E-04
12.875	-1.29E-02	-5.34E-03	-1.09E-03	8.48E-03	-1.34E-02	-1.70E-03
13.125	-1.11E-02	-3.57E-03	-4.04E-03	5.53E-03	-1.50E-02	-3.26E-03
13.375	-1.09E-02	-3.34E-03	-4.35E-03	5.22E-03	-1.37E-02	-2.00E-03
13.625	-1.29E-02	-5.34E-03	-2.88E-03	6.69E-03	-1.31E-02	-1.33E-03
13.875	-9.56E-03	-2.03E-03	-4.51E-03	5.06E-03	-1.05E-02	1.20E-03
14.125	-9.87E-03	-2.34E-03	-2.88E-03	6.69E-03	-1.17E-02	7.68E-06
14.375	-9.64E-03	-2.11E-03	-3.73E-03	5.84E-03	-1.41E-02	-2.37E-03
14.625	-1.02E-02	-2.65E-03	-4.27E-03	5.30E-03	-1.20E-02	-2.15E-04
14.875	-1.02E-02	-2.65E-03	-6.60E-03	2.97E-03	-1.23E-02	-5.86E-04
15.125	-9.87E-03	-2.34E-03	-5.59E-03	3.98E-03	-1.20E-02	-2.89E-04
15.375	-1.02E-02	-2.65E-03	-7.61E-03	1.96E-03	-1.26E-02	-8.83E-04
15.625	-7.18E-03	3.50E-04	-8.54E-03	1.03E-03	-1.02E-02	1.57E-03
15.875	-8.72E-03	-1.19E-03	-1.00E-02	-4.50E-04	-1.12E-02	5.27E-04
16.125	-7.79E-03	-2.65E-04	-1.20E-02	-2.39E-03	-8.83E-03	2.90E-03
16.375	-5.72E-03	1.81E-03	-1.04E-02	-8.38E-04	-1.18E-02	-6.66E-05
16.625	-7.64E-03	-1.11E-04	-9.24E-03	3.27E-04	-1.14E-02	3.79E-04
16.875	-8.95E-03	-1.42E-03	-1.00E-02	-4.50E-04	-1.21E-02	-3.64E-04
17.125	-7.95E-03	-4.19E-04	-1.08E-02	-1.23E-03	-1.16E-02	1.56E-04
17.375	-6.95E-03	5.80E-04	-6.60E-03	2.97E-03	-1.19E-02	-1.41E-04
17.625	-6.57E-03	9.64E-04	-9.32E-03	2.49E-04	-1.28E-02	-1.03E-03
17.875	-6.80E-03	7.34E-04	-1.04E-02	-8.38E-04	-1.04E-02	1.34E-03
18.125	-6.03E-03	1.50E-03	-1.19E-02	-2.31E-03	-1.19E-02	-1.41E-04
18.375	-6.49E-03	1.04E-03	-9.24E-03	3.27E-04	-1.11E-02	6.02E-04
18.625	-8.41E-03	-8.80E-04	-1.07E-02	-1.15E-03	-1.14E-02	3.79E-04
18.875	-7.18E-03	3.50E-04	-8.08E-03	1.49E-03	-1.32E-02	-1.48E-03
19.125	-6.80E-03	7.34E-04	-8.31E-03	1.26E-03	-1.17E-02	8.19E-05
19.375	-7.56E-03	-3.44E-05	-9.16E-03	4.04E-04	-1.16E-02	1.56E-04
19.625	-8.10E-03	-5.72E-04	-9.01E-03	5.60E-04	-1.21E-02	-3.64E-04
19.875	-8.87E-03	-1.34E-03	-1.23E-02	-2.78E-03	-1.21E-02	-3.64E-04
20.125	-1.00E-02	-2.49E-03	-9.63E-03	-6.16E-05	-1.20E-02	-2.15E-04
20.375	-7.33E-03	1.96E-04	-8.93E-03	6.37E-04	-1.16E-02	1.56E-04
20.625	-6.41E-03	1.12E-03	-1.03E-02	-6.83E-04	-1.08E-02	8.99E-04
20.875	-6.87E-03	6.57E-04	-8.78E-03	7.92E-04	-1.17E-02	8.19E-05
21.125	-7.26E-03	2.73E-04	-8.54E-03	1.03E-03	-1.40E-02	-2.29E-03
21.375	-7.18E-03	3.50E-04	-9.86E-03	-2.94E-04	-1.16E-02	1.56E-04
21.625	-7.41E-03	1.19E-04	-8.39E-03	1.18E-03	-1.25E-02	-7.35E-04
21.875	-9.56E-03	-2.03E-03	-1.14E-02	-1.85E-03	-1.14E-02	3.79E-04
22.125	-8.64E-03	-1.11E-03	-1.12E-02	-1.61E-03	-1.21E-02	-3.64E-04
22.375	-7.03E-03	5.03E-04	-8.08E-03	1.49E-03	-1.23E-02	-5.86E-04
22.625	-7.79E-03	-2.65E-04	-7.92E-03	1.65E-03	-1.10E-02	7.50E-04
22.875	-7.56E-03	-3.44E-05	-8.70E-03	8.70E-04	-1.18E-02	-6.66E-05
23.125	-7.49E-03	4.24E-05	-8.31E-03	1.26E-03	-1.20E-02	-2.15E-04
23.375	-1.02E-02	-2.65E-03	-8.08E-03	1.49E-03	-1.28E-02	-1.03E-03
23.625	-1.19E-02	-4.41E-03	-4.97E-03	4.60E-03	-1.00E-02	1.72E-03
23.875	-2.76E-02	-2.01E-02	3.53E-02	4.49E-02	-2.20E-02	-1.02E-02
24.125	-4.04E-02	-3.28E-02	6.09E-02	7.05E-02	-2.35E-02	-1.18E-02
24.375	6.17E-02	6.92E-02	2.14E-01	2.24E-01	7.89E-02	9.07E-02
24.625	-5.57E-03	1.96E-03	3.69E-02	4.64E-02	-1.57E-02	-3.93E-03
24.875	1.53E-02	2.29E-02	4.07E-02	5.02E-02	-1.30E-02	-1.25E-03
25.125	3.48E-02	4.24E-02	4.62E-02	5.58E-02	1.08E-02	2.25E-02
25.375	1.23E-01	1.30E-01	2.43E-01	2.52E-01	-5.05E-03	6.69E-03

Table 12. MAPO test number 59 data (Continued).

Time	x (g's)	x Corrected (g's)	y (g's)	y Corrected (g's)	z (g's)	z Corrected (g's)
25.625	4.71E-02	5.47E-02	1.30E-01	1.40E-01	-1.04E-03	1.07E-02
25.875	1.27E-02	2.03E-02	1.86E-01	1.96E-01	-9.65E-03	2.09E-03
26.125	1.96E-02	2.71E-02	2.27E-01	2.36E-01	-6.83E-03	4.91E-03
26.375	1.74E-02	2.49E-02	2.77E-01	2.87E-01	-1.78E-03	9.96E-03
26.625	1.96E-02	2.71E-02	3.52E-01	3.62E-01	-6.76E-03	4.98E-03
26.875	1.46E-02	2.22E-02	4.19E-01	4.29E-01	-4.23E-03	7.51E-03
27.125	1.82E-02	2.57E-02	5.09E-01	5.19E-01	-3.34E-03	8.40E-03
27.375	1.96E-02	2.72E-02	6.00E-01	6.09E-01	1.48E-04	1.19E-02
27.625	2.00E-02	2.76E-02	6.87E-01	6.97E-01	-1.63E-03	1.01E-02
27.875	1.42E-02	2.17E-02	7.90E-01	8.00E-01	8.17E-04	1.26E-02
28.125	8.88E-03	1.64E-02	8.70E-01	8.80E-01	9.65E-04	1.27E-02
28.375	9.19E-03	1.67E-02	9.36E-01	9.46E-01	3.19E-03	1.49E-02
28.625	1.59E-02	2.34E-02	9.97E-01	1.01E+00	5.94E-03	1.77E-02
28.875	1.14E-02	1.89E-02	1.04E+00	1.05E+00	6.61E-03	1.83E-02
29.125	4.04E-03	1.16E-02	1.08E+00	1.09E+00	9.65E-03	2.14E-02
29.375	-6.49E-04	6.88E-03	1.11E+00	1.11E+00	9.43E-03	2.12E-02
29.625	3.50E-03	1.10E-02	1.15E+00	1.16E+00	7.35E-03	1.91E-02
29.875	2.66E-03	1.02E-02	1.20E+00	1.21E+00	8.61E-03	2.03E-02
30.125	-9.49E-03	-1.96E-03	1.25E+00	1.26E+00	7.13E-03	1.89E-02
30.375	-1.49E-02	-7.33E-03	1.29E+00	1.30E+00	9.87E-03	2.16E-02
30.625	-9.64E-03	-2.11E-03	1.34E+00	1.35E+00	1.10E-02	2.27E-02
30.875	-1.16E-02	-4.03E-03	1.39E+00	1.40E+00	1.06E-02	2.24E-02
31.125	-2.50E-02	-1.75E-02	1.43E+00	1.44E+00	1.01E-02	2.18E-02
31.375	-2.49E-02	-1.73E-02	1.45E+00	1.46E+00	1.32E-02	2.50E-02
31.625	-1.51E-02	-7.56E-03	1.47E+00	1.48E+00	1.11E-02	2.29E-02
31.875	-1.54E-02	-7.87E-03	1.50E+00	1.51E+00	1.44E-02	2.61E-02
32.125	-2.40E-02	-1.65E-02	1.53E+00	1.54E+00	1.09E-02	2.27E-02
32.375	-1.71E-02	-9.56E-03	1.55E+00	1.56E+00	1.75E-02	2.93E-02
32.625	-1.59E-02	-8.33E-03	1.58E+00	1.59E+00	2.18E-02	3.36E-02
32.875	-2.10E-02	-1.35E-02	1.60E+00	1.61E+00	2.20E-02	3.38E-02
33.125	-2.45E-02	-1.69E-02	1.62E+00	1.63E+00	2.49E-02	3.67E-02
33.375	-2.12E-02	-1.36E-02	1.63E+00	1.64E+00	2.78E-02	3.96E-02
33.625	-1.77E-02	-1.02E-02	1.64E+00	1.65E+00	2.43E-02	3.60E-02
33.875	-2.67E-02	-1.92E-02	1.65E+00	1.65E+00	2.89E-02	4.06E-02
34.125	-1.76E-02	-1.00E-02	1.66E+00	1.67E+00	2.62E-02	3.79E-02
34.375	-1.27E-02	-5.18E-03	1.67E+00	1.68E+00	2.59E-02	3.76E-02
34.625	-1.36E-02	-6.10E-03	1.67E+00	1.68E+00	2.45E-02	3.62E-02
34.875	-1.05E-02	-2.95E-03	1.68E+00	1.69E+00	2.55E-02	3.73E-02
35.125	-1.42E-02	-6.64E-03	1.69E+00	1.70E+00	2.23E-02	3.41E-02
35.375	-1.39E-02	-6.41E-03	1.71E+00	1.72E+00	1.29E-02	2.47E-02
35.625	-1.29E-02	-5.41E-03	1.72E+00	1.73E+00	1.66E-02	2.84E-02
35.875	-1.04E-02	-2.88E-03	1.73E+00	1.74E+00	2.23E-02	3.41E-02
36.125	-7.49E-03	4.24E-05	1.74E+00	1.75E+00	2.15E-02	3.32E-02
36.375	-9.64E-03	-2.11E-03	1.74E+00	1.75E+00	3.13E-02	4.31E-02
36.625	-8.87E-03	-1.34E-03	1.76E+00	1.76E+00	3.48E-02	4.66E-02
36.875	-2.34E-03	5.19E-03	1.76E+00	1.77E+00	3.98E-02	5.15E-02
37.125	-9.33E-03	-1.80E-03	1.77E+00	1.78E+00	4.03E-02	5.20E-02
37.375	-1.14E-02	-3.88E-03	1.78E+00	1.79E+00	3.51E-02	4.69E-02
37.625	-7.41E-03	1.19E-04	1.77E+00	1.78E+00	2.82E-02	3.99E-02
37.875	-8.03E-03	-4.95E-04	1.76E+00	1.77E+00	1.48E-02	2.65E-02
38.125	-7.41E-03	1.19E-04	1.76E+00	1.77E+00	8.91E-03	2.06E-02
38.375	-9.41E-03	-1.88E-03	1.77E+00	1.78E+00	-5.20E-03	6.54E-03
38.625	-3.18E-03	4.35E-03	1.76E+00	1.77E+00	-1.86E-03	9.88E-03
38.875	-3.72E-03	3.81E-03	1.75E+00	1.76E+00	2.40E-02	3.57E-02
39.125	-6.33E-03	1.19E-03	1.76E+00	1.77E+00	2.93E-02	4.11E-02
39.375	-2.65E-04	7.27E-03	1.77E+00	1.78E+00	3.39E-02	4.57E-02
39.625	-7.56E-03	-3.44E-05	1.77E+00	1.78E+00	3.08E-02	4.25E-02
39.875	-1.70E-02	-9.49E-03	1.77E+00	1.78E+00	2.67E-02	3.85E-02

Table 13. MAPO test number 74 data.

Test File: MAPOTEST.074 Test Date: Wed, 12-11-1996 No. Channels: 3 Sam/sec: 128      Average      32 pt centered Start: 10:40:47:35    End: 10:41:27:39 Low-g Range start    10:40:57    (16.5 sec) end      10:41:06    (18.5 sec) Accelerometer Bias Average Interval (16 to 23 sec)						
Bias Values    x            -0.0075 (G's)            y            -0.0103 z            -0.0133						
Time Stamp Offset Between Data and Video    0 sec						
Time	x (G's)	x Corrected (G's)	y (G's)	y Corrected (G's)	z (G's)	z Corrected (G's)
0.125	-1.51E-01	-1.43E-01	-3.73E-02	-2.69E-02	-1.64E+00	-1.62E+00
0.375	-1.45E-01	-1.37E-01	-4.84E-02	-3.80E-02	-1.58E+00	-1.57E+00
0.625	-1.31E-01	-1.24E-01	-5.57E-02	-4.54E-02	-1.61E+00	-1.60E+00
0.875	-1.68E-01	-1.60E-01	-7.92E-03	2.41E-03	-1.69E+00	-1.68E+00
1.125	-1.64E-01	-1.56E-01	-2.28E-02	-1.25E-02	-1.66E+00	-1.65E+00
1.375	-1.84E-01	-1.77E-01	4.43E-02	5.46E-02	-1.71E+00	-1.70E+00
1.625	-1.64E-01	-1.57E-01	-5.37E-02	-4.33E-02	-1.64E+00	-1.63E+00
1.875	-1.95E-01	-1.87E-01	2.53E-02	3.56E-02	-1.69E+00	-1.68E+00
2.125	-1.45E-01	-1.37E-01	-2.66E-02	-1.62E-02	-1.66E+00	-1.65E+00
2.375	-1.91E-01	-1.83E-01	-2.96E-02	-1.93E-02	-1.67E+00	-1.65E+00
2.625	-1.93E-01	-1.85E-01	-2.94E-02	-1.90E-02	-1.66E+00	-1.65E+00
2.875	-2.17E-01	-2.09E-01	1.20E-02	2.23E-02	-1.68E+00	-1.67E+00
3.125	-1.85E-01	-1.77E-01	-1.14E-02	-1.09E-03	-1.63E+00	-1.62E+00
3.375	-2.15E-01	-2.08E-01	-2.24E-02	-1.20E-02	-1.69E+00	-1.68E+00
3.625	-1.94E-01	-1.87E-01	-3.50E-03	6.83E-03	-1.63E+00	-1.62E+00
3.875	-1.71E-01	-1.63E-01	-4.11E-02	-3.07E-02	-1.53E+00	-1.51E+00
4.125	-1.42E-01	-1.34E-01	-2.67E-02	-1.64E-02	-1.36E+00	-1.35E+00
4.375	-1.05E-01	-9.77E-02	5.90E-03	1.62E-02	-1.22E+00	-1.21E+00
4.625	-8.50E-02	-7.75E-02	-1.97E-02	-9.39E-03	-1.00E+00	-9.89E-01
4.875	-5.70E-02	-4.95E-02	-1.47E-02	-4.35E-03	-8.03E-01	-7.89E-01
5.125	-3.78E-02	-3.03E-02	-1.86E-02	-8.23E-03	-6.53E-01	-6.39E-01
5.375	-3.22E-02	-2.46E-02	-1.73E-02	-6.99E-03	-5.31E-01	-5.18E-01
5.625	-2.04E-02	-1.29E-02	-1.89E-02	-8.62E-03	-4.62E-01	-4.49E-01
5.875	-1.96E-02	-1.20E-02	-1.09E-02	-5.43E-04	-4.39E-01	-4.25E-01
6.125	-1.19E-02	-4.40E-03	-1.32E-02	-2.87E-03	-4.07E-01	-3.93E-01
6.375	-1.39E-02	-6.32E-03	-6.60E-03	3.73E-03	-3.99E-01	-3.86E-01
6.625	-1.03E-02	-2.71E-03	-6.37E-03	3.96E-03	-3.60E-01	-3.47E-01
6.875	-1.31E-02	-5.55E-03	-1.07E-02	-3.88E-04	-3.29E-01	-3.16E-01
7.125	-6.03E-03	1.52E-03	-8.08E-03	2.25E-03	-2.94E-01	-2.80E-01
7.375	-3.49E-03	4.05E-03	-1.07E-02	-3.88E-04	-2.62E-01	-2.49E-01
7.625	-1.02E-02	-2.63E-03	-6.06E-03	4.27E-03	-2.46E-01	-2.32E-01
7.875	-7.41E-03	1.34E-04	-6.60E-03	3.73E-03	-2.23E-01	-2.10E-01
8.125	-9.87E-03	-2.32E-03	-1.27E-02	-2.41E-03	-1.91E-01	-1.78E-01
8.375	-6.80E-03	7.49E-04	-1.27E-02	-2.41E-03	-1.78E-01	-1.64E-01
8.625	-7.72E-03	-1.73E-04	-1.22E-02	-1.86E-03	-1.50E-01	-1.37E-01
8.875	-3.72E-03	3.82E-03	-1.18E-02	-1.48E-03	-1.29E-01	-1.15E-01
9.125	-5.11E-03	2.44E-03	-1.03E-02	0.00E+00	-1.21E-01	-1.08E-01
9.375	-8.64E-03	-1.09E-03	-6.76E-03	3.57E-03	-1.02E-01	-8.88E-02
9.625	-1.06E-02	-3.09E-03	-4.04E-03	6.29E-03	-9.55E-02	-8.22E-02
9.875	-7.87E-03	-3.27E-04	-5.36E-03	4.97E-03	-8.92E-02	-7.59E-02
10.125	-6.87E-03	6.72E-04	-1.06E-02	-3.11E-04	-7.97E-02	-6.64E-02
10.375	-8.95E-03	-1.40E-03	-8.54E-03	1.79E-03	-7.97E-02	-6.64E-02
10.625	-8.79E-03	-1.25E-03	-9.86E-03	4.66E-04	-7.67E-02	-6.34E-02
10.875	-9.10E-03	-1.56E-03	-1.44E-02	-4.11E-03	-6.68E-02	-5.35E-02

Table 13. MAPO test number 74 data (Continued).

Time	x (G's)	x Corrected (G's)	y (G's)	y Corrected (G's)	z (G's)	z Corrected (G's)
11.125	-6.49E-03	1.06E-03	-1.23E-02	-2.02E-03	-6.47E-02	-5.14E-02
11.375	-6.41E-03	1.13E-03	-1.51E-02	-4.74E-03	-5.95E-02	-4.62E-02
11.625	-6.03E-03	1.52E-03	-1.63E-02	-5.98E-03	-5.40E-02	-4.07E-02
11.875	-8.56E-03	-1.02E-03	-1.48E-02	-4.43E-03	-4.62E-02	-3.29E-02
12.125	-5.95E-03	1.59E-03	-1.95E-02	-9.16E-03	-3.89E-02	-2.56E-02
12.375	-7.64E-03	-9.60E-05	-1.83E-02	-8.00E-03	-3.72E-02	-2.39E-02
12.625	-9.49E-03	-1.94E-03	-1.83E-02	-8.00E-03	-2.88E-02	-1.55E-02
12.875	-7.95E-03	-4.03E-04	-1.89E-02	-8.62E-03	-2.33E-02	-1.00E-02
13.125	-1.27E-02	-5.17E-03	-1.37E-02	-3.34E-03	-2.29E-02	-9.63E-03
13.375	-1.04E-02	-2.86E-03	-1.39E-02	-3.57E-03	-1.78E-02	-4.51E-03
13.625	-1.05E-02	-2.94E-03	-1.48E-02	-4.43E-03	-1.88E-02	-5.48E-03
13.875	-8.79E-03	-1.25E-03	-1.29E-02	-2.56E-03	-1.86E-02	-5.25E-03
14.125	-1.25E-02	-4.94E-03	-1.64E-02	-6.06E-03	-2.00E-02	-6.74E-03
14.375	-1.00E-02	-2.48E-03	-1.23E-02	-2.02E-03	-2.67E-02	-1.33E-02
14.625	-1.72E-02	-9.62E-03	-1.35E-02	-3.18E-03	-2.77E-02	-1.44E-02
14.875	-9.18E-03	-1.63E-03	-1.19E-02	-1.55E-03	-2.33E-02	-1.00E-02
15.125	-8.18E-03	-6.34E-04	-1.21E-02	-1.79E-03	-2.21E-02	-8.82E-03
15.375	-1.16E-02	-4.09E-03	-1.62E-02	-5.82E-03	-1.82E-02	-4.88E-03
15.625	-9.64E-03	-2.09E-03	-1.28E-02	-2.48E-03	-2.20E-02	-8.67E-03
15.875	-8.03E-03	-4.80E-04	-1.19E-02	-1.55E-03	-2.08E-02	-7.48E-03
16.125	-1.09E-02	-3.32E-03	-1.16E-02	-1.32E-03	-1.92E-02	-5.92E-03
16.375	-1.11E-02	-3.55E-03	-1.26E-02	-2.25E-03	-1.77E-02	-4.36E-03
16.625	-6.95E-03	5.95E-04	-1.06E-02	-2.33E-04	-1.80E-02	-4.73E-03
16.875	-5.95E-03	1.59E-03	-1.28E-02	-2.48E-03	-1.36E-02	-2.78E-04
17.125	-5.34E-03	2.21E-03	-9.09E-03	1.24E-03	-1.48E-02	-1.47E-03
17.375	-8.41E-03	-8.64E-04	-6.99E-03	3.34E-03	-1.25E-02	8.35E-04
17.625	-9.41E-03	-1.86E-03	-1.23E-02	-2.02E-03	-1.16E-02	1.73E-03
17.875	-8.18E-03	-6.34E-04	-9.55E-03	7.76E-04	-1.17E-02	1.58E-03
18.125	-9.33E-03	-1.79E-03	-1.10E-02	-6.21E-04	-1.34E-02	-5.57E-05
18.375	-6.80E-03	7.49E-04	-1.03E-02	0.00E+00	-1.09E-02	2.39E-03
18.625	-9.64E-03	-2.09E-03	-8.85E-03	1.48E-03	-1.35E-02	-2.04E-04
18.875	-1.32E-02	-5.63E-03	-1.52E-02	-4.89E-03	-1.66E-02	-3.25E-03
19.125	-4.00E-02	-3.24E-02	-4.23E-02	-3.20E-02	-3.93E-02	-2.60E-02
19.375	-8.79E-03	-1.25E-03	-1.55E-02	-5.20E-03	-2.67E-02	-1.33E-02
19.625	-8.95E-03	-1.40E-03	-1.49E-02	-4.58E-03	-2.29E-02	-9.63E-03
19.875	-2.11E-02	-1.35E-02	-2.92E-02	-1.89E-02	-3.95E-02	-2.62E-02
20.125	-3.18E-02	-2.42E-02	-1.81E-02	-7.76E-03	-2.61E-02	-1.28E-02
20.375	-1.53E-02	-7.78E-03	-1.75E-02	-7.14E-03	-1.57E-02	-2.36E-03
20.625	-1.37E-02	-6.17E-03	-1.46E-02	-4.27E-03	-1.95E-02	-6.14E-03
20.875	-1.16E-02	-4.09E-03	-1.53E-02	-4.97E-03	-2.21E-02	-8.82E-03
21.125	-1.56E-02	-8.01E-03	-9.09E-03	1.24E-03	-2.06E-02	-7.26E-03
21.375	-1.09E-02	-3.32E-03	-8.31E-03	2.02E-03	-1.56E-02	-2.28E-03
21.625	-9.25E-03	-1.71E-03	-4.43E-03	5.90E-03	-1.41E-02	-7.98E-04
21.875	-8.03E-03	-4.80E-04	-3.96E-03	6.37E-03	-1.51E-02	-1.84E-03
22.125	-1.10E-02	-3.48E-03	-5.52E-03	4.81E-03	-1.33E-02	1.86E-05
22.375	-7.79E-03	-2.50E-04	-1.22E-02	-1.86E-03	-1.02E-02	3.06E-03
22.625	-7.95E-03	-4.03E-04	-8.54E-03	1.79E-03	-1.29E-02	3.90E-04
22.875	-7.18E-03	3.65E-04	-8.62E-03	1.71E-03	-1.06E-02	2.69E-03
23.125	-6.95E-03	5.95E-04	-8.08E-03	2.25E-03	-1.17E-02	1.58E-03
23.375	-7.41E-03	1.34E-04	-8.85E-03	1.48E-03	-1.27E-02	6.12E-04
23.625	-8.10E-03	-5.57E-04	-1.04E-02	-7.76E-05	-1.09E-02	2.39E-03
23.875	-8.33E-03	-7.88E-04	-1.13E-02	-1.01E-03	-1.18E-02	1.50E-03
24.125	-8.18E-03	-6.34E-04	-1.17E-02	-1.40E-03	-1.16E-02	1.73E-03
24.375	-8.87E-03	-1.33E-03	-8.31E-03	2.02E-03	-1.34E-02	-5.57E-05
24.625	-8.41E-03	-8.64E-04	-1.07E-02	-3.88E-04	-1.20E-02	1.35E-03
24.875	-7.33E-03	2.11E-04	-8.62E-03	1.71E-03	-1.31E-02	1.67E-04
25.125	-5.64E-03	1.90E-03	-1.03E-02	7.76E-05	-1.02E-02	3.14E-03
25.375	-8.49E-03	-9.41E-04	-1.01E-02	2.33E-04	-1.28E-02	5.38E-04

Table 13. MAPO test number 74 data (Continued).

Time	x (G's)	x Corrected (G's)	y (G's)	y Corrected (G's)	z (G's)	z Corrected (G's)
25.625	-8.41E-03	-8.64E-04	-6.99E-03	3.34E-03	-1.44E-02	-1.10E-03
25.875	-7.56E-03	-1.92E-05	-9.32E-03	1.01E-03	-1.16E-02	1.73E-03
26.125	-9.49E-03	-1.94E-03	-1.03E-02	0.00E+00	-1.23E-02	9.84E-04
26.375	-8.64E-03	-1.09E-03	-7.84E-03	2.48E-03	-1.37E-02	-3.53E-04
26.625	-4.88E-03	2.67E-03	-1.47E-02	-4.35E-03	-1.26E-02	6.87E-04
26.875	-3.49E-03	4.05E-03	-1.90E-02	-8.70E-03	-1.28E-02	5.38E-04
27.125	-1.13E-01	-1.06E-01	-1.38E-01	-1.28E-01	8.29E-02	9.62E-02
27.375	-1.02E-02	-2.63E-03	-2.88E-03	7.45E-03	-1.77E-02	-4.36E-03
27.625	-1.29E-02	-5.32E-03	-1.56E-03	8.77E-03	-1.66E-02	-3.32E-03
27.875	-1.29E-02	-5.32E-03	-4.82E-03	5.51E-03	-1.45E-02	-1.17E-03
28.125	-1.29E-02	-5.32E-03	-4.97E-03	5.36E-03	-1.43E-02	-9.47E-04
28.375	-1.12E-02	-3.63E-03	9.29E-04	1.13E-02	-3.41E-03	9.89E-03
28.625	-6.57E-03	9.80E-04	2.12E-02	3.15E-02	9.43E-03	2.27E-02
28.875	-1.57E-02	-8.16E-03	3.64E-02	4.67E-02	-8.91E-03	4.40E-03
29.125	-3.96E-02	-3.21E-02	2.03E-02	3.07E-02	-2.55E-02	-1.22E-02
29.375	-8.02E-02	-7.26E-02	-1.10E-02	-6.99E-04	-1.09E-01	-9.55E-02
29.625	-1.56E-01	-1.49E-01	-1.75E-02	-7.22E-03	-1.97E-01	-1.83E-01
29.875	-3.84E-01	-3.76E-01	-6.09E-02	-5.05E-02	-5.51E-01	-5.37E-01
30.125	-1.14E-01	-1.06E-01	-4.33E-02	-3.30E-02	-1.58E-01	-1.45E-01
30.375	-1.18E-01	-1.10E-01	-3.63E-02	-2.60E-02	-1.28E-01	-1.15E-01
30.625	-7.55E-02	-6.79E-02	-1.02E-01	-9.16E-02	-3.77E-01	-3.64E-01
30.875	-7.47E-02	-6.72E-02	-1.31E-01	-1.20E-01	-3.56E-01	-3.43E-01
31.125	-2.33E-02	-1.58E-02	-2.16E-01	-2.06E-01	-3.88E-01	-3.74E-01
31.375	5.34E-02	6.10E-02	-2.79E-01	-2.68E-01	-4.42E-01	-4.29E-01
31.625	-2.34E-03	5.21E-03	-2.87E-01	-2.76E-01	-3.38E-01	-3.25E-01
31.875	-8.49E-03	-9.41E-04	-1.86E-01	-1.76E-01	-4.98E-01	-4.85E-01
32.125	-2.96E-02	-2.21E-02	1.96E-02	3.00E-02	-7.74E-01	-7.60E-01
32.375	-4.88E-03	2.67E-03	1.38E-02	2.41E-02	-7.14E-01	-7.00E-01
32.625	-2.23E-02	-1.48E-02	-1.66E-02	-6.29E-03	-7.95E-01	-7.81E-01
32.875	-2.22E-02	-1.47E-02	-1.42E-02	-3.88E-03	-8.57E-01	-8.44E-01
33.125	-2.75E-02	-1.99E-02	-1.01E-02	2.33E-04	-9.16E-01	-9.03E-01
33.375	-2.52E-02	-1.77E-02	-1.08E-02	-4.66E-04	-9.55E-01	-9.42E-01
33.625	-3.99E-02	-3.24E-02	-1.31E-02	-2.80E-03	-9.88E-01	-9.75E-01
33.875	-3.71E-02	-2.96E-02	-1.58E-02	-5.43E-03	-1.03E+00	-1.01E+00
34.125	-4.06E-02	-3.31E-02	-1.09E-02	-5.43E-04	-1.06E+00	-1.05E+00
34.375	-3.82E-02	-3.07E-02	-1.44E-02	-4.11E-03	-1.09E+00	-1.08E+00
34.625	-4.78E-02	-4.03E-02	-2.07E-02	-1.04E-02	-1.14E+00	-1.12E+00
34.875	-5.11E-02	-4.36E-02	-2.14E-02	-1.10E-02	-1.17E+00	-1.15E+00
35.125	-4.68E-02	-3.92E-02	-3.06E-02	-2.03E-02	-1.20E+00	-1.19E+00
35.375	-5.60E-02	-4.85E-02	-3.08E-02	-2.05E-02	-1.23E+00	-1.22E+00
35.625	-6.04E-02	-5.29E-02	-2.69E-02	-1.65E-02	-1.25E+00	-1.23E+00
35.875	-6.80E-02	-6.05E-02	-2.58E-02	-1.55E-02	-1.28E+00	-1.27E+00
36.125	-6.73E-02	-5.97E-02	-3.18E-02	-2.15E-02	-1.32E+00	-1.30E+00
36.375	-6.42E-02	-5.66E-02	-2.87E-02	-1.84E-02	-1.33E+00	-1.32E+00
36.625	-7.06E-02	-6.30E-02	-2.31E-02	-1.27E-02	-1.36E+00	-1.35E+00
36.875	-7.35E-02	-6.59E-02	-1.75E-02	-7.22E-03	-1.38E+00	-1.36E+00
37.125	-6.99E-02	-6.23E-02	-9.79E-03	5.43E-04	-1.39E+00	-1.37E+00
37.375	-7.23E-02	-6.48E-02	-1.27E-02	-2.33E-03	-1.41E+00	-1.39E+00
37.625	-7.65E-02	-6.89E-02	-1.02E-02	1.55E-04	-1.42E+00	-1.41E+00
37.875	-7.72E-02	-6.96E-02	-8.00E-03	2.33E-03	-1.45E+00	-1.44E+00
38.125	-7.50E-02	-6.75E-02	-8.39E-03	1.94E-03	-1.47E+00	-1.45E+00
38.375	-7.53E-02	-6.77E-02	-9.24E-03	1.09E-03	-1.47E+00	-1.46E+00
38.625	-7.95E-02	-7.19E-02	-7.22E-03	3.11E-03	-1.50E+00	-1.49E+00
38.875	-7.34E-02	-6.59E-02	-2.54E-02	-1.51E-02	-1.50E+00	-1.49E+00
39.125	-7.28E-02	-6.53E-02	-2.91E-02	-1.88E-02	-1.52E+00	-1.51E+00
39.375	-7.43E-02	-6.68E-02	-3.87E-02	-2.84E-02	-1.53E+00	-1.52E+00
39.625	-7.75E-02	-6.99E-02	-2.52E-02	-1.48E-02	-1.54E+00	-1.53E+00
39.875	-6.37E-02	-5.62E-02	-2.11E-02	-1.08E-02	-1.54E+00	-1.53E+00

Table 14. MAPO test number 90 data.

Test File: MAPOTEST.090 Test Date: Wed, 12-12-1996 No. Channels: 3 Sam/sec: 128      Average      32 pt centered Start: 10:16:23:97    End: 10:17:04:01 Low-g Range start    10:16:34    (10 sec) end      10:16:45    (21 sec) Accelerometer Bias Average Interval (14 to 21 sec)  Bias Values    x      -0.0077 (g's)          y      -0.0095 z      -0.0119 Time Stamp Offset Between Data and Video    1 sec						
Time	x (g's)	x Corrected (g's)	y (g's)	y Corrected (g's)	z (g's)	z Corrected (g's)
0.125	-1.38E-01	-1.31E-01	-2.11E-02	-1.17E-02	1.71E+00	1.73E+00
0.375	-1.50E-01	-1.43E-01	1.09E-02	2.04E-02	1.66E+00	1.67E+00
0.625	-1.35E-01	-1.27E-01	-1.30E-02	-3.50E-03	1.59E+00	1.60E+00
0.875	-1.47E-01	-1.39E-01	6.67E-03	1.61E-02	1.51E+00	1.52E+00
1.125	-1.40E-01	-1.32E-01	-1.71E-02	-7.61E-03	1.56E+00	1.57E+00
1.375	-1.60E-01	-1.53E-01	2.41E-02	3.35E-02	1.52E+00	1.53E+00
1.625	-1.59E-01	-1.52E-01	1.65E-02	2.60E-02	1.50E+00	1.51E+00
1.875	-1.33E-01	-1.25E-01	-2.02E-02	-1.07E-02	1.54E+00	1.55E+00
2.125	-1.52E-01	-1.44E-01	2.39E-02	3.34E-02	1.44E+00	1.45E+00
2.375	-1.23E-01	-1.15E-01	7.45E-03	1.69E-02	1.27E+00	1.28E+00
2.625	-1.11E-01	-1.04E-01	1.35E-02	2.30E-02	1.10E+00	1.11E+00
2.875	-9.85E-02	-9.08E-02	6.44E-03	1.59E-02	9.16E-01	9.28E-01
3.125	-6.70E-02	-5.92E-02	-4.66E-03	4.81E-03	7.46E-01	7.58E-01
3.375	-7.16E-02	-6.39E-02	-1.71E-03	7.76E-03	6.07E-01	6.19E-01
3.625	-4.68E-02	-3.91E-02	-2.14E-02	-1.20E-02	5.36E-01	5.48E-01
3.875	-3.88E-02	-3.11E-02	-9.24E-03	2.28E-04	4.50E-01	4.62E-01
4.125	-3.18E-02	-2.40E-02	-1.34E-02	-3.89E-03	3.86E-01	3.98E-01
4.375	-2.75E-02	-1.97E-02	-1.35E-02	-4.04E-03	3.72E-01	3.84E-01
4.625	-2.42E-02	-1.65E-02	-8.31E-03	1.16E-03	3.39E-01	3.51E-01
4.875	-2.48E-02	-1.70E-02	-1.32E-03	8.15E-03	3.21E-01	3.33E-01
5.125	-1.75E-02	-9.74E-03	1.16E-03	1.06E-02	3.06E-01	3.18E-01
5.375	-1.79E-02	-1.02E-02	4.97E-03	1.44E-02	2.74E-01	2.86E-01
5.625	-1.59E-02	-8.13E-03	1.05E-02	1.99E-02	2.50E-01	2.62E-01
5.875	-1.25E-02	-4.75E-03	1.52E-02	2.47E-02	2.17E-01	2.28E-01
6.125	-1.02E-02	-2.44E-03	1.16E-02	2.10E-02	1.87E-01	1.99E-01
6.375	-2.57E-03	5.17E-03	1.05E-02	1.99E-02	1.56E-01	1.68E-01
6.625	-5.87E-03	1.86E-03	1.46E-02	2.41E-02	1.27E-01	1.39E-01
6.875	-7.49E-03	2.49E-04	-8.04E-05	9.39E-03	1.21E-01	1.33E-01
7.125	-3.18E-03	4.55E-03	-2.80E-03	6.67E-03	1.01E-01	1.13E-01
7.375	-7.64E-03	9.54E-05	-8.70E-03	7.71E-04	1.08E-01	1.20E-01
7.625	7.34E-04	8.47E-03	-1.41E-02	-4.66E-03	1.14E-01	1.26E-01
7.875	-1.04E-02	-2.67E-03	-1.30E-02	-3.58E-03	1.22E-01	1.34E-01
8.125	-2.65E-03	5.09E-03	-9.09E-03	3.83E-04	1.25E-01	1.37E-01
8.375	-7.56E-03	1.72E-04	-8.16E-03	1.31E-03	1.28E-01	1.40E-01
8.625	-3.72E-03	4.01E-03	-6.84E-03	2.63E-03	1.12E-01	1.24E-01
8.875	-3.88E-03	3.86E-03	-1.48E-02	-5.36E-03	1.07E-01	1.19E-01
9.125	-8.79E-03	-1.06E-03	-1.37E-02	-4.20E-03	7.77E-02	8.96E-02
9.375	-3.42E-03	4.32E-03	-1.79E-02	-8.39E-03	5.11E-02	6.30E-02
9.625	-1.19E-03	6.55E-03	-1.64E-02	-6.92E-03	3.48E-02	4.68E-02
9.875	-6.95E-03	7.87E-04	-1.66E-02	-7.15E-03	1.14E-02	2.34E-02
10.125	-7.33E-03	4.03E-04	-1.61E-02	-6.60E-03	-1.48E-04	1.18E-02
10.375	-8.56E-03	-8.27E-04	-1.28E-02	-3.34E-03	-5.86E-03	6.07E-03
10.625	-9.56E-03	-1.83E-03	-9.09E-03	3.83E-04	-1.14E-02	5.02E-04
10.875	-9.33E-03	-1.60E-03	-1.03E-02	-8.59E-04	-1.31E-02	-1.13E-03

Table 14. MAPO test number 90 data (Continued).

Time	x (g's)	x Corrected (g's)	y (g's)	y Corrected (g's)	z (g's)	z Corrected (g's)
11.125	-1.06E-02	-2.90E-03	-9.79E-03	-3.16E-04	-1.37E-02	-1.73E-03
11.375	-2.88E-03	4.86E-03	-5.59E-03	3.88E-03	-8.98E-03	2.95E-03
11.625	-4.80E-03	2.94E-03	-1.05E-02	-1.01E-03	-5.35E-03	6.59E-03
11.875	-8.64E-03	-9.03E-04	-1.08E-02	-1.33E-03	1.65E-02	2.84E-02
12.125	-7.72E-03	1.85E-05	-1.26E-02	-3.11E-03	-2.52E-03	9.41E-03
12.375	-3.49E-03	4.24E-03	-4.35E-03	5.12E-03	1.38E-02	2.57E-02
12.625	-9.41E-03	-1.67E-03	6.18E-04	1.01E-02	1.20E-02	2.40E-02
12.875	-3.95E-03	3.78E-03	-3.13E-04	9.16E-03	1.17E-02	2.36E-02
13.125	-9.64E-03	-1.90E-03	-7.07E-03	2.40E-03	7.72E-03	1.97E-02
13.375	-5.26E-03	2.48E-03	-8.16E-03	1.31E-03	6.09E-03	1.80E-02
13.625	-6.80E-03	9.41E-04	-4.74E-03	4.73E-03	-5.86E-03	6.07E-03
13.875	-4.88E-03	2.86E-03	-8.85E-03	6.16E-04	-8.98E-03	2.95E-03
14.125	-4.95E-03	2.78E-03	-9.63E-03	-1.61E-04	-1.16E-02	3.53E-04
14.375	-9.64E-03	-1.90E-03	-9.16E-03	3.05E-04	-1.23E-02	-3.89E-04
14.625	-8.41E-03	-6.73E-04	-8.78E-03	6.93E-04	-1.23E-02	-3.89E-04
14.875	-8.03E-03	-2.89E-04	-8.70E-03	7.71E-04	-1.29E-02	-9.83E-04
15.125	-7.64E-03	9.54E-05	-9.16E-03	3.05E-04	-1.31E-02	-1.13E-03
15.375	-7.03E-03	7.10E-04	-9.24E-03	2.28E-04	-1.26E-02	-6.86E-04
15.625	-9.87E-03	-2.13E-03	-9.01E-03	4.60E-04	-1.18E-02	1.31E-04
15.875	-8.64E-03	-9.03E-04	-9.86E-03	-3.94E-04	-1.18E-02	1.31E-04
16.125	-8.18E-03	-4.42E-04	-9.86E-03	-3.94E-04	-1.12E-02	7.24E-04
16.375	-8.79E-03	-1.06E-03	-8.54E-03	9.26E-04	-1.25E-02	-5.38E-04
16.625	-8.72E-03	-9.80E-04	-9.16E-03	3.05E-04	-1.21E-02	-1.66E-04
16.875	-7.49E-03	2.49E-04	-9.47E-03	-5.35E-06	-1.44E-02	-2.47E-03
17.125	-7.03E-03	7.10E-04	-8.78E-03	6.93E-04	-1.32E-02	-1.28E-03
17.375	-7.72E-03	1.85E-05	-9.24E-03	2.28E-04	-1.22E-02	-3.15E-04
17.625	-1.16E-02	-3.82E-03	-9.16E-03	3.05E-04	-1.31E-02	-1.13E-03
17.875	-7.10E-03	6.33E-04	-9.09E-03	3.83E-04	-1.14E-02	5.02E-04
18.125	-7.79E-03	-5.83E-05	-1.10E-02	-1.48E-03	-1.11E-02	8.73E-04
18.375	-7.10E-03	6.33E-04	-1.38E-02	-4.35E-03	-9.87E-03	2.06E-03
18.625	-5.57E-03	2.17E-03	-9.94E-03	-4.71E-04	-1.06E-02	1.32E-03
18.875	-7.56E-03	1.72E-04	-8.85E-03	6.16E-04	-1.28E-02	-8.35E-04
19.125	-8.03E-03	-2.89E-04	-1.07E-02	-1.25E-03	-1.08E-02	1.10E-03
19.375	-7.03E-03	7.10E-04	-9.86E-03	-3.94E-04	-1.04E-02	1.54E-03
19.625	-7.03E-03	7.10E-04	-1.12E-02	-1.71E-03	-1.08E-02	1.17E-03
19.875	-5.95E-03	1.79E-03	-1.02E-02	-7.04E-04	-1.14E-02	5.76E-04
20.125	-6.87E-03	8.64E-04	-8.31E-03	1.16E-03	-1.22E-02	-2.41E-04
20.375	-7.95E-03	-2.12E-04	-7.15E-03	2.32E-03	-1.22E-02	-3.15E-04
20.625	-8.64E-03	-9.03E-04	-8.93E-03	5.38E-04	-1.08E-02	1.10E-03
20.875	-6.64E-03	1.09E-03	-8.93E-03	5.38E-04	-1.28E-02	-8.35E-04
21.125	-7.41E-03	3.26E-04	-8.93E-03	5.38E-04	-1.18E-02	1.31E-04
21.375	-5.64E-03	2.09E-03	-9.32E-03	1.50E-04	-1.22E-02	-3.15E-04
21.625	-7.33E-03	4.03E-04	-1.23E-02	-2.88E-03	-1.89E-02	-7.00E-03
21.875	1.09E-01	1.17E-01	1.45E-01	1.55E-01	8.83E-02	1.00E-01
22.125	-5.82E-02	-5.05E-02	4.24E-02	5.19E-02	1.77E-01	1.89E-01
22.375	-1.24E-02	-4.67E-03	-8.63E-02	-7.68E-02	-5.30E-02	-4.11E-02
22.625	1.11E-02	1.88E-02	-2.36E-04	9.23E-03	-3.27E-02	-2.07E-02
22.875	7.27E-03	1.50E-02	3.00E-02	3.94E-02	-1.48E-02	-2.91E-03
23.125	-8.49E-03	-7.50E-04	-1.82E-02	-8.70E-03	-3.60E-02	-2.41E-02
23.375	-6.10E-03	1.63E-03	-1.92E-02	-9.71E-03	-2.39E-02	-1.20E-02
23.625	-4.72E-03	3.02E-03	-1.26E-02	-3.11E-03	-4.11E-02	-2.91E-02
23.875	-2.34E-03	5.40E-03	-1.28E-02	-3.34E-03	-3.58E-02	-2.38E-02
24.125	-7.49E-03	2.49E-04	-2.98E-02	-2.03E-02	-2.98E-02	-1.79E-02
24.375	2.73E-04	8.01E-03	-1.27E-02	-3.19E-03	-4.48E-02	-3.28E-02
24.625	-1.26E-02	-4.90E-03	-2.02E-03	7.45E-03	-2.58E-02	-1.39E-02
24.875	4.16E-02	4.93E-02	-2.98E-02	-2.03E-02	1.33E-02	2.52E-02
25.125	7.19E-03	1.49E-02	4.84E-02	5.78E-02	3.62E-02	4.82E-02
25.375	1.04E-02	1.82E-02	1.71E-03	1.12E-02	-3.34E-03	8.59E-03

Table 14. MAPO test number 90 data (Continued).

Time	x (g's)	x Corrected (g's)	y (g's)	y Corrected (g's)	z (g's)	z Corrected (g's)
25.625	-2.65E-03	5.09E-03	-1.47E-02	-5.21E-03	6.01E-03	1.79E-02
25.875	1.13E-02	1.90E-02	2.22E-02	3.17E-02	4.05E-02	5.25E-02
26.125	1.03E-02	1.80E-02	-1.26E-02	-3.11E-03	3.07E-02	4.27E-02
26.375	6.42E-03	1.42E-02	-3.88E-03	5.58E-03	3.59E-02	4.79E-02
26.625	8.65E-03	1.64E-02	-1.33E-02	-3.81E-03	5.56E-02	6.75E-02
26.875	1.56E-02	2.34E-02	-1.25E-02	-3.03E-03	7.79E-02	8.98E-02
27.125	7.50E-03	1.52E-02	-9.86E-03	-3.94E-04	1.15E-01	1.27E-01
27.375	7.42E-03	1.52E-02	-8.39E-03	1.08E-03	1.72E-01	1.84E-01
27.625	9.19E-03	1.69E-02	-1.17E-02	-2.26E-03	2.33E-01	2.45E-01
27.875	1.87E-02	2.65E-02	1.47E-02	2.41E-02	2.91E-01	3.03E-01
28.125	1.57E-02	2.35E-02	-1.53E-02	-5.83E-03	3.60E-01	3.72E-01
28.375	1.33E-02	2.11E-02	-1.48E-02	-5.36E-03	4.51E-01	4.63E-01
28.625	8.65E-03	1.64E-02	-1.65E-02	-6.99E-03	5.38E-01	5.50E-01
28.875	1.73E-03	9.47E-03	-2.06E-02	-1.11E-02	6.48E-01	6.60E-01
29.125	8.88E-04	8.62E-03	-1.97E-02	-1.03E-02	7.66E-01	7.78E-01
29.375	-4.88E-03	2.86E-03	-9.55E-03	-8.30E-05	8.56E-01	8.68E-01
29.625	-1.51E-02	-7.36E-03	-7.30E-03	2.17E-03	9.49E-01	9.61E-01
29.875	-2.68E-02	-1.90E-02	-5.83E-03	3.64E-03	1.03E+00	1.04E+00
30.125	-3.16E-02	-2.39E-02	8.51E-04	1.03E-02	1.07E+00	1.08E+00
30.375	-3.39E-02	-2.62E-02	8.69E-03	1.82E-02	1.11E+00	1.12E+00
30.625	-4.01E-02	-3.23E-02	1.13E-02	2.07E-02	1.13E+00	1.15E+00
30.875	-4.97E-02	-4.19E-02	9.78E-03	1.92E-02	1.17E+00	1.18E+00
31.125	-5.29E-02	-4.52E-02	7.53E-03	1.70E-02	1.21E+00	1.22E+00
31.375	-5.63E-02	-4.85E-02	-8.04E-05	9.39E-03	1.24E+00	1.25E+00
31.625	-6.21E-02	-5.44E-02	-7.46E-03	2.01E-03	1.26E+00	1.27E+00
31.875	-6.31E-02	-5.54E-02	-1.49E-02	-5.44E-03	1.29E+00	1.30E+00
32.125	-6.46E-02	-5.68E-02	-1.30E-02	-3.50E-03	1.31E+00	1.32E+00
32.375	-6.44E-02	-5.67E-02	-1.10E-02	-1.56E-03	1.34E+00	1.35E+00
32.625	-7.04E-02	-6.27E-02	-1.20E-02	-2.49E-03	1.37E+00	1.38E+00
32.875	-7.10E-02	-6.33E-02	-1.02E-02	-7.04E-04	1.40E+00	1.41E+00
33.125	-6.68E-02	-5.91E-02	-6.99E-03	2.48E-03	1.41E+00	1.42E+00
33.375	-6.26E-02	-5.48E-02	-6.29E-03	3.18E-03	1.43E+00	1.44E+00
33.625	-7.26E-02	-6.49E-02	-1.41E-02	-4.59E-03	1.45E+00	1.46E+00
33.875	-6.81E-02	-6.04E-02	-6.45E-03	3.02E-03	1.46E+00	1.47E+00
34.125	-6.64E-02	-5.87E-02	-1.12E-02	-1.71E-03	1.49E+00	1.50E+00
34.375	-6.97E-02	-6.20E-02	-5.13E-03	4.34E-03	1.53E+00	1.54E+00
34.625	-8.11E-02	-7.34E-02	-4.04E-03	5.43E-03	1.55E+00	1.56E+00
34.875	-7.40E-02	-6.62E-02	-2.64E-03	6.83E-03	1.57E+00	1.59E+00
35.125	-7.79E-02	-7.02E-02	-2.36E-04	9.23E-03	1.58E+00	1.59E+00
35.375	-8.64E-02	-7.87E-02	-4.04E-03	5.43E-03	1.60E+00	1.61E+00
35.625	-8.03E-02	-7.25E-02	3.18E-03	1.26E-02	1.61E+00	1.62E+00
35.875	-7.57E-02	-6.80E-02	-3.03E-03	6.44E-03	1.61E+00	1.63E+00
36.125	-8.35E-02	-7.57E-02	-8.57E-04	8.61E-03	1.60E+00	1.61E+00
36.375	-7.83E-02	-7.05E-02	-9.24E-03	2.28E-04	1.58E+00	1.59E+00
36.625	-6.54E-02	-5.77E-02	-9.40E-03	7.23E-05	1.56E+00	1.57E+00
36.875	-6.60E-02	-5.82E-02	-9.55E-03	-8.30E-05	1.56E+00	1.57E+00
37.125	-7.20E-02	-6.43E-02	-2.23E-02	-1.28E-02	1.56E+00	1.57E+00
37.375	-7.43E-02	-6.66E-02	-1.10E-02	-1.56E-03	1.56E+00	1.57E+00
37.625	-6.70E-02	-5.92E-02	-1.19E-02	-2.41E-03	1.56E+00	1.58E+00
37.875	-7.10E-02	-6.33E-02	-7.30E-03	2.17E-03	1.55E+00	1.57E+00
38.125	-6.75E-02	-5.98E-02	-2.56E-03	6.90E-03	1.54E+00	1.56E+00
38.375	-6.60E-02	-5.82E-02	-1.23E-02	-2.80E-03	1.54E+00	1.55E+00
38.625	-6.09E-02	-5.32E-02	-6.60E-03	2.87E-03	1.52E+00	1.54E+00
38.875	-5.87E-02	-5.09E-02	-9.71E-03	-2.38E-04	1.52E+00	1.54E+00
39.125	-6.23E-02	-5.45E-02	-5.98E-03	3.49E-03	1.52E+00	1.53E+00
39.375	-4.65E-02	-3.88E-02	-1.23E-02	-2.80E-03	1.53E+00	1.54E+00
39.625	-5.60E-02	-4.83E-02	-2.10E-03	7.37E-03	1.52E+00	1.54E+00
39.875	-5.84E-02	-5.07E-02	-1.06E-02	-1.09E-03	1.53E+00	1.54E+00

Table 15. MAPO test number 97 data.

Test File: MAPOTEST.097 Test Date: Wed, 12-12-1996 No. Channels: 3 Sam/sec: 128      Average      32 pt centered Start: 10:28:37:17    End: 10:29:17:21 Low-g Range start      10:28:48      (10 sec) end      10:29:01      (24 sec) Accelerometer Bias Average Interval (20 to 24 sec)  Bias Values <i>x</i> -0.0078 (g's) <i>y</i> -0.0090 <i>z</i> -0.0119 Time Stamp Offset Between Data and Video      0 sec						
Time	<i>x</i> (g's)	<i>x</i> Corrected (g's)	<i>y</i> (g's)	<i>y</i> Corrected (g's)	<i>z</i> (g's)	<i>z</i> Corrected (g's)
0.125	-1.47E-01	-1.39E-01	1.72E+00	1.73E+00	2.15E-02	3.34E-02
0.375	-1.58E-01	-1.50E-01	1.69E+00	1.70E+00	-7.42E-05	1.18E-02
0.625	-1.22E-01	-1.14E-01	1.60E+00	1.61E+00	5.42E-02	6.61E-02
0.875	-1.13E-01	-1.05E-01	1.45E+00	1.45E+00	1.90E-02	3.09E-02
1.125	-1.07E-01	-9.89E-02	1.20E+00	1.21E+00	-9.95E-03	1.96E-03
1.375	-9.07E-02	-8.29E-02	9.66E-01	9.75E-01	-3.31E-02	-2.12E-02
1.625	-5.04E-02	-4.26E-02	7.31E-01	7.40E-01	8.02E-03	1.99E-02
1.875	-3.54E-02	-2.76E-02	5.99E-01	6.08E-01	8.54E-03	2.04E-02
2.125	-4.32E-02	-3.54E-02	5.43E-01	5.52E-01	-1.93E-02	-7.40E-03
2.375	-3.92E-02	-3.14E-02	4.66E-01	4.75E-01	-8.24E-03	3.66E-03
2.625	-3.61E-02	-2.83E-02	4.38E-01	4.47E-01	-9.50E-03	2.40E-03
2.875	-2.59E-02	-1.80E-02	4.30E-01	4.39E-01	-9.06E-03	2.85E-03
3.125	-2.77E-02	-1.99E-02	4.10E-01	4.19E-01	-1.64E-02	-4.50E-03
3.375	-2.02E-02	-1.24E-02	3.88E-01	3.97E-01	-1.92E-02	-7.25E-03
3.625	-1.92E-02	-1.14E-02	3.30E-01	3.39E-01	-1.20E-02	-1.22E-04
3.875	-1.73E-02	-9.51E-03	2.93E-01	3.02E-01	-7.42E-03	4.48E-03
4.125	-1.42E-02	-6.44E-03	2.68E-01	2.77E-01	-5.72E-03	6.19E-03
4.375	-1.22E-02	-4.37E-03	2.24E-01	2.33E-01	-8.76E-03	3.14E-03
4.625	-9.87E-03	-2.06E-03	1.94E-01	2.03E-01	-1.32E-02	-1.31E-03
4.875	-1.15E-02	-3.67E-03	1.63E-01	1.72E-01	-1.21E-02	-1.97E-04
5.125	-1.38E-02	-5.98E-03	1.31E-01	1.40E-01	-1.77E-02	-5.84E-03
5.375	-1.39E-02	-6.06E-03	1.01E-01	1.10E-01	-1.56E-02	-3.69E-03
5.625	-1.13E-02	-3.44E-03	6.13E-02	7.03E-02	-1.48E-02	-2.94E-03
5.875	-1.19E-02	-4.06E-03	4.35E-02	5.24E-02	-1.54E-02	-3.54E-03
6.125	-1.36E-02	-5.83E-03	3.21E-02	4.10E-02	-1.28E-02	-8.65E-04
6.375	-1.31E-02	-5.29E-03	8.77E-03	1.77E-02	-1.06E-02	1.29E-03
6.625	-1.06E-02	-2.83E-03	4.03E-03	1.30E-02	-9.73E-03	2.18E-03
6.875	-1.03E-02	-2.52E-03	-1.01E-03	7.95E-03	-1.06E-02	1.29E-03
7.125	-9.25E-03	-1.45E-03	-3.03E-03	5.93E-03	-9.06E-03	2.85E-03
7.375	-9.33E-03	-1.52E-03	6.96E-04	9.66E-03	-9.65E-03	2.25E-03
7.625	-1.09E-02	-3.06E-03	-1.32E-03	7.64E-03	-8.02E-03	3.89E-03
7.875	-1.63E-02	-8.52E-03	1.27E-02	2.16E-02	-4.60E-03	7.30E-03
8.125	-1.50E-02	-7.21E-03	1.65E-02	2.55E-02	-1.19E-03	1.07E-02
8.375	-1.50E-02	-7.21E-03	2.49E-02	3.39E-02	2.23E-04	1.21E-02
8.625	-1.19E-02	-4.06E-03	2.76E-02	3.65E-02	-4.31E-03	7.60E-03
8.875	-1.24E-02	-4.60E-03	2.75E-02	3.64E-02	-4.23E-03	7.67E-03
9.125	-9.64E-03	-1.83E-03	3.39E-02	4.29E-02	-6.68E-03	5.22E-03
9.375	-1.13E-02	-3.52E-03	2.83E-02	3.73E-02	-4.38E-03	7.52E-03
9.625	-1.60E-02	-8.21E-03	2.05E-02	2.95E-02	-4.16E-03	7.75E-03
9.875	-1.26E-02	-4.83E-03	1.86E-02	2.76E-02	-5.12E-03	6.78E-03
10.125	-1.20E-02	-4.21E-03	4.58E-03	1.35E-02	-7.28E-03	4.63E-03
10.375	-1.58E-02	-7.98E-03	7.37E-03	1.63E-02	-6.46E-03	5.45E-03
10.625	-8.18E-03	-3.71E-04	6.05E-03	1.50E-02	-5.86E-03	6.04E-03
10.875	-1.43E-02	-6.52E-03	9.86E-03	1.88E-02	-7.35E-03	4.55E-03

Table 15. MAPO test number 97 data (Continued).

Time	x (g's)	x Corrected (g's)	y (g's)	y Corrected (g's)	z (g's)	z Corrected (g's)
11.125	-1.33E-02	-5.52E-03	8.46E-03	1.74E-02	-5.64E-03	6.26E-03
11.375	-1.09E-02	-3.14E-03	6.96E-04	9.66E-03	-7.57E-03	4.33E-03
11.625	-1.26E-02	-4.83E-03	3.65E-03	1.26E-02	-7.72E-03	4.18E-03
11.875	-1.28E-02	-4.98E-03	5.35E-03	1.43E-02	-5.72E-03	6.19E-03
12.125	-1.85E-02	-1.07E-02	5.04E-03	1.40E-02	-7.05E-03	4.85E-03
12.375	-1.73E-02	-9.51E-03	9.70E-03	1.87E-02	-1.31E-02	-1.16E-03
12.625	-1.55E-02	-7.67E-03	8.54E-03	1.75E-02	-1.61E-02	-4.21E-03
12.875	-1.61E-02	-8.28E-03	9.39E-03	1.84E-02	-1.54E-02	-3.54E-03
13.125	-1.43E-02	-6.52E-03	8.85E-03	1.78E-02	-1.69E-02	-4.95E-03
13.375	-1.56E-02	-7.82E-03	9.78E-03	1.87E-02	-1.63E-02	-4.35E-03
13.625	-1.31E-02	-5.29E-03	7.84E-03	1.68E-02	-1.60E-02	-4.06E-03
13.875	-1.31E-02	-5.29E-03	3.72E-03	1.27E-02	-1.49E-02	-3.02E-03
14.125	-1.48E-02	-6.98E-03	6.13E-03	1.51E-02	-1.49E-02	-3.02E-03
14.375	-1.33E-02	-5.52E-03	6.67E-03	1.56E-02	-1.51E-02	-3.17E-03
14.625	-8.87E-03	-1.06E-03	4.73E-03	1.37E-02	-1.47E-02	-2.79E-03
14.875	-1.54E-02	-7.59E-03	7.14E-03	1.61E-02	-1.69E-02	-5.02E-03
15.125	-1.26E-02	-4.75E-03	7.14E-03	1.61E-02	-1.71E-02	-5.17E-03
15.375	-1.37E-02	-5.90E-03	7.53E-03	1.65E-02	-1.59E-02	-3.98E-03
15.625	-1.26E-02	-4.75E-03	5.82E-03	1.48E-02	-1.54E-02	-3.54E-03
15.875	-1.46E-02	-6.75E-03	5.28E-03	1.42E-02	-1.76E-02	-5.69E-03
16.125	-1.19E-02	-4.06E-03	3.34E-03	1.23E-02	-1.63E-02	-4.43E-03
16.375	-1.23E-02	-4.52E-03	5.90E-03	1.49E-02	-1.49E-02	-3.02E-03
16.625	-8.87E-03	-1.06E-03	1.94E-03	1.09E-02	-1.74E-02	-5.47E-03
16.875	-1.19E-02	-4.06E-03	-1.56E-03	7.41E-03	-1.37E-02	-1.83E-03
17.125	-1.16E-02	-3.75E-03	-1.48E-03	7.49E-03	-1.18E-02	1.00E-04
17.375	-9.49E-03	-1.68E-03	3.85E-04	9.35E-03	-1.37E-02	-1.83E-03
17.625	-7.41E-03	3.98E-04	-4.97E-03	3.99E-03	-1.18E-02	1.00E-04
17.875	-8.87E-03	-1.06E-03	-5.05E-03	3.91E-03	-1.24E-02	-4.93E-04
18.125	-1.16E-02	-3.75E-03	-5.05E-03	3.91E-03	-1.42E-02	-2.28E-03
18.375	-9.02E-03	-1.22E-03	-7.61E-03	1.35E-03	-1.31E-02	-1.16E-03
18.625	-7.72E-03	9.04E-05	-7.46E-03	1.51E-03	-1.28E-02	-8.65E-04
18.875	-1.09E-02	-3.06E-03	-3.57E-03	5.39E-03	-1.11E-02	7.69E-04
19.125	-1.11E-02	-3.29E-03	-4.12E-03	4.85E-03	-9.65E-03	2.25E-03
19.375	-8.41E-03	-6.01E-04	-7.61E-03	1.35E-03	-1.27E-02	-7.90E-04
19.625	-8.26E-03	-4.47E-04	-9.71E-03	-7.44E-04	-1.09E-02	9.91E-04
19.875	-9.49E-03	-1.68E-03	-2.56E-03	6.40E-03	-1.33E-02	-1.38E-03
20.125	-4.11E-03	3.70E-03	-8.54E-03	4.20E-04	-1.28E-02	-9.39E-04
20.375	-9.02E-03	-1.22E-03	-8.54E-03	4.20E-04	-1.21E-02	-1.97E-04
20.625	-1.02E-02	-2.37E-03	-9.09E-03	-1.23E-04	-1.11E-02	7.69E-04
20.875	-1.23E-02	-4.44E-03	-6.84E-03	2.13E-03	-1.31E-02	-1.16E-03
21.125	-9.79E-03	-1.98E-03	-8.23E-03	7.31E-04	-1.24E-02	-4.93E-04
21.375	-8.56E-03	-7.55E-04	-9.01E-03	-4.57E-05	-1.08E-02	1.14E-03
21.625	-8.18E-03	-3.71E-04	-8.54E-03	4.20E-04	-1.31E-02	-1.16E-03
21.875	-4.64E-03	3.16E-03	-1.03E-02	-1.37E-03	-1.05E-02	1.36E-03
22.125	-8.10E-03	-2.94E-04	-9.16E-03	-2.01E-04	-1.18E-02	1.00E-04
22.375	-8.95E-03	-1.14E-03	-8.54E-03	4.20E-04	-1.18E-02	1.00E-04
22.625	-5.57E-03	2.24E-03	-8.62E-03	3.43E-04	-1.37E-02	-1.83E-03
22.875	-7.49E-03	3.21E-04	-7.46E-03	1.51E-03	-1.31E-02	-1.24E-03
23.125	-9.02E-03	-1.22E-03	-1.02E-02	-1.21E-03	-1.11E-02	8.43E-04
23.375	-5.49E-03	2.32E-03	-1.05E-02	-1.52E-03	-1.17E-02	2.49E-04
23.625	-6.41E-03	1.40E-03	-9.86E-03	-9.00E-04	-1.05E-02	1.44E-03
23.875	-9.18E-03	-1.37E-03	-9.79E-03	-8.22E-04	-1.08E-02	1.14E-03
24.125	-5.80E-03	2.01E-03	-9.16E-03	-2.01E-04	-1.20E-02	-1.22E-04
24.375	-8.95E-03	-1.14E-03	-9.55E-03	-5.89E-04	-1.31E-02	-1.16E-03
24.625	-8.72E-03	-9.08E-04	-8.23E-03	7.31E-04	-1.05E-02	1.36E-03
24.875	-6.10E-03	1.70E-03	-9.71E-03	-7.44E-04	-1.25E-02	-6.42E-04
25.125	-4.24E-02	-3.46E-02	-3.34E-03	5.62E-03	-1.77E-02	-5.76E-03
25.375	-6.91E-02	-6.13E-02	1.18E-02	2.08E-02	-3.79E-02	-2.60E-02

Table 15. MAPO test number 97 data (Continued).

Time	x (g's)	x Corrected (g's)	y (g's)	y Corrected (g's)	z (g's)	z Corrected (g's)
25.625	-6.28E-02	-5.50E-02	-2.97E-02	-2.08E-02	-3.53E-02	-2.34E-02
25.875	-5.40E-02	-4.62E-02	-3.00E-02	-2.10E-02	-5.56E-02	-4.37E-02
26.125	-4.36E-02	-3.58E-02	-3.38E-02	-2.48E-02	-8.55E-02	-7.36E-02
26.375	-1.91E-02	-1.13E-02	-9.09E-03	-1.23E-04	-4.45E-02	-3.26E-02
26.625	-2.44E-02	-1.66E-02	-6.58E-02	-5.69E-02	-4.46E-02	-3.27E-02
26.875	-2.74E-02	-1.96E-02	-9.71E-02	-8.82E-02	-5.32E-02	-4.13E-02
27.125	-3.08E-02	-2.30E-02	-1.01E-01	-9.17E-02	-7.14E-02	-5.95E-02
27.375	-1.55E-02	-7.67E-03	-8.18E-02	-7.29E-02	-5.01E-02	-3.82E-02
27.625	3.73E-03	1.15E-02	-2.10E-02	-1.21E-02	-2.44E-02	-1.25E-02
27.875	1.61E-02	2.39E-02	-6.60E-03	2.36E-03	-2.41E-02	-1.21E-02
28.125	2.72E-02	3.50E-02	1.34E-02	2.23E-02	-4.96E-02	-3.77E-02
28.375	-3.94E-02	-3.16E-02	1.44E-01	1.53E-01	-2.00E-03	9.90E-03
28.625	-1.04E-01	-9.66E-02	2.36E-01	2.45E-01	-1.86E-02	-6.66E-03
28.875	-2.19E-01	-2.11E-01	7.37E-01	7.46E-01	8.98E-02	1.02E-01
29.125	1.23E-01	1.31E-01	6.62E-01	6.71E-01	1.45E-02	2.64E-02
29.375	2.83E-02	3.61E-02	8.20E-01	8.29E-01	1.40E-01	1.52E-01
29.625	-1.99E-02	-1.20E-02	9.15E-01	9.24E-01	2.74E-02	3.93E-02
29.875	-3.87E-02	-3.09E-02	1.03E+00	1.04E+00	4.40E-02	5.59E-02
30.125	-5.00E-02	-4.22E-02	1.15E+00	1.16E+00	4.80E-02	5.99E-02
30.375	-6.06E-02	-5.28E-02	1.27E+00	1.27E+00	5.37E-02	6.56E-02
30.625	-7.20E-02	-6.42E-02	1.34E+00	1.35E+00	5.15E-02	6.34E-02
30.875	-8.15E-02	-7.37E-02	1.41E+00	1.42E+00	5.03E-02	6.22E-02
31.125	-7.58E-02	-6.80E-02	1.45E+00	1.46E+00	5.03E-02	6.22E-02
31.375	-7.83E-02	-7.05E-02	1.47E+00	1.48E+00	6.58E-02	7.78E-02
31.625	-7.78E-02	-7.00E-02	1.51E+00	1.52E+00	7.93E-02	9.12E-02
31.875	-7.89E-02	-7.11E-02	1.53E+00	1.54E+00	9.50E-02	1.07E-01
32.125	-8.06E-02	-7.28E-02	1.55E+00	1.56E+00	1.02E-01	1.14E-01
32.375	-6.90E-02	-6.11E-02	1.56E+00	1.57E+00	1.03E-01	1.15E-01
32.625	-7.50E-02	-6.71E-02	1.59E+00	1.59E+00	8.54E-02	9.74E-02
32.875	-7.84E-02	-7.06E-02	1.61E+00	1.61E+00	9.01E-02	1.02E-01
33.125	-7.38E-02	-6.60E-02	1.62E+00	1.62E+00	8.71E-02	9.90E-02
33.375	-7.46E-02	-6.68E-02	1.62E+00	1.63E+00	8.17E-02	9.36E-02
33.625	-7.00E-02	-6.22E-02	1.63E+00	1.64E+00	7.17E-02	8.36E-02
33.875	-7.55E-02	-6.77E-02	1.65E+00	1.66E+00	5.35E-02	6.54E-02
34.125	-7.19E-02	-6.41E-02	1.67E+00	1.68E+00	5.17E-02	6.36E-02
34.375	-7.50E-02	-6.72E-02	1.68E+00	1.69E+00	4.82E-02	6.01E-02
34.625	-7.39E-02	-6.61E-02	1.69E+00	1.70E+00	5.49E-02	6.68E-02
34.875	-6.58E-02	-5.80E-02	1.70E+00	1.71E+00	6.16E-02	7.35E-02
35.125	-6.40E-02	-5.62E-02	1.71E+00	1.71E+00	6.61E-02	7.81E-02
35.375	-5.86E-02	-5.08E-02	1.71E+00	1.71E+00	7.14E-02	8.33E-02
35.625	-6.16E-02	-5.38E-02	1.71E+00	1.72E+00	6.46E-02	7.65E-02
35.875	-4.86E-02	-4.08E-02	1.70E+00	1.71E+00	7.52E-02	8.71E-02
36.125	-5.19E-02	-4.41E-02	1.70E+00	1.71E+00	6.61E-02	7.81E-02
36.375	-5.80E-02	-5.02E-02	1.69E+00	1.70E+00	6.02E-02	7.21E-02
36.625	-5.89E-02	-5.11E-02	1.69E+00	1.70E+00	4.54E-02	5.73E-02
36.875	-4.92E-02	-4.14E-02	1.67E+00	1.68E+00	4.45E-02	5.64E-02
37.125	-4.81E-02	-4.03E-02	1.66E+00	1.67E+00	4.02E-02	5.21E-02
37.375	-4.77E-02	-3.99E-02	1.66E+00	1.67E+00	4.46E-02	5.65E-02
37.625	-3.88E-02	-3.10E-02	1.66E+00	1.67E+00	4.76E-02	5.95E-02
37.875	-3.62E-02	-2.84E-02	1.67E+00	1.68E+00	5.11E-02	6.30E-02
38.125	-3.04E-02	-2.26E-02	1.67E+00	1.68E+00	5.89E-02	7.08E-02
38.375	-2.62E-02	-1.84E-02	1.67E+00	1.68E+00	6.25E-02	7.44E-02
38.625	-2.69E-02	-1.91E-02	1.67E+00	1.68E+00	6.18E-02	7.37E-02
38.875	-2.31E-02	-1.53E-02	1.67E+00	1.68E+00	6.25E-02	7.44E-02
39.125	-3.25E-02	-2.47E-02	1.66E+00	1.66E+00	5.15E-02	6.34E-02
39.375	-1.70E-02	-9.21E-03	1.62E+00	1.63E+00	4.65E-02	5.85E-02
39.625	-1.92E-02	-1.14E-02	1.60E+00	1.61E+00	4.03E-02	5.22E-02
39.875	-1.70E-02	-9.21E-03	1.58E+00	1.59E+00	4.17E-02	5.36E-02

Table 16. MAPO test number 106 data.

Test File: MAPOTEST.106 Test Date: Wed, 12-12-1996 No. Channels: 3 Sam/sec: 128      Average      32 pt centered Start: 10:46:27:83    End: 10:47:07:87 Low-g Range start      10:46:33      (5 sec) end      10:46:41      (13 sec) Accelerometer Bias Average Interval (14 to 17 sec)						
Bias Values    x      -0.0078 (g's)          y      -0.0101 z      -0.0128 Time Stamp Offset Between Data and Video      0 sec						
Time	x (g's)	x Corrected (g's)	y (g's)	y Corrected (g's)	z (g's)	z Corrected (g's)
0.125	-1.99E-01	-1.91E-01	-4.97E-03	5.09E-03	-1.69E+00	-1.68E+00
0.375	-1.89E-01	-1.81E-01	-1.46E-02	-4.53E-03	-1.71E+00	-1.70E+00
0.625	-1.93E-01	-1.85E-01	-8.93E-03	1.13E-03	-1.70E+00	-1.69E+00
0.875	-2.15E-01	-2.07E-01	-2.10E-03	7.97E-03	-1.74E+00	-1.73E+00
1.125	-1.77E-01	-1.69E-01	-3.32E-02	-2.32E-02	-1.65E+00	-1.64E+00
1.375	-1.94E-01	-1.86E-01	-1.67E-02	-6.63E-03	-1.66E+00	-1.65E+00
1.625	-1.84E-01	-1.76E-01	-5.27E-02	-4.27E-02	-1.66E+00	-1.65E+00
1.875	-2.05E-01	-1.98E-01	-3.94E-02	-2.93E-02	-1.70E+00	-1.68E+00
2.125	-1.97E-01	-1.89E-01	-2.80E-02	-1.80E-02	-1.67E+00	-1.66E+00
2.375	-2.11E-01	-2.03E-01	-1.81E-02	-8.03E-03	-1.67E+00	-1.66E+00
2.625	-2.28E-01	-2.20E-01	-7.77E-03	2.30E-03	-1.68E+00	-1.66E+00
2.875	-2.01E-01	-1.93E-01	-1.82E-02	-8.18E-03	-1.60E+00	-1.59E+00
3.125	-1.48E-01	-1.41E-01	-1.75E-02	-7.41E-03	-1.43E+00	-1.42E+00
3.375	-1.29E-01	-1.21E-01	-2.03E-02	-1.02E-02	-1.19E+00	-1.18E+00
3.625	-1.15E-01	-1.08E-01	-1.03E-02	-2.63E-04	-9.58E-01	-9.45E-01
3.875	-8.32E-02	-7.53E-02	-6.29E-03	3.77E-03	-7.90E-01	-7.77E-01
4.125	-7.38E-02	-6.60E-02	-1.02E-02	-1.08E-04	-6.55E-01	-6.42E-01
4.375	-5.03E-02	-4.24E-02	-2.13E-02	-1.12E-02	-5.25E-01	-5.12E-01
4.625	-4.93E-02	-4.14E-02	-3.01E-02	-2.01E-02	-4.61E-01	-4.48E-01
4.875	-4.18E-02	-3.40E-02	-2.28E-02	-1.28E-02	-4.39E-01	-4.26E-01
5.125	-4.34E-02	-3.55E-02	-2.07E-02	-1.07E-02	-3.73E-01	-3.60E-01
5.375	-3.25E-02	-2.46E-02	-1.65E-02	-6.40E-03	-3.04E-01	-2.91E-01
5.625	-2.91E-02	-2.12E-02	-8.47E-03	1.60E-03	-2.80E-01	-2.67E-01
5.875	-2.25E-02	-1.47E-02	-9.01E-03	1.06E-03	-2.61E-01	-2.48E-01
6.125	-2.35E-02	-1.56E-02	-1.03E-02	-1.85E-04	-2.44E-01	-2.31E-01
6.375	-2.04E-02	-1.26E-02	-1.09E-02	-8.06E-04	-2.34E-01	-2.21E-01
6.625	-1.59E-02	-8.10E-03	4.72E-01	4.82E-01	-2.29E-01	-2.16E-01
6.875	-1.11E-02	-3.26E-03	-2.01E-02	-1.00E-02	-2.19E-01	-2.07E-01
7.125	-1.25E-02	-4.64E-03	-2.05E-02	-1.04E-02	-2.07E-01	-1.94E-01
7.375	-8.72E-03	-8.75E-04	-2.31E-02	-1.31E-02	-1.82E-01	-1.69E-01
7.625	-1.12E-02	-3.33E-03	-2.17E-02	-1.16E-02	-1.74E-01	-1.61E-01
7.875	-7.18E-03	6.62E-04	-1.48E-02	-4.69E-03	-1.60E-01	-1.47E-01
8.125	-7.95E-03	-1.06E-04	-1.03E-02	-2.63E-04	-1.23E-01	-1.10E-01
8.375	-1.10E-02	-3.18E-03	-5.90E-03	4.16E-03	-1.01E-01	-8.80E-02
8.625	-1.08E-02	-2.95E-03	-5.46E-04	9.52E-03	-7.67E-02	-6.39E-02
8.875	-1.04E-02	-2.57E-03	3.03E-03	1.31E-02	-5.20E-02	-3.92E-02
9.125	-1.08E-02	-2.95E-03	1.71E-03	1.18E-02	-4.36E-02	-3.08E-02
9.375	-9.64E-03	-1.80E-03	-2.02E-03	8.04E-03	-3.67E-02	-2.39E-02
9.625	-8.87E-03	-1.03E-03	-7.07E-03	3.00E-03	-2.85E-02	-1.57E-02
9.875	-7.26E-03	5.85E-04	-1.20E-02	-1.89E-03	-3.67E-02	-2.40E-02
10.125	-8.87E-03	-1.03E-03	-1.59E-02	-5.85E-03	-3.82E-02	-2.54E-02
10.375	-7.33E-03	5.08E-04	-1.69E-02	-6.86E-03	-4.30E-02	-3.02E-02
10.625	-7.87E-03	-2.96E-05	-1.85E-02	-8.41E-03	-4.17E-02	-2.89E-02
10.875	-6.18E-03	1.66E-03	-2.06E-02	-1.05E-02	-3.91E-02	-2.63E-02

Table 16. MAPO test number 106 data (Continued).

Time	x (g's)	x Corrected (g's)	y (g's)	y Corrected (g's)	z (g's)	z Corrected (g's)
11.125	-9.87E-03	-2.03E-03	-1.78E-02	-7.72E-03	-3.46E-02	-2.18E-02
11.375	-8.26E-03	-4.14E-04	-1.73E-02	-7.25E-03	-2.12E-02	-8.37E-03
11.625	-7.26E-03	5.85E-04	-1.83E-02	-8.26E-03	-2.86E-02	-1.58E-02
11.875	-6.80E-03	1.05E-03	-1.42E-02	-4.14E-03	-3.10E-02	-1.82E-02
12.125	-8.03E-03	-1.83E-04	-1.09E-02	-8.06E-04	-1.71E-02	-4.36E-03
12.375	-8.10E-03	-2.60E-04	-1.01E-02	-2.99E-05	-1.34E-02	-5.71E-04
12.625	-1.00E-02	-2.18E-03	-1.25E-02	-2.44E-03	-2.04E-02	-7.62E-03
12.875	-9.79E-03	-1.95E-03	-1.78E-02	-7.72E-03	-2.51E-02	-1.23E-02
13.125	-1.03E-02	-2.49E-03	-1.30E-02	-2.98E-03	-1.63E-02	-3.54E-03
13.375	-5.72E-03	2.12E-03	-1.13E-02	-1.27E-03	-1.52E-02	-2.43E-03
13.625	-7.64E-03	2.01E-04	-1.45E-02	-4.46E-03	-1.95E-02	-6.66E-03
13.875	-8.33E-03	-4.91E-04	-1.17E-02	-1.66E-03	-1.52E-02	-2.43E-03
14.125	-1.02E-02	-2.33E-03	-1.27E-02	-2.59E-03	-1.76E-02	-4.80E-03
14.375	-9.95E-03	-2.10E-03	-1.08E-02	-7.29E-04	-1.78E-02	-5.03E-03
14.625	-4.95E-03	2.89E-03	-9.94E-03	1.25E-04	-1.26E-02	1.71E-04
14.875	-3.65E-03	4.20E-03	-1.09E-02	-8.06E-04	-1.10E-02	1.80E-03
15.125	-8.18E-03	-3.37E-04	-1.06E-02	-4.96E-04	-1.21E-02	6.91E-04
15.375	-9.79E-03	-1.95E-03	-9.32E-03	7.47E-04	-1.25E-02	2.46E-04
15.625	-1.02E-02	-2.33E-03	-9.09E-03	9.79E-04	-1.31E-02	-2.74E-04
15.875	-8.10E-03	-2.60E-04	-9.79E-03	2.81E-04	-1.13E-02	1.51E-03
16.125	-6.18E-03	1.66E-03	-1.04E-02	-3.40E-04	-1.18E-02	9.88E-04
16.375	-9.41E-03	-1.57E-03	-1.02E-02	-1.08E-04	-1.22E-02	5.43E-04
16.625	-8.87E-03	-1.03E-03	-9.16E-03	9.02E-04	-1.17E-02	1.06E-03
16.875	-5.03E-03	2.81E-03	-1.00E-02	4.78E-05	-1.06E-02	2.18E-03
17.125	-7.49E-03	3.55E-04	-8.08E-03	1.99E-03	-1.19E-02	9.14E-04
17.375	-8.10E-03	-2.60E-04	-1.03E-02	-2.63E-04	-1.28E-02	2.28E-05
17.625	-8.49E-03	-6.44E-04	-9.47E-03	5.91E-04	-1.17E-02	1.06E-03
17.875	-6.95E-03	8.92E-04	-1.03E-02	-2.63E-04	-1.18E-02	9.88E-04
18.125	-7.95E-03	-1.06E-04	-1.43E-02	-4.22E-03	7.42E-04	1.35E-02
18.375	-9.64E-03	-1.80E-03	1.36E-02	2.37E-02	2.17E-02	3.45E-02
18.625	-2.07E-02	-1.29E-02	-2.33E-03	7.73E-03	-1.63E-03	1.12E-02
18.875	-1.91E-02	-1.12E-02	-1.58E-04	9.91E-03	-1.31E-02	-3.48E-04
19.125	-7.33E-02	-6.54E-02	-6.37E-02	-5.37E-02	2.03E-01	2.16E-01
19.375	-2.36E-02	-1.58E-02	-1.74E-02	-7.33E-03	-2.72E-02	-1.44E-02
19.625	-6.03E-03	1.81E-03	-2.66E-02	-1.66E-02	-1.05E-02	2.32E-03
19.875	-1.29E-02	-5.10E-03	-3.63E-02	-2.63E-02	-8.02E-03	4.77E-03
20.125	-9.79E-03	-1.95E-03	-3.34E-03	6.72E-03	-1.75E-02	-4.73E-03
20.375	-6.18E-03	1.66E-03	-9.24E-03	8.24E-04	-1.22E-02	6.17E-04
20.625	-1.04E-02	-2.57E-03	-8.70E-03	1.37E-03	-1.32E-02	-4.23E-04
20.875	-7.49E-03	3.55E-04	-5.83E-03	4.24E-03	-1.35E-02	-7.20E-04
21.125	-4.26E-03	3.58E-03	-3.11E-03	6.96E-03	-2.02E-02	-7.40E-03
21.375	5.04E-04	8.35E-03	8.93E-03	1.90E-02	-3.91E-02	-2.63E-02
21.625	6.42E-03	1.43E-02	3.10E-03	1.32E-02	-5.13E-02	-3.85E-02
21.875	9.57E-03	1.74E-02	-4.58E-03	5.48E-03	-5.46E-02	-4.18E-02
22.125	1.23E-02	2.01E-02	-6.45E-03	3.62E-03	-5.37E-02	-4.10E-02
22.375	1.10E-02	1.89E-02	-4.97E-03	5.09E-03	-3.94E-02	-2.66E-02
22.625	2.30E-02	3.09E-02	-1.39E-02	-3.83E-03	-3.61E-02	-2.33E-02
22.875	-3.72E-03	4.12E-03	6.96E-04	1.08E-02	-2.12E-02	-8.37E-03
23.125	-1.34E-02	-5.56E-03	8.38E-03	1.84E-02	-9.21E-03	3.59E-03
23.375	-6.80E-03	1.05E-03	2.10E-02	3.10E-02	-3.49E-03	9.30E-03
23.625	-5.26E-03	2.58E-03	-1.32E-03	8.74E-03	-2.29E-02	-1.01E-02
23.875	-1.00E-02	-2.18E-03	-2.40E-02	-1.39E-02	-3.53E-02	-2.25E-02
24.125	-5.57E-03	2.28E-03	-2.24E-02	-1.24E-02	-1.96E-02	-6.81E-03
24.375	-3.11E-03	4.73E-03	-3.73E-02	-2.73E-02	-2.95E-02	-1.68E-02
24.625	3.04E-03	1.09E-02	-4.89E-02	-3.88E-02	-1.80E-02	-5.25E-03
24.875	-4.88E-03	2.97E-03	-1.03E-02	-2.63E-04	-2.29E-02	-1.01E-02
25.125	5.04E-04	8.35E-03	-9.63E-03	4.36E-04	-1.56E-03	1.12E-02
25.375	4.96E-03	1.28E-02	-1.24E-02	-2.36E-03	9.35E-03	2.21E-02

Table 16. MAPO test number 106 data (Continued).

Time	x (g's)	x Corrected (g's)	y (g's)	y Corrected (g's)	z (g's)	z Corrected (g's)
25.625	9.49E-03	1.73E-02	-1.50E-02	-4.92E-03	1.97E-02	3.25E-02
25.875	8.03E-03	1.59E-02	6.60E-03	1.67E-02	1.21E-02	2.49E-02
26.125	7.80E-03	1.56E-02	1.58E-02	2.58E-02	1.06E-02	2.34E-02
26.375	1.13E-02	1.91E-02	6.21E-03	1.63E-02	0.00E+00	1.28E-02
26.625	1.24E-02	2.03E-02	9.29E-04	1.10E-02	-4.90E-03	7.89E-03
26.875	9.88E-03	1.77E-02	2.17E-03	1.22E-02	-1.78E-03	1.10E-02
27.125	4.65E-03	1.25E-02	-1.87E-03	8.20E-03	-1.20E-02	8.39E-04
27.375	5.11E-03	1.30E-02	-1.18E-02	-1.74E-03	-9.35E-03	3.44E-03
27.625	4.50E-03	1.23E-02	-3.61E-02	-2.60E-02	-1.60E-02	-3.17E-03
27.875	-9.56E-04	6.89E-03	-6.41E-02	-5.41E-02	-2.62E-02	-1.34E-02
28.125	-5.95E-03	1.89E-03	-1.82E-02	-8.18E-03	-2.95E-02	-1.68E-02
28.375	-1.03E-03	6.81E-03	-1.69E-02	-6.86E-03	-2.96E-02	-1.68E-02
28.625	-1.28E-02	-4.95E-03	-3.66E-02	-2.65E-02	-4.70E-02	-3.42E-02
28.875	-5.18E-03	2.66E-03	-4.67E-02	-3.66E-02	-5.35E-02	-4.07E-02
29.125	-1.69E-02	-9.02E-03	-1.32E-03	8.74E-03	-5.31E-02	-4.03E-02
29.375	-4.66E-02	-3.88E-02	-2.51E-02	-1.50E-02	-2.03E-01	-1.90E-01
29.625	3.58E-03	1.14E-02	-1.96E-02	-9.58E-03	-3.23E-01	-3.10E-01
29.875	9.11E-03	1.70E-02	-2.80E-06	1.01E-02	-2.61E-01	-2.48E-01
30.125	1.05E-02	1.83E-02	-1.65E-02	-6.47E-03	-3.65E-01	-3.52E-01
30.375	5.57E-03	1.34E-02	-5.28E-03	4.78E-03	-4.43E-01	-4.30E-01
30.625	-9.56E-04	6.89E-03	-1.26E-02	-2.51E-03	-5.09E-01	-4.96E-01
30.875	-1.00E-02	-2.18E-03	-4.27E-03	5.79E-03	-6.02E-01	-5.89E-01
31.125	-1.41E-02	-6.25E-03	-1.37E-02	-3.60E-03	-7.09E-01	-6.96E-01
31.375	-2.40E-02	-1.62E-02	-1.40E-02	-3.91E-03	-8.52E-01	-8.39E-01
31.625	-3.02E-02	-2.24E-02	-9.55E-03	5.14E-04	-9.86E-01	-9.73E-01
31.875	-4.31E-02	-3.52E-02	-1.16E-02	-1.58E-03	-1.08E+00	-1.06E+00
32.125	-5.74E-02	-4.96E-02	-1.08E-02	-7.29E-04	-1.16E+00	-1.15E+00
32.375	-6.96E-02	-6.17E-02	-1.70E-02	-6.94E-03	-1.22E+00	-1.21E+00
32.625	-6.66E-02	-5.87E-02	-1.86E-02	-8.49E-03	-1.26E+00	-1.25E+00
32.875	-7.13E-02	-6.34E-02	-2.70E-02	-1.70E-02	-1.30E+00	-1.29E+00
33.125	-8.05E-02	-7.26E-02	-2.42E-02	-1.42E-02	-1.35E+00	-1.33E+00
33.375	-8.17E-02	-7.39E-02	-2.95E-02	-1.94E-02	-1.36E+00	-1.35E+00
33.625	-8.02E-02	-7.23E-02	-3.11E-02	-2.10E-02	-1.38E+00	-1.36E+00
33.875	-8.12E-02	-7.33E-02	-2.86E-02	-1.85E-02	-1.39E+00	-1.38E+00
34.125	-8.16E-02	-7.38E-02	-2.85E-02	-1.84E-02	-1.39E+00	-1.38E+00
34.375	-8.47E-02	-7.69E-02	-2.88E-02	-1.87E-02	-1.42E+00	-1.41E+00
34.625	-8.63E-02	-7.85E-02	-2.14E-02	-1.14E-02	-1.46E+00	-1.45E+00
34.875	-8.96E-02	-8.18E-02	-1.82E-02	-8.10E-03	-1.48E+00	-1.47E+00
35.125	-9.34E-02	-8.55E-02	-2.22E-02	-1.21E-02	-1.48E+00	-1.47E+00
35.375	-8.22E-02	-7.43E-02	-2.14E-02	-1.14E-02	-1.50E+00	-1.49E+00
35.625	-8.43E-02	-7.65E-02	-2.62E-02	-1.61E-02	-1.52E+00	-1.51E+00
35.875	-8.66E-02	-7.88E-02	-2.51E-02	-1.50E-02	-1.54E+00	-1.52E+00
36.125	-8.40E-02	-7.62E-02	-3.28E-02	-2.28E-02	-1.54E+00	-1.53E+00
36.375	-8.26E-02	-7.48E-02	-2.73E-02	-1.72E-02	-1.54E+00	-1.53E+00
36.625	-7.66E-02	-6.88E-02	-2.91E-02	-1.91E-02	-1.56E+00	-1.54E+00
36.875	-8.49E-02	-7.71E-02	-2.76E-02	-1.75E-02	-1.57E+00	-1.56E+00
37.125	-7.38E-02	-6.60E-02	-2.07E-02	-1.07E-02	-1.58E+00	-1.56E+00
37.375	-7.56E-02	-6.78E-02	-1.82E-02	-8.10E-03	-1.57E+00	-1.56E+00
37.625	-7.85E-02	-7.06E-02	-1.19E-02	-1.82E-03	-1.59E+00	-1.57E+00
37.875	-6.77E-02	-5.98E-02	-2.10E-02	-1.10E-02	-1.57E+00	-1.56E+00
38.125	-6.35E-02	-5.57E-02	-1.46E-02	-4.53E-03	-1.56E+00	-1.55E+00
38.375	-6.14E-02	-5.35E-02	-6.14E-03	3.93E-03	-1.55E+00	-1.54E+00
38.625	-6.61E-02	-5.83E-02	-1.35E-02	-3.45E-03	-1.58E+00	-1.57E+00
38.875	-6.18E-02	-5.40E-02	-2.25E-02	-1.25E-02	-1.60E+00	-1.59E+00
39.125	-6.75E-02	-5.97E-02	-1.03E-02	-2.63E-04	-1.61E+00	-1.60E+00
39.375	-5.74E-02	-4.96E-02	-6.52E-03	3.54E-03	-1.62E+00	-1.61E+00
39.625	-6.83E-02	-6.05E-02	-1.40E-03	8.67E-03	-1.64E+00	-1.63E+00
39.875	-6.23E-02	-5.44E-02	-1.79E-03	8.28E-03	-1.66E+00	-1.65E+00

## REFERENCES

1. Glover, D.: "NASA Cryogenic Fluid Management Space Experiment Efforts 1960–1990," *AIAA Paper 91–3538*, AIAA/NASA/OAI Conference on Advanced SEI Technologies, September 4–6, 1991.
2. Hastings, L.J.; and Schmidt, G.R.: "The Marshall Space Flight Center Cryogenic Fluid Management Program," *AIAA Paper 93–4224*, AIAA Space Programs and Technologies Conference and Exhibit, September 21–23, 1993.
3. Takeda, T.; and Nishigaki, K.: "Shape Deformation of the Gas-Liquid Interface of Liquid Oxygen in High-Magnetic Fields," *Physical Review A*, Vol. 43, No. 4, pp. 2081–2083, February 15, 1991.
4. Hendricks, R.: "Paramagnetic Propellant Orientation," *AIAA Paper 91–2325*, AIAA/SAE/ASME/ASEE 27th Joint Propulsion Conference and Exhibit, June 24–26, 1991.
5. Paine, C.G.; and Seidel, G.M.: "Magnetic Levitation of Condensed Hydrogen," *American Institute of Physics Review of Scientific Instruments*, Vol. 62, No. 12, pp. 3022–3024, December 1991.
6. Hastings, L.J.; Tucker, S.P.; and Huffaker, C.F.: "CFM Technology Needs for Future Space Transportation Systems," *AIAA Paper 91–3474*, AIAA/NASA/OAI Conference on Advanced SEI Technologies, September 4–6, 1991.
7. Dominick, S.; and Driscoll, S.: "Fluid Acquisition and Resupply Experiment (FARE 1) Flight Results," *AIAA Paper 93–2424*, AIAA/SAE/ASME/ASEE 29th Joint Propulsion Conference and Exhibit, June 28–30, 1993.
8. "Low Gravity Propellant Control Using Capillary Devices in Large Scale Cryogenic Vehicles," *Design Handbook, Report No. GDC–DDB70–006*, Convair Division of General Dynamics, Contract NAS8–21465, August 1970.
9. Meserole, J.S.; and Jones, O.S.: "Pressurant Effects on Cryogenic Liquid Acquisition Devices," *Journal of Spacecraft and Rockets*, Vol. 30, No. 2, pp. 236–243, March April 1993.
10. "JSC Reduced Gravity Program User's Guide," *JSC 22803*, NASA Lyndon B. Johnson Space Center, November 1996.
11. "Design, Inspection and Certification of Pressure Vessels and Pressurized Systems," *JHB 1710 Rev. B*, NASA Lyndon B. Johnson Space Center, March 1994.
12. "JSC Safety Manual," *JSCM 1700 Rev. D*, NASA Lyndon B. Johnson Space Center, September 1989.

13. "Instruction for Preparation of Hazard Analysis for JSC Ground Operations," *JSC-17773, Rev. B*, NASA Lyndon B. Johnson Space Center, December 1984.
14. Myshkis, A.D.; Babskii, V.G.; Kopachevskii, N.D.; Slobozhanin, L.A.; and Tyuptsov, A.D.: "Low-Gravity Fluid Mechanics," Springer-Verlag, New York, 1987.
15. Hastings, L.J.; and Rutherford, R.: "Low Gravity Liquid-Vapor Interface Shapes in Axisymmetric Containers and a Computer Solution," *NASA TM X-53790*, MSFC, October 7, 1968.
16. Flanders, P.I.: "An Alternating-Gradient Magnetometer," *Journal of Applied Physics*, Vol. 63 (3), pp. 3940–3945, April 15, 1988.

REPORT DOCUMENTATION PAGE			Form Approved OMB No. 0704-0188	
Public reporting burden for this collection of information is estimated to average 1 hour per response, including the time for reviewing instructions, searching existing data sources, gathering and maintaining the data needed, and completing and reviewing the collection of information. Send comments regarding this burden estimate or any other aspect of this collection of information, including suggestions for reducing this burden, to Washington Headquarters Services, Directorate for Information Operation and Reports, 1215 Jefferson Davis Highway, Suite 1204, Arlington, VA 22202-4302, and to the Office of Management and Budget, Paperwork Reduction Project (0704-0188), Washington, DC 20503				
1. AGENCY USE ONLY (Leave Blank)	2. REPORT DATE March 2000	3. REPORT TYPE AND DATES COVERED Technical Memorandum		
4. TITLE AND SUBTITLE Magnetically Actuated Propellant Orientation Experiment, Controlling Fluid Motion With Magnetic Fields in a Low-Gravity Environment (MSFC Center Director's Discretionary Fund Final Report, Project No. 93-18)			5. FUNDING NUMBERS	
6. AUTHORS J.J. Martin and J.B. Holt				
7. PERFORMING ORGANIZATION NAME(S) AND ADDRESS(ES) George C. Marshall Space Flight Center Marshall Space Flight Center, AL 35812			8. PERFORMING ORGANIZATION REPORT NUMBER M-975	
9. SPONSORING/MONITORING AGENCY NAME(S) AND ADDRESS(ES) National Aeronautics and Space Administration Washington, DC 20546-0001			10. SPONSORING/MONITORING AGENCY REPORT NUMBER NASA/TM-2000-210129	
11. SUPPLEMENTARY NOTES Prepared by Propulsion Research Center, Space Transportation Directorate				
12a. DISTRIBUTION/AVAILABILITY STATEMENT Unclassified-Unlimited Subject Category 15 Nonstandard Distribution			12b. DISTRIBUTION CODE	
13. ABSTRACT (Maximum 200 words)  This report details the results of a series of fluid motion experiments to investigate the use of magnets to orient fluids in a low-gravity environment. The fluid of interest for this project was liquid oxygen (LO <sub>2</sub> ) since it exhibits a paramagnetic behavior (is attracted to magnetic fields). However, due to safety and handling concerns, a water-based ferromagnetic mixture (produced by Ferrofluidics Corporation) was selected to simplify procedures. Three ferromagnetic fluid mixture strengths and a nonmagnetic water baseline were tested using three different initial fluid positions with respect to the magnet. Experiment accelerometer data were used with a modified computational fluid dynamics code termed CFX-4 (by AEA Technologies) to predict fluid motion. These predictions compared favorably with experiment video data, verifying the code's ability to predict fluid motion with and without magnetic influences. Additional predictions were generated for LO <sub>2</sub> with the same test conditions and geometries used in the testing. Test hardware consisted of a cylindrical Plexiglas tank (6-in. bore with 10-in. length), a 6,000-G rare Earth magnet (10-in. ring), three-axis accelerometer package, and a video recorder system. All tests were conducted aboard the NASA Reduced-Gravity Workshop, a KC-135A aircraft.				
14. SUBJECT TERMS propellant orientation, propellant resettling, propellant transfer, propellant acquisition, magnetic control, magnetism, paramagnetic, ferromagnetic, liquid oxygen, cryogenics, low gravity, and reduced gravity			15. NUMBER OF PAGES 106	
			16. PRICE CODE A06	
17. SECURITY CLASSIFICATION OF REPORT Unclassified	18. SECURITY CLASSIFICATION OF THIS PAGE Unclassified	19. SECURITY CLASSIFICATION OF ABSTRACT Unclassified	20. LIMITATION OF ABSTRACT Unlimited	